FEASIBILITY OF RECYCLING SEWAGE SLUDGE ASH AS CONSTRUCTION MATERIALS

CHEN ZHEN

PhD

THE HONG KONG POLYTECHNIC UNIVERSITY

2019

THE HONG KONG POLYTECHNIC UNIVERSITY

DEPARTMENT OF CIVIL AND ENVIRONMENTAL ENGINEERING

FEASIBILITY OF RECYCLING SEWAGE SLUDGE ASH AS CONSTRUCTION MATERIALS

CHEN ZHEN

A thesis submitted in partial fulfilment of the

requirements for the degree of Doctor of Philosophy

July 2018

CERTRIFICATE OF ORIGINALITY

I hereby declare that this thesis is my own work and that, to the best of my knowledge and belief, it reproduces no material previously published or written, nor material that has been accepted for the award of any other degree or diploma, except where due acknowledgement has been made in the text.

_____ (Signed)

CHEN ZHEN (Name of student)

ABSTRACT

Sewage sludge ash (SSA) is generated from incinerating dewatered sewage sludge. As most SSA still need to be disposed of at landfills, the management of SSA becomes an environmental issue. Many places including Hong Kong face growing pressure in waste management due to limited landfilling capacity around cities and strong objections to their operation by the public. Dumping wastes in landfills is not a sustainable means of managing wastes. To relieve the burden on landfills, it is highly desirable to increase the recycling of wastes. One major approach is the use of wastes in construction products. The huge consumption of construction materials can effectively reduce some wastes by this means. The focus of the PhD study was on the recycling of SSA as construction materials. The study consists of three parts. First, use of SSA as partial cement replacements for making cement mortars. Second, use of SSA as partial cement replacements for making concrete blocks. Last, blending SSA with ground granulated blast-furnace slag (GGBS) to produce geopolymers.

For producing cement mortars the effects of the SSA on the compressive and flexural strength of the cement mortars were studied. These effects were compared with those of pulverized fly ash (PFA) and fine sewage sludge ash (FSSA) which was prepared by grinding the SSA in a ball mill for 3 hours. Methods for characterization the

properties included Frattini pozzolanic activity, compressive strength, flexural strength, drying shrinkage, Isothermal Conduction Calorimetry, mercury intrusion porosimetry, XRD, SEM and EDX tests. The results showed that the SSA and FSSA exhibited lower pozzolanic activities compared with PFA, but the cement mortars prepared with up to 20% SSA or FSSA yielded strength values comparable to those of the PFA cement mortars. The SSA and FSSA contributed to the strength through (i) acceleration of the rate of cement hydration at early stages while PFA did not produce this effect, (ii) the preservation of cumulative pore volume of the paste with low SSA or FSSA content up to 10%, and (iii) the formation of brushite, a kind of binding phase, in SSA or FSSA cement pastes at late ages. Unfortunately, SSA caused higher drying shrinkage in mortars due to increasing content of mesopores with sizes less than 0.025 μm. This undesirable effect was greater with the FSSA. Findings of the study filled the gap in knowledge about strength development in mortars containing a small amount of SSA despite its low pozzolanic activity.

Given the difficulty in achieving good workability in cement mortars incorporating SSA due to its hydrophilic nature, the second application of SSA in making precast concrete blocks was studied. This recycling method only require a small quantity of water to give a dry but cohesive mix which is then compressed into standard moulds. In this study, SSA was used as a partial substitution of cement together with recycled glass cullet for partial substitution of natural aggregates to produce concrete blocks.

Through investigating the hardened density, water absorption, compressive strength, drying shrinkage, alkali silica reaction of the concrete blocks, it was found that the benefits and drawbacks of SSA and glass cullet aggregates were complimentary to each other. The porous nature of SSA absorbed more water in mixing resulting in high shrinkage. While glass cullet in the mix, being hydrophobic, substantially reduced shrinkage of the blocks. On the other hand, expansion due to alkali silica reaction caused by the reactive glass cullet aggregates could in turn be controlled by the SSA present in the blocks. Other findings in this study included use of SSA increased the water demand and more water was needed to attain suitable consistency in making concrete blocks while the FSSA with smoother particles and less pores required slightly less water and the blending of 20% SSA or FSSA in the binder increased the water absorption values of the concrete blocks but the effects on hardened densities were not obvious. Besides, leaching tests conducted on both the SSA and the concrete blocks showed full compliance with regulations. This combined use of the two types of wastes, i.e., SSA and glass cullet, is innovative and successful.

Another complimentary use of two wastes is blending GGBS with SSA in equal proportion to form an aluminosilicate precursor for synthesizing geopolymer pastes. In studying this application, the effects of alkali dosage, expressed as weight percentage of Na_2O to the mixed solids, and modulus which represented the molar

ratio of SiO_2 to Na_2O in the mixed sodium hydroxide (NaOH) and sodium silicate (Na_2SiO_3) alkaline solution were assessed. Through various tests including compressive strength, XRD, QXRD, FTIR, SEM and EDX, insights into the microstructure of geopolymer and variations caused by different alkalinity was gained. SSA was found to be transformed in the geopolymerization and the quartz and hematite crystals in it were largely dissolved by the alkaline solution. Optimum alkali dosage of 4.0% and modulus of 0.95 could produce a geopolymer of maximum strength of 32.81 MPa. The main reaction product of the optimum mixture was a C-(N)-A-S-H gel with Fe substitutions. The drying shrinkage of all specimens were less than 0.06% at the age of 14 days. This study built up a theoretical basis for recycling SSA as aluminum silicate sources for producing geopolymer.

PUBLICATIONS ARISING FROM THE THESIS

Academic Journal Papers

Chen, Z., Poon, C.S.*, 2017. Comparing the use of sewage sludge ash and glass powder in cement mortars. Environmental Technology 38 (11), 1390-1398.

Chen, Z., Poon, C.S.*, 2017. Comparative studies on the effects of sewage sludge ash and fly ash on cement hydration and properties of cement mortars. Construction and Building Materials 154, 791-803.

Chen, Z., Li, J.S., Poon, C.S.*, 2018. Combined use of sewage sludge ash and recycled glass cullet for the production of concrete blocks. Journal of Cleaner Production 171, 1447-1459.

Chen, Z., Li, J.S., Zhan, B.J., Sharma, U., Poon, C.S.*, 2018. Compressive strength and microstructural properties of dry-mixed geopolymer pastes synthetized from GGBS and sewage sludge ash. Construction and Building Materials 182, 597-607.

Conference Papers

Chen, Z., Poon, C.S.*, 2015. Maximizing the recycling of waste glass as construction materials. International Conference on Solid Waste 2015, Hong Kong.

Chen, Z., Poon, C.S.*, 2016. Recycling of sewage sludge ash (SSA) as construction materials. 2016 International Concrete Sustainability Conference, Washington, D. C., America.

ACKNOWLEGEMENTS

I would like to express my heartfelt gratitude to my supervisor, Prof. C.S. Poon, for giving me the opportunity to carry out the research project. Thank the Environment and Conservation Fund, the Woo Wheelock Green Fund and the Hong Kong Polytechnic University (Project of Strategic Importance) for giving funding supports.

In addition, Prof. Poon provided solid academic and technical supports throughout my study. Without his patient guidance and insightful criticism, the completion of this thesis would not have been possible. My research and analytical skills have been greatly improved while working under Prof. Poon. His care and advice added strength in overcoming many difficulties. Many thanks and appreciation to Prof. Poon.

I would like to express my thanks to the technicians in the laboratories. With their assistance, my experiments were performed smoothly and orderly in a tight schedule due to the late supply of sewage sludge ash, my study material. Many experimental skills I acquired in the laboratories are valuable for my future work.

Thanks are due to all researchers who work in Prof. Poon's team during the period of my PhD study. Prof. Poon's team has many good colleagues who were very

knowledgeable and helpful rendering great support to my work.

Last but not the least, special thanks goes to my boyfriend who stood by me at all times, lifting my spirit when I was down and supporting me in everything. Seriously, without him, I could not clear so many hurdles.

TABLE OF CONTENTS

LIST OF FIGURES

LIST OF TABLES

LIST OF ABBREVIATIONS

AFt	Ettringite
ASR	Alkali Silica Reaction
BET	Brunauer Emmett Teller
$Ca(OH)_2$	Portlandite
C-A-S-H	Calcium Aluminate Silicate Hydrate
C&D	Construction and Demolition
C_2S	Belite
C_3S	Alite
C-S-H	Calcium Silicate Hydrate
DTA	Differential Thermal Analysis
EDX	Energy Dispersive X-ray
EPA	Environmental Protection Agency
EPD	Environmental Protection Department
FSSA	Fine Sewage Sludge Ash
FTIR	Fourier Transform Infrared Spectroscopy
FTS	Flow Table Spread
GC	Glass Cullet
GGBS	Ground Granulated Blast-Furnace Slag
ICC	Isothermal Conduction Calorimetry

ICDD	International Centre for Diffraction Data
LOI	Loss of Ignition
MIP	Mercury Intrusion Porosimetry
MK	Metakaolin
NA	Natural Aggregates
NaOH	Sodium Hydroxide
N-A-S-H	Sodium Aluminate Silicate Hydrate
Na_2SiO_3	Sodium Silicate
OPC	Ordinary Portland Cement
PDF	Powder Diffraction File
PFA	Pulverized Fly Ash
QXRD	Semi-Quantitative X-ray Diffraction
SAI	Strength Activity Index
SCM	Supplementary Cementitious Material
SEM	Scanning Electron Microscopy
SSA	Sewage Sludge Ash
TCLP	Toxicity Characteristic Leaching Procedure
TGA	Thermogravimetric Analysis
W/B	Water/Binder
W/C	Water/Cement

XRD	X-ray Diffraction
XRF	X-ray Fluorescence

CHAPTER 1 – INTRODUCTION

1.1 Background

Hong Kong faces growing pressure in waste management due to its limited landfilling capacity and strong objections to its extension by the public (News.gov.hk, 2013). Dumping wastes in landfills is not a sustainable means of managing waste. Sewage sludge is generated from the treatment of wastewater. In Hong Kong about 1000 tonnes of dewatered sewage sludge were produced every day in 2014 as reported by the Environmental Protection Department (EPD) (2014). They were disposed of in landfills in the past. In 2015, the Hong Kong government commissioned a mega-sized sewage sludge incinerator, the largest one in the world up to date, to treat sludge. This treatment method can generally convert dewatered sewage sludge into ash of 30% of the original weight after combustion of organics and vaporization of water (EPD, 2017). Sludge is incinerated in a fluidized bed in the incineration process. The ash is then collected by a dedust system and cyclone separators. Two types of ash are generated in this process: one is incinerated sewage sludge ash, i.e., SSA, and the other is air pollution control residues. The focus of this PhD study is SSA. Despite its smaller volume after incineration, SSA still needs to be disposal of in landfills at the moment. For sustainable waste management, various means of recycling SSA to reduce the burden on landfills are needed.

1.2 Research Objectives

The application of SSA in construction products has attracted interest in conducting this PhD study. The huge consumption of construction materials can significantly reduce the waste through recycling. In this study, the SSA was used to replace cement as a supplementary cementitious material (SCM) to produce cement mortars and concrete blocks. It was also used to mix with ground granulated blast-furnace slag (GGBS) to synthesize geopolymer pastes. In all, the objectives of this study can be summarized as follows:

(1) To evaluate potential chemical and microstructural factors governing the mechanical properties of cement pastes containing SSA.

(2) To evaluate the benefits of the combined use of SSA as a cement replacement and recycled construction and demolition (C&D) aggregates or glass cullet (GC) as a partial substitution of natural aggregates (NA) in concrete blocks.

(3) To understand the process of geopolymerization of SSA with GGBS and to evaluate the effects of alkalinity conditions on the process.

1.3 Thesis Outline

This chapter introduces the background and purposes of the PhD study. The focuses of the remaining chapters of this thesis are as follows:

Chapter 2 presents an overview of the findings from past studies about the effects of SSA on the properties of concretes and geopolymers. The potential environmental risks from leaching of metal(loid)s associated with those applications as revealed in some studies are also reviewed in this chapter.

Chapter 3 describes the research methodologies employed in studying the various construction applications incorporating the SSA. It provides information on the chemical and physical properties of the materials, the proportioning and mixing of the ingredients, the curing conditions of test specimens and the experimental methods for evaluating the products.

Chapter 4 discusses the mechanisms behind some beneficial effects of the SSA on the strength development of cement mortars through a comparison study with PFA and fine sewage sludge ash (FSSA).

Chapter 5 discusses the properties of concrete blocks using SSA as a cement replacement together with recycled C&D aggregates or GC as a partial substitution of NA.

Chapter 6 discusses geopolymerization of mixes of GGBS and SSA in equal weight under binary alkaline activators, namely, sodium hydroxide (NaOH) and sodium silicate (Na_2SiO_3), with different Na_2O contents and moduli.

Chapter 7 summarizes the findings and draws conclusions on this PhD study followed by giving recommendations for future research.

CHAPTER 2 – LITERATURE REVIEW

2.1 Introduction

Among those potential reuse applications of SSA, many studies have been conducted on sintering materials containing SSA, including clay with SSA to produce bricks and tiles (Anderson, 2002; Chen and Lin, 2009a), clay and sewage sludge with SSA to produce lightweight aggregates (Cheeseman and Virdi, 2005; Chiou et al., 2006), and SSA alone or with additives including clay, glass powder and limestone to manufacture ceramic and glass-ceramic products (Park et al., 2003; Wang et al., 2012). Besides, as phosphate rich reserve is limited but the demand for phosphate is high (Xu et al., 2012), many studies have been conducted on recovery of phosphate from SSA by different processes (Niu and Shen, 2017; Li et al., 2018) as SSA typically contain 13-25% phosphate by weight in the form of P_2O_5 (Adam et al., 2009). There were also studies on some less usual recycling applications of SSA. They include soil stabilization in combination with $Ca(OH)_2$ or cement (Lin, et al., 2007; Chen and Lin, 2009) and addition to asphalt as mineral filler to replace limestone (Al Sayed et al., 1995).

Another application of SSA is using it as a SCM to replace cement. Portland cement is the most widely used binder material in building and other infrastructure

construction. However, cement production utilizes natural resources, consumes high energy and generates huge amounts of carbon dioxide. In view of growing environmental concerns, there is a need to explore alternative cementing materials for sustainability. Waste materials, such as PFA and GGBS, have been beneficially recycled as partial replacement of cement in concrete. Many studies have also focused on using other wastes, such as municipal solid waste incineration bottom ash (Li et al., 2012), rice husk ash (Gursel et al., 2016), palm oil fuel ash (Alsubari et al., 2016), etc. to substitute small amounts of cement for concrete production. This chapter presents an overview of the chemical and physical characteristics of SSA together with its effects on the properties of cement-based materials from findings of previous studies.

Typical source materials for making geopolymers are those rich in silicon (Si) and aluminum (Al). The synthetization of geopolymers is an environmental-friendly process in which three-dimensional aluminosilicate materials are synthesized (Habert et al., 2011; Turner and Collins, 2013). The process involves the dissolution of Si and Al species from the precursors by an alkaline media as well as possible surface hydration of particles of the precursors, followed by coagulation and gelation of the dissolved minerals into monomers which undergo further polycondensation to form a gel and subsequently hardened geopolymer structure (Davidovits, 1994). Geopolymers are promising materials to replace cement as alternative binder

materials in construction works because they exhibited equal or even superior mechanical (Mehta and Siddique, 2016; Lahoti et al., 2017), durability (Bakharev, 2005; Koenig et al., 2017) and high temperature (Kong and Sanjayan, 2008; Yang et al., 2017) properties compared with cement. SSA can be a potential precursor for synthesizing geopolymers because its main components are SiO_2, Al_2O_3 and CaO as revealed in previous studies (Franz, 2008; Kosior-Kazberuk, 2011). However, not many researches have been conducted in this field. A summary of published data on using SSA as a base material for synthesizing geopolymers has been included in this chapter.

2.2 Chemical Characteristics and Physical Properties of SSA Recorded in the Literature

2.2.1 Oxide Compositions and Metal(loid) Element Contents

Sewage treatment plant often handles domestic and industrial sewage together (Baeyens and Puyvelde, 1994). SSA which is a residue of incinerating sewage sludge therefore contains some common oxides and elements. Table 2.1 and Table 2.2 give average chemical compositions of major oxides and trace metal(loid) elements in SSA respectively presented by Cyr et al. (2007) from reviewing a number of articles. Major oxide components of SSA (SiO_2, CaO, Al_2O_3 and Fe_2O_3) shown in Table 2.1

are similar to those of common cementitious materials such as PFA, silica fume and metakaolin (MK). The special oxide compositions of SSA indicate that it can be used for partial replacement of Portland cement in producing cement paste, mortar, and concrete. The special oxide compositions also show possible use of SSA as an aluminosilicate source for the production of geopolymers.

The sulfur content (SO_3) in SSA noted by Cyr et al. (2007) ranged from 0.01% to 12.4% by weight. In Monzó et al. (1999)'s research, it was shown that high sulfur content did not seem to influence the compressive strength of mortars containing SSA and cement with different tricalcium aluminate contents.

It can be seen from Table 2.2 that SSA contains a range of metal(loid)s like Ba, Zn, Cu and Pb, some of which in high concentrations. It is therefore probable that these metal(loid)s may leach out in some applications of SSA. Cyr et al. (2007) presented that the amount of metal(loid)s leached from SSA-containing mortars was slightly higher than that from the reference mortar without SSA but it remained of the same order of magnitude. Chen et al. (2013) studied the leaching contaminants from mortar and concrete with different SSA contents with monoliths cured for 3 months. They found that only Mo and Se at concentrations above their threshold limits leached from the SSA powder, and no contaminants including Mo and Se leached at concentrations exceeding the limits in the concrete monoliths. They then concluded

that mixing SSA with cement and sand to produce mortar and concrete was a good method for stabilizing SSA.

To achieve better performance in stabilizing SSA in cement-based materials, Cyr et al. (2012) found that the use of MK led to a significant decrease in soluble fractions and metal(loid)s released from the binder matrix. They considered that the effect came from decreased permeability of the pastes, increased adsorption potential for metal(loid) ions, reaction of metal(loid) ions with cement and MK compounds during the hydration process, and possibly adsorption of metal(loid)s in the clay minerals of MK. However, it is noted that the study was conducted using a large amount of MK relative to SSA, its effectiveness had not been fully explored. Greater benefit can be achieved if further studies confirm that lesser proportions of MK also perform well.

The actual composition of SSA generated in a particular place would deviate from the average composition due to different sources of wastewater, furnace temperatures and diverse additives introduced into the sludge processing systems. The actual composition should be checked and monitored to assess the changing properties of SSA collected from a plant before utilization.

Table 2.1 Average composition of oxides in SSA noted in the literature (Cyr et al., 2007)

Oxide	wt. %	Oxide	wt. %
SiO_2	36.1	Na_2O	0.9
Al_2O_3	14.2	K_2O	1.3
Fe_2O_3	9.2	TiO_2	1.1
CaO	14.8	MgO	2.4
P_2O_5	11.6	MnO	0.3
SO_3	2.8	Loss of ignition (LOI)	6.1

Table 2.2 Average contents of metal(loid) elements in SSA noted in the literature (Cyr et al., 2007)

Element	mg/kg	Element	mg/kg
As	87	Pb	600
Ba	4142	Sb	35
Cd	20	Sn	400
Co	39	Sr	539
Cr	452	V	35
Cu	1962	Zn	3512
Ni	671		

2.2.2 Mineralogy Compositions

The common crystalline minerals in SSA are quartz (SiO_2), calcite ($CaCO_3$) and hematite (Fe_2O_3) and the proportions of amorphous and semi-crystalline phases in SSA range from 35% to 75%, as summarized in the book of Dhir et al. (2017). Variation in the mineralogy compositions of SSA is expected as it is derived from sewage sludge which varies widely in composition. Mineralogy composition of SSA significantly affects its reactivity in any recycling processes.

A study conducted by Dhir et al. (2001) demonstrated that the amount and composition of the amorphous and semi-crystalline portion of SSA influenced the material's performance. In general, the extent of hydration reaction was defined by the amorphous and semi-crystalline phase CaO/SiO_2 ratio and Al_2O_3/SiO_2 ratio. The contribution when used in combination with Portland cement improved as the composition of the amorphous and semi-crystalline fraction approached the region defined by Smolczyk (1980) as being inhabited by latent hydraulic materials, as shown on the CaO-SiO_2-Al_2O_3 ternary diagram in Fig. 2.1. Such a region was defined by the relationships $0.5 < CaO/SiO_2 < 2.0$ and $0.1 < Al_2O_3/SiO_2 < 0.6$. Also shown in Fig. 2.1 are positions of four kinds of SSA based on their amorphous and semi-crystalline CaO, Al_2O_3 and SiO_2 compositions found by Dhir et al. (2001). It was claimed that the SSAs lay very close to the shadow zone and may undergo hydraulic

reactions.

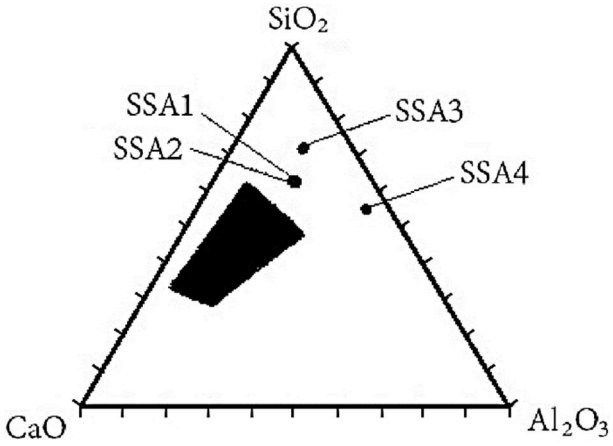

Fig. 2.1 Positions of latent hydraulic materials defined by Smolczyk (1980) and four kinds of SSA on a ternary diagram (Dhir et al., 2001)

2.2.3 Morphology, Specific Gravity, Fineness and Grading

The morphology of SSA is one of the basic characteristics that has been widely reported in the literature (Donatello and Cheeseman, 2013; Lynn et al., 2015; Dhir et al., 2017). Generally, SSA particles were irregular in shape and their surface was rough and porous.

The average values of specific gravity, specific surface area in Blaine and Brunauer Emmett Teller (BET) of SSA obtained in the literature and calculated by Cyr et al. (2007) were 2.61, 450 m^2/kg and 15100 m^2/kg respectively. The BET test can

measure surface area at the scale of nitrogen molecules, but the flowing air method in the Blaine test cannot interrogate all parts of the surface area. It was reported that the BET test can measure surface area in the range of 686 m^2/kg to 2000 m^2/kg while the Blaine test can only measure surface area from 349 m^2/kg to 545 m^2/kg (Ferraris and Garboczi, 2013). Therefore, the Blaine test is less sensitive than the BET test in measuring surface areas. It was also mentioned in one article (Arvaniti et al., 2015) that the Blaine surface area would be smaller than the BET surface area when particles were porous or rough in surface. The particle sizes of SSA ranged from 8 μm to 200 μm, with a mean diameter of 44 μm (Cyr et al., 2007). Dhir et al. (2017) through a review of large amount of experimental data reported in the literature found that the average specific gravity, specific surface area in Blaine and BET of SSA were 2.6, 335 m^2/kg and 10800 m^2/kg respectively. The size of SSA particles ranged from 8 μm to 263 μm with an average value of 49 μm (Dhir et al., 2017). From the studies of Cyr et al. (2007) and Dhir et al. (2017), SSA was lighter than conventional Portland cement and had very large BET specific surface area. Cyr et al. (2007) pointed out that the very high BET specific surface area of SSA was due to the irregular grains of SSA and their open porosity. Chen et al. (2013) also stated that SSA had much higher porosity than cement, sand and gravel. In the research of Chen et al. (2013), the porosity of SSA from some incinerated household wastewater sludge in France was about 76% by volume.

Pan et al. (2003) studied the change in specific gravity and fineness of ground SSA after different grinding time in a ball mill. Test results are shown in Table 2.3. It was noted that, the specific gravity and BET specific surface area showed little change with grinding time, but the Blaine fineness of SSA increased significantly with grinding time in the first 60 min and remained almost constant thereafter. Pan et al. (2003) explained that within the limit of the grinding machine, SSA particles were progressively broken into finer particles in the first hour but the increase in outer surface area was relatively insignificant compared with the inner pore surface area in view of the highly porous nature of SSA. Monzó et al. (1999) studied the influences of chemical composition and fineness of SSA on the mechanical strength of mortar by comparing samples with different granulometric distributions of SSA. It was claimed that fineness might have more dominant influence than chemical composition on the chemical reactivity of SSA-containing mortars. Lin et al. (2008) also found that for small particle of SSA, the main influence factor was the particle size rather than the chemical compositions.

Table 2.3 Specific gravity and fineness of SSA after grinding

(Pan et al., 2003)

Properties / Grinding time (min)	Specific gravity	Specific surface area in Blaine (m^2/kg)	Specific surface area in BET (m^2/kg)
10	2.48	496	11588
20	2.61	780	10906
30	-	846	11774
60	2.54	975	11020
120	2.45	979	11666
180	2.67	993	11521
360	2.60	872	12487

2.3 Use of SSA as Cement Substitutions in Cement Mortar and Concrete

2.3.1 Influence of SSA on Cement Hydration

Relatively little attention has been paid to the effects of SSA on cement hydration including comparison with other SCMs in this respect. Portland cement consists of the following crystalline phases: alite ($3CaO \cdot SiO_2$ or C_3S), belite ($2CaO \cdot SiO_2$ or C_2S), tricalcium aluminate ($3CaO \cdot Al_2O_3$ or C_3A), ferrite ($4C \cdot A \cdot Fe_2O_3$ or C_4AF) and

gypsum ($CaSO_4 \cdot 2H_2O$ or CSH_2). Decades of research have shown that Portland cement hydration involves a series of complex and interdependent chemical reactions which results in the formation of C-S-H (calcium silicate hydrate) gels with a typical Ca/Si ratio of 1.5-2.2 (Puertas et al., 2011), portlandite ($Ca(OH)_2$ or CH) and ettringite ($C_6AS_3H_{32}$ or AFt). The main hydration reactions are exothermic and calorimetry data almost invariably reveals four distinctive peaks, i.e., the initial dissolution phase, the induction period, the acceleration period and the deceleration period (Bullard et al., 2011). With partial substitution of the cement by SCMs, the effects of these materials on the cement hydration process need to be examined.

From the limited calorimetry data published, Cyr et al. (2007) found that the adding SSA to mixtures would cause short delay in cement hydration and explained that this may be due to the presence of metal(loid)s in SSA and the dilution effect on cement since replacement of cement by SSA led to less thermal activation of cement. Nevertheless, the total heat evolved per gram of cement in early 96 hours increased with the content of SSA in mortars and was larger than that of the control mix. The authors attributed this phenomenon to the rapid activity of SSA in the mortar or its activation effect on cement hydration. However, their later studies showed that there was no improvement in the strength of mortar.

A study by Dyer et al. (2011) on SSA obtained from 4 sources in the UK revealed that the ashes had retardation effects on cement hydration. Furthermore, apparent secondary peaks appeared in the heat evolution curves, the magnitude of which were dependent on the proportions of SSA in the pastes. The authors attributed this phenomenon to the transformation of AFt to Al_2O_3-Fe_2O_3-mono (AFm) due to the exhaustion of sulfate in the pastes.

Chen et al. (2013) said that when mixed with cement including replacing cement in partial, the size of SSA would affect a lot the hydration process. The smaller particles of cement would react first and crystallize at the close proximity of particles during the time of curing. The smaller particles of SSA would act as binder while the bigger particles which are less reactive would act as fillers.

2.3.2 Pozzolanic Activity of SSA

There are various methods which aim at assessing the potential for pozzolanic activity of a material (see Table 2.4).

Table 2.4 Summary of common methods for assessing pozzolanic activity

Method	Principle of test and interpretation of results

EN 196-5 (2005), or Frattini test	The test is directly linked to the requirements for CEM IV cements as defined in BS EN 197-1 (2011). The blended cement, i.e., cement + SCMs, is tested directly instead of the SCM alone. 20 g of blended cement is mixed with 100 ml of deionized water in a container, which is then sealed and placed in an oven at 40°C for either 8 days or 15 days. The contents of the container are then filtered and the filtrate is tested for alkalinity and calcium concentration by chemical titration and results for $[Ca^{2+}]$ and $[OH^-]$ are plotted on the solubility curve for $Ca(OH)_2$. Any result below the solubility curve is deemed to be indicative of a pozzolanic cement.
ASTM C311, or strength activity index (SAI) test	The SAI of a material is defined as the ratio of the compressive strength of the test mortar to that of the control (pure cement) mortar at the same age. The control mortar is prepared by mixing the cement, standard sand and water at the ratio of 1 : 2.75 : 0.484 and cast in 50 mm mortar cubes. The test mortar is prepared with 20% of the cement replaced by the test material. The workability of the test mortars is kept within ±5 mm of that of the control mortar by varying the water content. A SAI greater than 75% after 7 days or 28 days infers the test material being a good pozzolan (ASTM C618, 2012).
Analysis of pastes by simultaneous	Blended cement pastes are prepared and cured under conditions identical to those for curing a control paste containing no SCM. Paste

thermogravimetric analysis (TGA) and differential thermal analysis (DTA)	specimens are ground to fine powders and dried. A small part (mg) is then placed in a special balance where both weight change and heat flow can be monitored inside a furnace under programmed conditions. $Ca(OH)_2$ content is measured by determining the above background weight loss that coincides with an endothermic peak around 400-650°C associated with the dihydroxylation of $Ca(OH)_2$ (Taylor et al., 1985 and 1985a). Results from the blended paste and the control paste are compared. A lower $Ca(OH)_2$ content in the blended paste indicates a positive pozzolanic activity of the test material. However, an apparent consumption of $Ca(OH)_2$ may be due to carbonation as well. Therefore, data should be checked for significant $CaCO_3$ formation.
Saturated lime method, or modified Frattini test	The saturated lime method is a simplified Frattini method developed by Luxan et al. (1989) and modified by Yu et al. (1999), Payá et al. (2001) and Frías et al. (2008). This method is more widely used in research studies for assessing pozzolanic activities of materials (García et al., 2008; Donatello and Cheeseman, 2010; Tironi et al., 2013; Chhaiba et al., 2018). 1 g of the test material is mixed with 75 ml of saturated lime solution, i.e., a controlled quantity of $Ca(OH)_2$, instead of cement and water used in the Frattini test. Curing of specimens is performed in an oven maintained at 40ºC for 1, 3, 7, 28 and 90 days. The Ca^{2+} is removed by reaction with the test material and at the end

	of each curing period the solution is filtered and tested for Ca^{2+} remaining in it. The loss of Ca^{2+} from the solution is the Ca^{2+} fixed by the test material. A higher fixation of Ca^{2+} indicates a greater pozzolanic activity of the test material.

It should be noted that the TGA and DTA analyses, as well as the saturated lime method are not suitable for assessing the pozzolanic activity of the SSA in this study because $Ca(OH)_2$ in the SSA cement pastes may not solely be consumed in the pozzolanic reaction and transformed into a cementitious compound. It may also be consumed by the amorphous iron phosphate in the SSA as stated by Dyer et al. (2011).

Regarding the SAI method, it was developed for use only with fly ash. Care should therefore be taken when applying this test in any evaluation of other materials as a proof of their own pozzolanic activities because other factors can also affect strength development in blended cement pastes and mortars, especially porosity, which will be influenced by any changes in water/cement (w/c) ratio or workability and consistency caused by the introduction of SCMs. The SAI test, when considered alone, may fail to provide a clear and unequivocal demonstration of the pozzolanic reaction of the test material. When assessing the potential for pozzolanic activity of a new material such as SSA from a new source, it is prudent to consider results from more test methods.

The pozzolanic activity of SSA from various sources has been measured in previous studies. Pan et al. (2003) pointed out two major disadvantages of using SSA as a mineral admixture to replace cement partially from previous researches. First, the low pozzolanic activity. Second, the high water demand of SSA-containing mortar compared with ordinary cement mortar caused difficulty in maintaining both the water/binder (w/b) ratio and workability of SSA-containing mortar simultaneously. Pan et al. (2003) found a linear relationship, as shown in Fig. 2.2, between SSA fineness and SAI, from testing mortars with 20% cement replaced by SSA of different fineness and w/b material ratio of 0.6. Accordingly, SAI value approximately increased 5% when SSA fineness increased per 100 m^2/kg. This result indicated that pozzolanic activity of SSA primarily occurred at the outer surface rather than in the pore space of SSA since the inner pores were blocked during early hydration. Although the increase of SSA fineness could effectively improve SAI values, they still fell below 100% due to lesser content of amorphous silicon oxide in SSA than that in pure cement.

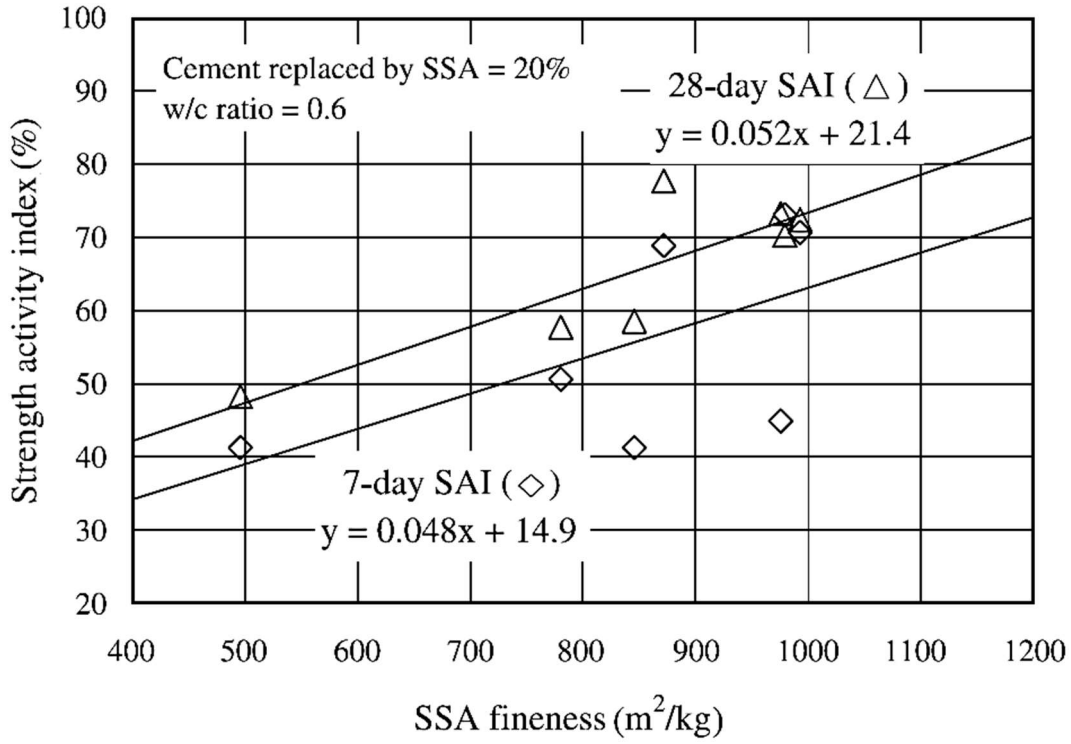

Fig. 2.2 Effect of fineness on pozzolanic activity of SSA (Pan et al., 2003)

Cyr et al. (2007) got results showing that mortars with 25% and 50% of cement replaced by SSA reached 92% and 84% at 3 months, indicating positive effect of SSA which might be related to moderate long-term pozzolanic activity due to limited content of SiO_2 and AlO_2 (Table 2.1) in SSA. In contrast, Donatello et al. (2010) concluded that SSA had no pozzolanic activity after conducting Frattini and SAI tests.

Dyer et al. (2011) considered that the reaction of SSA as a SCM should not be simply regarded as pozzolanic activity because the hydration products of SSA in combination with cement composed apparent quantities of AFm products. It was highly probable that the amorphous fraction of SSA supplied additional aluminum

and iron in the hydration reaction to form AFm. The authors compared the amorphous compositions (Al_2O_5 + Fe_2O_3) of four kinds of SSA with the magnitude of secondary peaks in the hydration heat curves and found that there was a positive relationship of the amorphous content with the secondary peak heat evolution. Through a series of simulation experiments to check the reactions amongst $FePO_4$, cement, $Ca(OH)_2$ and SSA, the authors believed that at least some proportions of aluminum and iron presented in amorphous phosphate-bearing phases in SSA indeed took part in the hydration reaction in SSA-cement pastes.

In the study by Halliday et al. (2012), the strength values decreased with more SSA added in mortar or concrete mixes, indicating limited pozzolanic activity of SSA. Tests of SAI with cement mortars containing 20% SSA showed that indices increased with time but some indices were lower than expected. The authors attributed this to the friable nature of SSA rather than the chemical compositions and believed that mechanical grinding would benefit the strength development. While indices increased with time at replacement level of 20%, indices reduced with time at replacement level of 10% SSA. The authors considered that at low replacement level, strength was mainly developed from the hydration of cement which masked the contribution of SSA.

2.3.3 Influence of SSA on Mortar Workability

Monzó et al. (2003) studied the influence of different size fractions of SSA on the workability of mortars with 15% of cement replaced by SSA by the flow table spread (FTS) method according to ASTM C109 (2013). FTS value is the average of two vertical diameters of the flow. It was found that the workability decreased as particle size decreased. Monzó et al. (2003) explained that coarse particles had lower specific surface area than fine particles and required less water for surface saturation.

Lin et al. (2008) studied the combined effect of SSA particle sizes and nano-SiO_2 on SSA-containing mortar and found that, as the particle size of SSA became smaller, the consistency of mortar became stable, and the addition of nano-SiO_2 had slight positive effect in increasing the consistency of SSA-containing mortars. Pan et al. (2003) also found that mortar workability decreased when cement was partially replaced by SSA. They further found that when the fineness of SSA increased through mechanical grinding, the workability of SSA-containing mortars increased due to the lubricant effect and morphology improvement. However, the optimal workability of SSA-containing mortars was still lower than the control mortar due to the porous and water adsorption nature of SSA. It should be noted that the finding of Pan et al. (2003) was conflicting with that of Monzó et al. (2003). More researches are needed to understand further the relationship between mortar workability and SSA fineness.

Many studies had reported that adding SSA to mortar or concrete mixes led to significantly greater water demand for keeping good workability in mixes (Cyr et al., 2007; Chen et al., 2013) due to the very great surface area and porosity of SSA taking up water. In the research of Cyr et al. (2007), when SSA replaced cement by 25% and 50%, the water content had to be increased by 17% and 34% respectively to maintain the same workability. Monzó et al. (2003) studied the influence of SSA content on the workability of the SSA-containing mortars. FTS of mortars with cement replaced by SSA in the range of 0% to 30% and containing different water contents, namely 200 ml and 225 ml were measured. It was found that increasing percentage of SSA led to a decrease in workability of mortars but the effect was proportionally less significant. Moreover, when the replacement ratio was high (30%), the workability became very low. Monzó et al. (2003) explained that this behavior was due to the irregular morphology of SSA particles and high water adsorption on SSA particle surface and in internal pores of SSA. Wang et al. (2005) stated that the high water demand during the initial mixing of SSA was due to its high calcium content.

To improve the workability of SSA-containing mortars, Monzó et al. (2003) also studied the effectiveness of adding superplasticizer to mortars with different SSA percentages. It was found that as the amount of superplasticizer increased, the

workability of the SSA-containing mortars increased. With the same superplasticizer content, the workability of mortars decreased as the content of SSA increased. Lynn et al. (2015) reported that the water absorption of SSA was ranged from 8% to 20%. Although the reduction in workability can be compensated by adding superplasticizers, this incurs additional costs.

2.3.4 Influence of SSA on Compressive and Flexural Strength

The majority of data published in this regard focused solely on measurement of strength. Most literatures reported that mortar or concrete of normal strength could be produced with small amount of cement replaced by SSA. However, information on how SSA affects the properties of cement mortars is limited given the modest pozzolanic activities of most SSA. For this reason, results will only be briefly summarized for the purpose of putting them in context.

Monzó et al. (1999) found that replacing cement with SSA up to 30% did not reduce the compressive and flexural strength of mortars cured with 40^{o}C water and suggested that this was due to the pozzolanic properties of SSA.

Pinarli (2000) conducted a study on the use of SSA to substitute cement in concrete production and found that the compressive strength of concrete with up to 10% of

cement replaced by SSA was not adversely affected although the setting times were longer with increasing SSA content.

SSA can be used to replace ordinary Portland cement (OPC) to up to 30% in cement mortar and 10% in high performance concrete without lowering the 28-day compressive strength (Fontes et al., 2004).

Cyr et al. (2007) tested the compressive strength and flexural strength of mortars with 25% and 50% of cement replaced by SSA. Superplasticizer was added to the mortars to maintain w/b material ratio of 0.5. Test results showed that SSA caused reduction in both strength compared to reference mortars, but such reductions became less over time.

Chen et al. (2013) substituted cement by SSA at different ratios, from 0%, 10%, 20%, 25% to 30%, to produce mortar, and found that with increasing amount of SSA in the mixes, the compressive and flexural strength decreased more. However, at a low replacement ratio of 10% the compressive strength of the mortar monoliths is similar to that of the blank.

Ing et al. (2016) also reported similar or higher strength values in mortars containing up to 10% SSA in the binder compared to the blank.

Particle size of SSA is another factor affecting the development of strength in SSA-containing mortars. Lin et al. (2008) compared the compressive strength of mortars with 20% of cement replaced by SSA of 1 μm, 10 μm, and 75 μm. Test results showed that smaller sizes of SSA gave higher compressive strengths at all curing times. Lin et al. (2008) explained that the larger specific surface areas of small SSA particles provided larger reaction areas and allowed greater pozzolanic activity resulting in higher compressive strength of the mortars.

Chen et al. (2013) in their study noted that the characteristics of SSA in terms of particle size and elemental composition fell within an intermediate range between cement and sand. They considered that SSA added to mortar and concrete mixes possibly acted as substitutes of both cement and sand. From strength consideration of concrete mixes, they found that the most appropriate ratios were 10% substitution of cement and 2% substitution of sand because the level of strength to be confidently achieved could satisfy the technical requirements for residential and light commercial building.

It should be noted that, although high porosity is a primary characteristic of SSA as reported in many studies (Lin and Weng, 2001; Chiou et al., 2006; Smol et al., 2015),

the relationship between the pore structure and mechanical properties of the paste has not been reported.

Dhir et al. (2017) also expressed in their book that most studies on porosity of SSA-containing mortar or concrete actually involved different types of water absorption tests but not in-depth microstructure analysis.

2.4 Use of SSA as Cement Substitution in Concrete Blocks

Little effort has been devoted to the research of using SSA as a cement substitute in the production of precast concrete blocks. Given the difficulties in controlling the w/b ratio and workability in cement mortars and concrete incorporating SSA, the application of SSA in making precast concrete blocks may be more suitable for the recycling of the waste because only a small quantity of water is needed to give a dry but cohesive mix suitable for the production of concrete blocks by the compression method using moulds (Kou et al., 2012; Lam et al., 2007; Poon et al., 2002).

As revealed from limited literature in this subject, SSA was found to have minor effect on the density of precast concrete blocks. Reduced density and increased density were reported by Pérez-Carrión et al. (2014) and Baeza-Brotons et al. (2014) respectively with increasing SSA content in the binder up to 20%.

The water absorption of concrete blocks containing SSA was lower than that of concrete blocks without SSA (Baeza-Brotons et al., 2014) but the capillary absorption values of SSA blocks were comparable to or less than those of the SSA free blocks (Baeza-Brotons et al., 2014; Pérez-Carrión et al., 2014; Nagarjuna, 2015).

Concrete blocks incorporating SSA to replace up to 20% OPC gave slightly lower strength values compared to the SSA free control blocks (Baeza-Brotons et al., 2014; Pérez-Carrión et al., 2014; Nagarjuna, 2015).

Dhir et al. (2017) in their book advised that these losses in strength were manageable. The absolute losses in mean strength from the SSA free control blocks to the blocks containing 20% SSA in the binder were 0.3 MPa and 3.5 MPa respectively as reported by Pérez-Carrión et al. (2014) and Baeza-Brotons et al. (2014). Dhir et al. (2017) recommended the use of SSA in concrete blocks in suitable circumstances considering the appropriate strength requirements. However, these previous studies did not assess the durability performance of the blocks such as drying shrinkage and alkali-silica expansion if reactive aggregates were used. Besides, data on leachability of metal(loid)s from concrete blocks containing SSA was also absent.

On the other hand, aggregates are major constituents in making concrete blocks. Normally, NA such as river sand and crushed stones are used. Studies were conducted in the past on using different types of wastes such as C&D aggregates and GC to partially or completely replace NA for making concrete blocks. Schuur (2000) showed that the mechanical properties of new bricks made entirely from crushed clay brick waste could be comparable or even better than those made with natural sand. Poon and Chan (2006) also showed that the incorporation of demolition aggregates had minor effects on the compressive strength of the blocks. Besides, Turgut and Yahlizade (2009) reported that 20% substitution of fine NA by GC gave comparable compressive strength with the control blocks. Ling and Poon (2014) reported that crushed cathode ray tube glass could be used as alternative fine aggregates to produce good quality concrete blocks with compressive strength greater than 45 MPa. In Hong Kong, it has been demonstrated that concrete blocks made with C&D and GC aggregates comply with local standards for civil engineering works and are being commercialized (Ling et al., 2013). Highways Authority already requires precast concrete paving units to incorporate C&D and GC aggregates to encourage recycling of these two types of wastes (Highways Department, 2014).

2.5 Use of SSA as an Aluminosilicate Precursor for Synthesizing Geopolymers

The knowledge on geopolymerization of SSA or its effects on other geopolymers remain limited. SSA is a potential source material of geopolymer by composition. It is rich in SiO_2, Al_2O_3 and CaO, which are the most active compounds for geopolymerization.

From the limited literature available, one study in the production of geopolymer concrete at ambient temperature using PFA and SSA as precursors and NaOH and Na_2SiO_3 as alkaline activators revealed that mechanical strength decreased with more incorporation of SSA (Paulnath et al., 2016).

Another study on the geopolymerization of PFA and SSA with NaOH and Na_2SiO_3 under 80^{o}C steam reported that SSA could improve mechanical strength of PFA-based geopolymer pastes with the best result attained at a ratio of 1 part SSA to 3 parts PFA (Yamaguchi and Ikeda, 2010).

For MK, it was shown in studies that SSA made little contribution to geopolymerization when blended with MK, particularly at ambient temperature (Istuque et al., 2016).

On the other hand, more encouraging results were obtained in two studies which showed improved geopolymerization of GGBS with SSA added and NaOH as

alkaline activator. The best result was achieved at a ratio of 1 part SSA to 4 parts GGBS (Akasaki et al., 2015) or 7 parts SSA mixed with 2 parts quick lime and 1 part GGBS (Chakraborty et al., 2017). This result supports the use of SSA for partial replacement of GGBS in producing geopolymers. Drying shrinkage of SSA based mortar was also evaluated in the study (Chakraborty et al., 2017). It was reported that the drying shrinkage of mortars increased with the addition of NaOH and quick lime but such an effect could be counterbalanced by the use of appropriate amounts of GGBS.

2.6 Summary

It is clear from the literature that with SiO_2, Al_2O_3 and CaO as the main components, there is a potential to use SSA as a SCM to partially replace cement or as an aluminosilicate precursor for synthesizing geopolymers. Leaching tests should be performed because SSA is obtained from incineration of sewage sludge in which metal(loid)s may be accumulated.

Previous studies revealed that SSA has apparent effects on two major properties of fresh mortar and concrete, namely, cement hydration and workability. It is noted that the amount and composition of amorphous phase CaO, Al_2O_3 and SiO_2 in SSA influenced the hydration reaction in SSA-containing mortar and concrete. Generally,

increasing percentage of SSA led to decreasing mortar workability, but the effect of SSA fineness on workability is inconsistent among some studies possibly due to different means of getting the finer fractions for testing.

Most studies reported a modest change in compressive strength of mortar and concrete when SSA was used to replace cement up to 10%. In higher replacement ratio, strength decreased as SSA content increased. Furthermore, the size of SSA particles may also affect its properties, finer SSA would give higher strength than coarser SSA. The application of SSA using dry-mixed compression method may be more suitable for the recycling of the waste given the difficulties in controlling the w/b ratio and workability in cement mortars and concrete incorporating SSA.

In order to understand better how porous SSA would affect cement hydration and strength development in mortar and concrete, the pore structures of hydrating cement pastes should be studied.

For SSA to be produced from the new incinerator in Hong Kong, its characteristics may be quite different from those of SSA used in the literature due to different incineration technologies and sewage treatment process adopted in Hong Kong. How the chemical composition, morphology and fineness of local SSA affect the cement hydration, workability and more importantly the compressive strength need to be

evaluated through in depth studies. Although there are very few pollution industries operating in Hong Kong leaving very low content of metal(loid)s in foul water, vigorous tests on leaching from SSA-containing products would still be necessary to alleviate environmental concern about potential leaching of metal(loid)s coming from SSA.

CHAPTER 3 – METHODOLOGY

3.1 Introduction

The methodology adopted in this study was through series of experiments with appropriate scientific tests to evaluate the benefits of different applications of the SSA as construction materials and to gain knowledge of material transformation in such applications. Section 3.2 describes the experimental work carried out in connection with using SSA as a SCM to produce cement pastes and mortars. Section 3.3 describes the experimental work undertaken related to the application of SSA as a SCM alone and in combination with recycled aggregates to produce concrete blocks. Section 3.4 describes the experimental work associated with the use of SSA as an aluminosilicate precursor in combination with GGBS to produce geopolymer pastes under the effects of different alkali content and modulus.

3.2 Preparation and Investigation of Cement Pastes and Mortars

3.2.1 Materials

A certain amount of OPC was replaced by PFA, SSA or FSSA respectively to produce the cement paste or mortar. The chemical and physical properties of OPC, PFA, SSA

and FSSA are summarized in Table 3.1. The method for testing specific gravity follows BS EN 196-6 : 2010. Specific gravity is the ratio of the density of a material to the density of water. The density is determined by pycnometer using the kerosene displacement method. For the X-ray fluorescence (XRF), laser size diffraction and nitrogen BET tests, samples were sent to outside laboratories for testing. The major oxide components in the SSA and FSSA studied were SiO_2, Fe_2O_3, Al_2O_3 and CaO. The contents of SiO_2 and Al_2O_3 were lower than the respective mean values of 32.8% and 14.2% reported by Dhir et al. (2017). However, the contents of Fe_2O_3 in the SSA and FSSA were much higher than the mean value of 11.3% reported due to the use of ferric chloride in the primary treatment of sewage in Hong Kong. There were high levels of phosphate in the SSA and FSSA. Phosphate comes from many sources including food, drinks, detergents, polishing agents in toothpaste, bath solutions, animal wastes and fermented plants. It can also be noted from Table 3.1 that the specific gravity, fineness and specific surface area of SSA increased with grinding. The specific gravities of OPC, PFA, SSA and FSSA were 3.09, 2.51, 2.33 and 2.74 respectively. The very high BET surface areas of SSA and FSSA were due to their irregular grain shapes and open porosities as revealed below.

The particle size distribution curves of OPC, PFA, SSA and FSSA are shown in Fig. 3.1. From the results, it can be seen that SSA was much coarser than PFA but FSSA was much finer than PFA.

The morphologies of PFA, SSA and FSSA particles are shown in Fig. 3.2. As compared to PFA which was mostly spherical in shape with a smooth surface, the original SSA particles were irregular in shape and contained many isolated and open pores. After grinding, the irregular grains of SSA were broken into smoother particles with fewer pores observed.

To identify the crystalline components in SSA, only FSSA was tested. Fig. 3.3 and Table 3.2 show the results of mineralogical and semi-quantitative X-ray diffraction (QXRD) analyses respectively. It can be seen from Fig. 3.3 that the dominant crystalline components of FSSA (SSA) were quartz (SiO_2, Powder Diffraction File, i.e., PDF #03-065-0466), hematite (Fe_2O_3, PDF #01-085-0987), magnetite (Fe_3O_4, PDF #01-075-0449), leucite ($KAlSi_2O_6$, PDF #01-075-0550) and albite ($NaAlSi_3O_8$, PDF #01-089-6428). Fig. 3.3 also reveals that PFA contained crystalline phases like quartz (SiO_2), hematite (Fe_2O_3), magnetite (Fe_3O_4) and mullite ($3Al_2O_3{\cdot}2SiO_2$, PDF #01-085-1460). The results of semi-quantitative analyses shown in Table 3.2 reveal that FSSA (SSA) contained a lower proportion of other non-crystalline (amorphous and semi-crystalline) phases compared to PFA (53.11% vs. 82.97%).

Table 3.1 Oxide compositions and physical properties of the tested materials

Oxide (wt. %)	OPC	PFA	SSA	FSSA	Test method
MgO	1.47	3.97	3.15	3.16	
Al_2O_3	3.77	18.9	12.2	12.26	
SiO_2	19.3	44.2	27.7	27.91	
CaO	63.8	11.87	10.4	10.47	
TiO_2	0.26	1.05	0.52	0.52	
Fe_2O_3	3.08	11.34	18.2	18.32	XRF
SO_3	5.38	1.76	6.10	6.13	
MnO	0.06	0.24	0.24	0.24	
K_2O	0.69	1.65	1.88	1.89	
Na_2O		1.32	7.28	7.32	
P_2O_5		0.41	9.72	9.77	
LOI	2.08	3.28	1.97	2.01	
Specific gravity	3.09	2.51	2.33	2.74	BS EN 196-6 : 2010
Mean diameter (μm)	19	38	60	6	Laser size diffraction
BET (m^2/kg)	533	559	1329	17366	Nitrogen BET

Note: Only one large batch of SSA was collected to do the research. There were no material changes in the nature of SSA ever time.

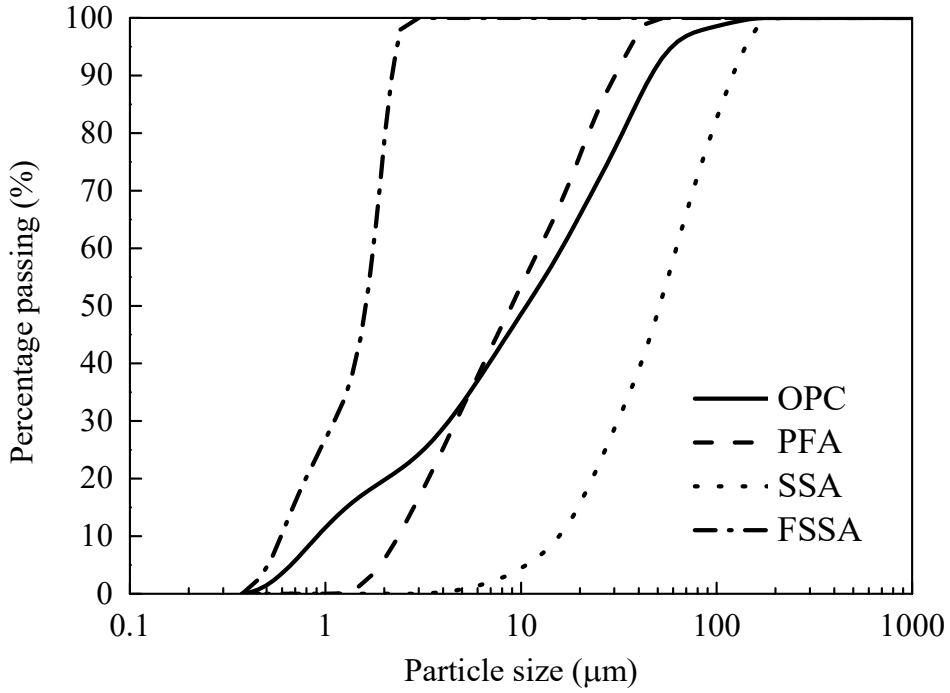

Fig. 3.1. Particle size distributions of the tested materials

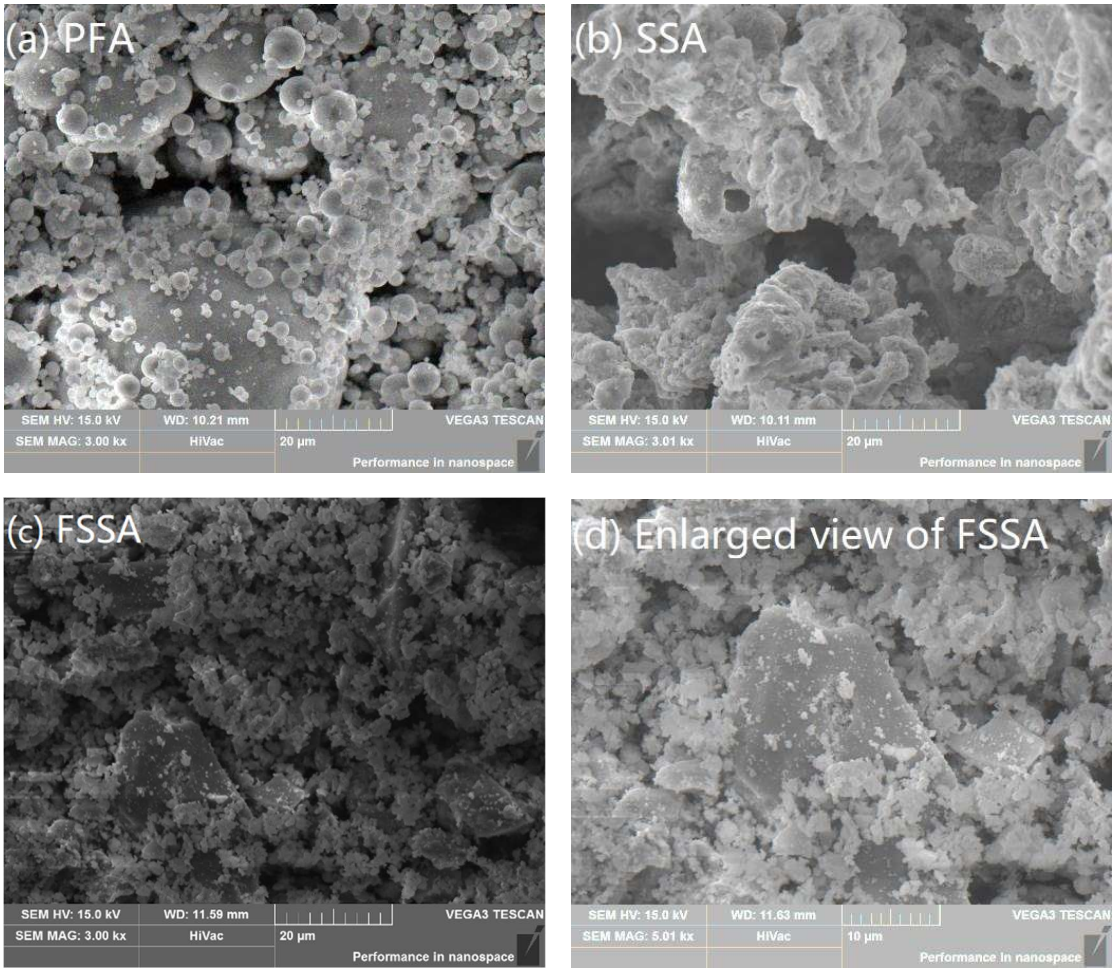

Fig. 3.2. Images of PFA, SSA and FSSA

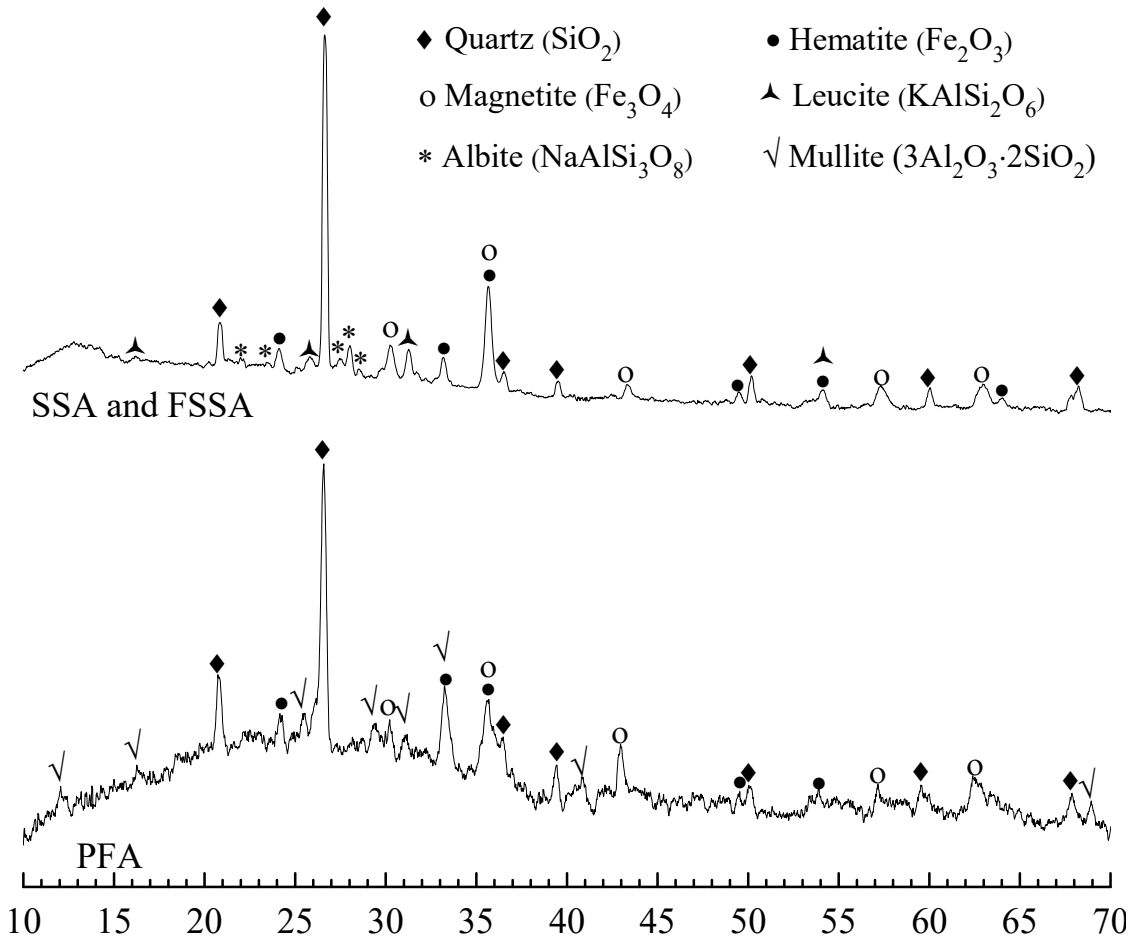

Fig. 3.3. Mineralogy of PFA and FSSA (SSA)

Table 3.2 Mineralogical compositions of PFA and FSSA (SSA) (wt. %)

	Quartz	Hematite	Magnetite	Leucite	Albite	Mullite	Others
PFA	7.26	1.38	1.68	-	-	6.71	82.97
SSA and FSSA	24.03	1.04	12.20	2.10	7.52	-	53.11

3.2.2 Proportioning, Mixing and Curing

Paste and mortar specimens were prepared in this study. The OPC and PFA were commercially available in Hong Kong. The SSA was provided by the sludge incinerator in Hong Kong. The FSSA was obtained by further grinding SSA in a laboratory ball mill for three hours. The w/b ratio was kept at 0.484 in all the mixes. Two types of paste specimens were prepared. One type was pure OPC, PFA, SSA or FSSA paste. Another type was OPC blended with PFA, SSA or FSSA which were used to replace 5%, 10% or 20% of OPC respectively. For the mortar mixes, standard sand with particle sizes ranging from 0.5 mm to 1 mm was used as the aggregate. An ASTM C109 (2013) mortar made with OPC, standard sand and water at a ratio of 1 : 2.75 : 0.484 was prepared as the control mix, which gave a mini slump cone flow value of around 175 mm on average. To prepare the test mortars, PFA, SSA or FSSA was used separately to replace 5%, 10% and 20% by weight of the OPC. A superplasticizer ADVA 109 (GRACE Construction Products, Hong Kong) with a specific gravity of 1.045, containing no chloride additives was added to the test mortars. The content of superplasticizer was around 0.28% by mass of the binder in the cement mortar containing SSA or FSSA. A vibrating table was used to compact the mortars. The mortars for testing the workability changes of the fresh mixes were prepared using the same mix proportions without the addition of the superplasticizer. A summary of the mix proportions is provided in Table 3.3.

The mixing of the pastes and mortar samples followed the same procedure: first, the binder materials together with sand, if required, were mixed for 2 mins at a low speed. Next, water with or without superplasticizer was added and the mixing was continued for 1 min. Afterwards, the bottom of the mixer was scraped manually with a steel trowel to avoid materials sticking to the bottom. Finally, the mixing was continued at a higher speed for 2 more mins. The freshly mixed materials were then cast into steel moulds and vibrated for 1 min to remove air bubbles. After troweling the surface, the moulds were covered with a polyethylene sheet to prevent moisture loss.

Table 3.3 Mix proportions of the paste and mortar mixes

Type	Material	Sample ID				Test
Paste	Binder	Control	Pure	1	0.95 OPC + 0.05 PFA/SSA/FSSA	Hydration heat Pore structure Crystallization Morphology
					0.90 OPC + 0.10 PFA/SSA/FSSA	
					0.80 OPC + 0.20 PFA/SSA/FSSA	
	Water	0.484				
Mortar	Binder	Control		1	0.95 OPC + 0.05 PFA/SSA/FSSA	Workability Strength Drying shrinkage
					0.90 OPC + 0.10 PFA/SSA/FSSA	
					0.80 OPC + 0.20 PFA/SSA/FSSA	
	Water	0.484				
	Sand	2.75				

Specimens for flexural and compressive strength tests were cast in 40 × 40 × 160 mm prismatic moulds. For microstructure analyses, 50 × 50 × 50 mm cube moulds were used. After 1 day, the specimens were demoulded and placed in a 23°C water tank until testing. Other 25 × 25 × 285 mm prismatic moulds were used for preparation of the specimens for testing drying shrinkage. The demoulded specimens were immersed in a 23°C water tank for 2 days prior to measuring the initial length. The specimens were then placed in an environmental chamber at 23 ± 2°C and 50 ± 5% relative humidity to monitor length changes.

3.2.3 Experimental Methods

The oxide compositions were analyzed by a Rigaku Supermini200-type XRF spectrometer. Tests were carried out on pressed powder specimens with a Pd X-ray source working at 4 mA and 50 kV.

The particle size distributions of the powder materials were tested on a Malvern Instrument's Spraytec laser diffraction system with a measuring range from 0.020 μm to 2 mm.

The morphologies and element compositions of gold-coated specimens were examined using scanning electron microscopy (SEM) and energy dispersive X-ray (EDX) spectroscopy (TESCAN VEGA3).

The X-ray diffraction (XRD) test requires grinding the specimens to a very fine form. To conduct the XRD test on the blended cement paste, pellet specimens were ground to form powder specimens in a ceramic bowl. The XRD apparatus used was a Rigaku Smartlab 9kW diffractometer with 20 mA and 40 kV, Kb-filtered CuKa radiation. An angular range of 10-70^{o} 2θ in a step interval of 0.01^{o} and a scan speed of 1.2^{o}/min was adopted throughout the tests. The peaks were identified by PDXL Rigaku

software using a XRD pattern database International Centre for Diffraction Data PDF (ICDD PDF).

Semi-quantitative QXRD tests for quantification of the crystalline and amorphous phases in the specimens were performed using the Rietveld refinement method. Twenty percent by weight of corundum was added to each specimen as the internal standard for conducting the quantification analysis. The specimens mixed with corundum was ground in an agate mortar to pass through a 45 μm sieve to obtain optimal particle dispersion and fineness.

The procedures for conducting the Isothermal Conduction Calorimetry (ICC) test were based on ASTM C1679-09 (2009). ICC tests were conducted by a model I-Cal 4000 calorimeter manufactured by Calmetrix Inc. The heat evolution was measured under a constant temperature set at 21°C. Since most of the heat was generated at the early stages and the peak evolution rate normally occurred within 24 hours, the hydration heat was continuously monitored for a period of 48 hours. Each reported result is the average of measurements from two specimens.

The pozzolanic activities of PFA, SSA and FSSA were assessed by the Frattini test. The test was carried out according to the method specified in EN 196-5 (2005). The control specimen was prepared with 100% OPC mixed with 100 ml of deionized

water. The tested specimens were made of 80% OPC and 20% PFA, SSA or FSSA by mass. The specimens were then stored in sealed containers at 40°C for 8 days. The concentrations of [Ca^{2+}] and [OH^-] in the filtered solutions were measured and compared with the saturation isotherm of calcium hydroxide at the same temperature. Two specimens were tested for each material.

The FTS method, which followed BS EN 1015 (1999), was used to study the influence of PFA, SSA or FSSA on the workability of the mortar mixes. No superplasticizer was added to the mix in this test.

For the specimens prepared for the strength tests, superplasticizer was added in order to achieve similar workability while keeping the same w/b ratio in different mixes. Three-point bending tests for flexural strength were carried out in conformity with ASTM C348-97 (2002). The broken portions in the flexural test were used to obtain the equivalent compressive strength according to ASTM C349 (2008). The compressive strength tests were conducted using a Denison compression machine which applied load at a rate of 0.6 MPa/sec. Each reported value was the average of measurements from three specimens.

The paste specimens were prepared for performing the mercury intrusion porosimetry (MIP) tests according to BS 7591 Part 1 (1992). After reaching the

required curing ages, the specimens were crushed into small pellets of about 2.36 mm in diameter and soaked in acetone for one week to stop the hydration reaction followed by one further week of dehydration by changing to a new portion of acetone. The solvents were decanted and the pellet specimens were dried in a vacuum oven at 60°C until the time for measurement using a Micromeritics AutoPore IV 9500 equipment with a measuring pressure ranging from 0.01 to 207 MPa. With a setting of contact angle of 140° (Day and Marsh, 1988; Taylor, 1997) and a constant surface tension of mercury of 485 dynes/cm (Taylor, 1997), the MIP test could measure the pore diameter of the paste specimens ranging from about 0.007 to 144 μm. The result was the mean of two measurements.

The standard test method ASTM C596-01 (2009) was used to determine the drying shrinkage of the cement mortar with different PFA, SSA or FSSA contents. The initial lengths of bar specimens were measured using the length comparator after the specimens were water cured for two days after demoulding. The specimens were then transferred to a drying chamber (23 ± 2°C and 50 ± 5% relative humidity). Further measurements were made at 1, 4, 7, 28, 56, 90 and 112 days. The reported length change was the average of measurements from two specimens.

3.3 Preparation and Investigation of Concrete Blocks

3.3.1 Materials

The binder materials used in this part of the study included OPC, PFA, SSA and FSSA. Their chemical and physical properties have been reported in section 3.2.1. Table 3.4 gives the total and leachable metal(loid) concentrations in the FSSA (SSA). It shows that the FSSA (SSA) contained some metal(loid)s with varying concentrations. The total concentrations of Zn and Cu were rather high, followed by Sr, Cr and Ba. Similar results were also reported in previous studies (Franz, 2008; Xu et al., 2012). However, the amounts of different metal(loid)s that could leach out by the Toxicity Characteristic Leaching Procedure (TCLP) test were limited. The ash can be considered as a non-hazardous waste.

All the aggregates used were smaller than 5 mm. The natural aggregate (NA) used was a crushed granite. The recycled C&D aggregates were derived from demolition of buildings and mainly comprised crushed concrete rubbles. The glass cullet (GC) was obtained from crushing clean mix-coloured post-consumer beverage bottles. Both the recycled C&D aggregates and GC were provided by a waste recycling company in Hong Kong.

The physical properties of the three types of aggregates are shown in Table 3.5. It can be seen that the density of the natural granite aggregates was higher than those

of recycled aggregates and GC. The water absorptivity of recycled aggregates was very much higher than that of NA but the water absorptivity of GC was about zero. The fineness modulus of each aggregates was determined according to ASTM C33/C33M (2016). All the moduli of the aggregates fell within the ASTM limiting range from 2.3 to 3.1 for concrete fine aggregates. The grading curves of all the aggregates lay within the grading limits for fine aggregates recommended in ASTM C33/C33M (2016) as shown in Fig. 3.4.

Table 3.4 Total metal(loid) contents in FSSA (SSA) and TCLP leaching concentrations

Metal(loid)	Total content (mg/kg)	Leachate by TCLP (mg/L)	TCLP limit (mg/L)
Sb	3.6	0.0065	–
As	12.4	0.052	5
Ba	172.8	0.035	100
Cd	< DL	0.0165	1
Cr	185.2	< DL	5
Cu	1062	2.46	–
Pb	67.6	0.036	5
Ni	134.8	0.0885	–
Co	2.8	0.005	–
Se	25.6	0.122	1
Sr	428.8	4.012	–
Ag	1.6	< DL	5
Zn	1755.2	2.601	–

DL: detection limit.

Table 3.5 Properties of aggregates

Properties	NA	C&D aggregates	GC
Saturated-surface-dry density (kg/m^3)	2620	2310	2500
Water absorption (%)	1.25	10.50	0
Fineness modulus	2.91	2.70	2.77

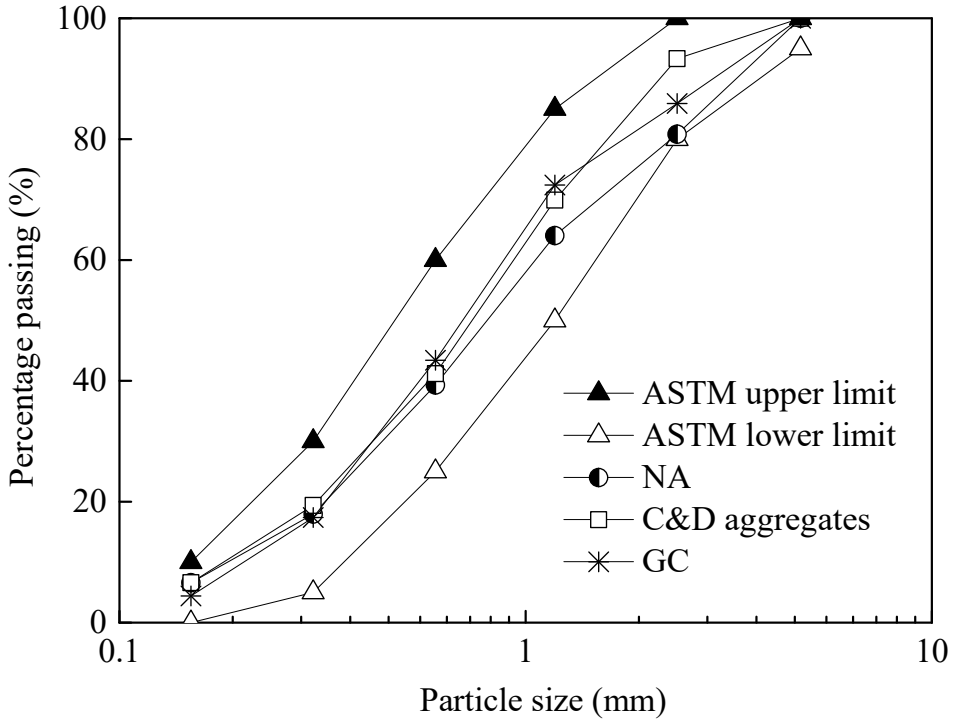

Fig. 3.4. Particle size distributions of aggregates

3.3.2 Proportioning, Mixing and Curing

A series of tests were conducted to determine the properties of the blocks with different constituents of waste materials. The control mix was made with OPC and NA. Recycled aggregates derived from C&D waste and crushed beverage GC were incorporated separately for replacing NA. SSA was used to partially replace cement as a binder. FSSA obtained from grinding SSA and PFA were also used at the same replacement levels for comparison of performance. The concrete block specimens were cast by a dry-mixed method (Lee et al., 2013; Ling and Poon, 2014). The w/b ratio was not specified using this method. The aggregates/binder ratio was fixed at 3. For assessing the effects of recycled C&D aggregates on properties of the concrete blocks, the composition of the binder was fixed at 80% OPC and 20% SSA. The recycled aggregate blocks contained either 20% or 50% C&D aggregates as replacement of NA. For blocks made with recycled GC to replace part of NA, either PFA, SSA or FSSA was added to replace 10% or 20% by weight of the OPC.

In the dry-mixed method, the mixes were prepared with just sufficient amount of water to achieve cohesion but with no workability. In this moisture state, no excess water would be squeezed out from the specimen during the moulding process. Binder and aggregates were first mixed for 3 min in a laboratory mechanical mixer. Afterwards, water was added and the mixture was further mixed for another 3 min. The fresh concrete with zero slump value was then placed into steel moulds. The blocks for the determination of hardened density, water absorption and compressive

strength were cast in cylindrical steel moulds with an internal diameter of 50 mm and a height of 50 mm while prismatic specimens with dimensions of 25 mm by 25 mm by 285 mm were prepared for measuring the dimension changes due to drying shrinkage and alkali-silica expansion. After manual casting, a compression force of 60 kN was applied for 30 seconds to compact the materials in the mould. The dry-mixed casting method allows instant demoulding of the specimens for highly efficient production. After one day of air curing, the specimens for the determination of hardened density, water absorption and compressive strength were cured in water at temperature of 23 ± 3 °C until the day of testing.

3.3.3 Experimental Methods

The experimental methods for conducting the XRF, laser size diffraction, SEM, XRD and QXRD of the materials and concrete blocks were the same as the aforementioned in section 3.2.3.

To measure the total concentration of metal(loid)s in the FSSA, i.e., SSA, the aqua regia strong acid digestion technique following BS EN 13657 (2002) was used. According to the Environmental Protection Agency (EPA)'s TCLP protocol EPA Method 1311 (1990), an acetic acid solution with a pH of 2.88 was used to extract metal(loid)s from both FSSA as well as crushed fragments from cast blocks

containing FSSA at a liquid to solid ratio of 20 in a rotary tumbler for 18 hrs. The TCLP method was developed to simulate scenarios of landfilling and to estimate the worst-case leaching conditions on disintegrated landfill wastes due to prolonged aging effects (Li et al., 2017). The concentrations of metal(loid)s were determined by using an inductively coupled plasma-atomic emission spectrometry (ICP-AES, Perkin Elmer Optima 3300DV). The results given are the averages of two measurements.

The pozzolanic activities of the PFA, SSA and FSSA were assessed by the Frattini test and the SAI test. The procedures of the tests are summarized in Table 2.4. The FTS method (BS EN 1015, 1999) was used to test the workability of different mortars. The FTS tests were conducted on mortar cubes of 50 mm. The control mortar was prepared with 100% OPC at a w/b ratio of 0.484 and an aggregates/binder ratio of 2.75. Standard sand with particle sizes ranging from 0.5 mm to 1 mm were used as the aggregates. The tested specimens were prepared with PFA, SSA or FSSA replacing up to 20% of OPC. The w/b ratio was maintained at 0.484 without adding superplasticizer.

The densities at saturated surface dry condition of the aggregates and the cylindrical block specimens at the age of 28 days were determined according to BS 812 (1995) for aggregates and BS 1881-114 (1983) for hardened concretes respectively. The

densities of the aggregates and blocks are the ratios of their weights at saturated surface dry condition to the weights of equal volumes of water. The reported results were the average values of three specimens.

The compressive strength values of the cylindrical block specimens were determined using a common universal testing machine with a maximum capacity of 3000 kN. A loading rate of 0.6 MPa/sec was applied to the block specimens. Three specimens of each mix were tested to give average results.

The water absorption of different aggregates and the cylindrical block specimens made with these aggregates were determined in accordance with BS 812 (1995) and AS/NZS 4456 (2003) respectively. In both tests, the weights of the specimens after wiped dry on their surface and the weights of the same specimens after oven dried were compared. The water absorption value was the amount of water absorbed from the oven dry state to the saturated surface dry state, expressed as a weight percentage of the oven dry state. Each result presented was the average value of three specimens.

The drying shrinkage tests were conducted following the procedures in BS 6073 (1981). According to the standard, 285 mm long bar specimens were first wrapped by plastic films to prevent loss of moisture during curing at room temperature and then placed in a drying chamber with the temperature controlled at 23 ± 2 ^{o}C and the

relative humidity controlled at 50 ± 5%. The percentage changes in lengths of the specimens after the drying process were checked regularly. Each result was the average of two specimens. This method for evaluating the drying shrinkage of dry-mixed specimens was reported in previous studies (Zhan and Poon, 2015; Xuan et al., 2016).

Alkali silica reaction (ASR) is the reaction between the alkaline pore solution in the cement matrix and the reactive silica in the aggregates. The product of this chemical reaction can cause deleterious cracking in the hardened concrete in the presence of moisture. It is a concern in mixing GC with cement because glass contains reactive silica. For assessing this potential problem, an accelerated ASR test was carried out on bar specimens in accordance with ASTM C1567 (2013). GC were used as the only fine aggregates in the bar specimens. The binder in the control bar was pure OPC while the binders in the test bars were OPC blended with PFA, SSA or FSSA. The bar specimens were demoulded 24 hours after casting followed by immersing in a water tank at about 80^{o}C for another 24 hours. The initial lengths of the bar specimens were then measured using a length comparator. The specimens were then transferred in a 1 M NaOH solution at about 80^{o}C and their lengths were measured periodically for 14 days. Two specimens for each mix were tested to give an average result. Expansion of less than 0.1% at the end of 14 days indicates insignificant ASR.

3.4 Preparation and Investigation of Geopolymer Pastes

3.4.1 Materials

The GGBS precursor was obtained commercially and the SSA precursor was directly collected from the sewage sludge incinerator in Hong Kong. GGBS and SSA were analyzed for oxide compositions, particle size distribution, mineralogy and morphology using XRF, laser size diffraction, XRD and SEM respectively. The oxide compositions of GGBS, SSA and mixed solids are shown in Table 3.6. The mixed solids were prepared by mixing GGBS and SSA on a 1 to 1 basis by mass. A large amount of the SSA was used to confirm the function of the SSA in the geopolymerization process as well as to maximize the recycling of the waste. CaO, SiO_2 and Al_2O_3 were the most abundant components presented in GGBS. Fig. 3.5 shows the particle size distributions of GGBS, SSA and the mixed solids. From the results, it can be seen that the GGBS was finer than the SSA. The particle size distribution of the GGBS was ranged from 0.869 μm to 33 μm and that of the SSA was ranged from 2.92 μm to 194.2 μm. The mixed solids had a continuous non-homogeneous grading.

Table 3.6 Oxide compositions of GGBS, SSA and mixed solids

Oxide (wt. %)	GGBS	SSA	Mixed solids
MgO	7.32	3.15	5.65
Al_2O_3	14.22	12.20	13.71
SiO_2	34.78	27.78	30.88
CaO	38.38	10.42	24.44
TiO_2	0.71	0.52	0.60
Fe_2O_3	0.27	18.23	9.75
SO_3	2.86	6.10	4.08
MnO	0.37	0.24	0.33
K_2O	0.77	1.88	1.23
Na_2O	-	7.28	3.24
P_2O_5	-	9.72	5.06
LOI	0.13	2.48	1.00

Mixed solids: mixture of GGBS and SSA in equal weight

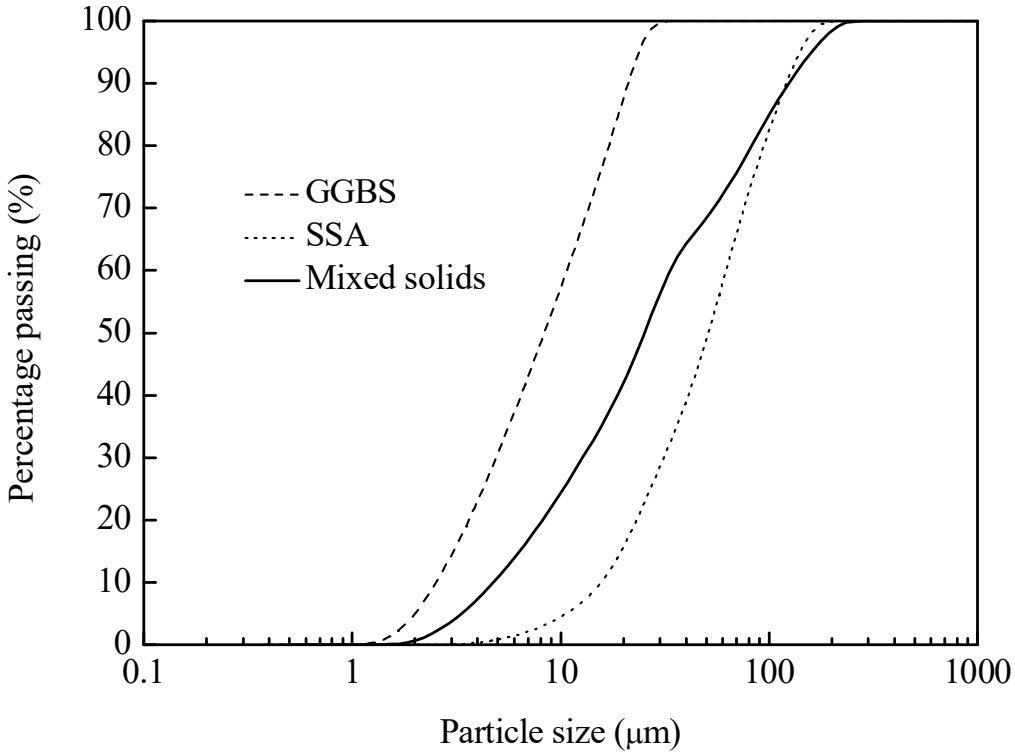

Fig. 3.5. Particle size distributions of GGBS, SSA and mixed solids

Mixture of NaOH and water glass i.e. Na_2SiO_3 was used as an activator. NaOH with purity of 98% in pellet form and Na_2SiO_3 comprising 28.3% SiO_2, 8.6% Na_2O and 58.4% water by weight were purchased commercially. The NaOH solution was prepared by dissolving NaOH pellets in water. The solution was stirred for at least 10 mins to ensure all the pellets were dissolved. After cooling, the NaOH solution was mixed thoroughly with Na_2SiO_3 in prescribed proportions to prepare the alkaline solution.

3.4.2 Proportioning, Mixing and Curing

The mix proportions of specimens are shown in Table 3.7. Pastes were made by mixing the mixed solids with the alkaline solutions. The alkaline solutions were prepared to achieve different weight percentages of Na_2O to the mixed solids (3.5%, 4.0% and 4.5%) and moduli (0.60, 0.95 and 1.30). The modulus is the SiO_2/Na_2O molar ratio in a mixed alkaline solution. The Na_2O in the solution included the Na_2O in both the NaOH and Na_2SiO_3. By applying the dry-mixed method to prepare the specimens, only a small amount of water (water/mixed solids ratio of 0.2) was required to produce a paste with enough consistency but with no workability (zero slump). The water content included water in the Na_2SiO_3 and additional water added to the mixture.

The geopolymer pastes were prepared using the dry-mixed compression method. The GGBS and SSA powder were placed in a laboratory mechanical mixer and mixed for 5 mins. The alkaline solution was then added and the mixture was further mixed for another 5 mins. All the mixes achieved similar cohesion but with no workability. The specimens to be used for the determination of compressive strength were cast in steel cylindrical moulds of 50 mm internal diameter and 50 mm height. Subsequently, a compression force of 60 kN was applied for 30 secs to compact the materials in the moulds. No excess solution would be squeezed out from the specimens during the process. The dry-mixed casting method allowed instant demoulding of the specimens which were left undisturbed at room temperature in air until the time of testing.

Table 3.7 Mix proportions of the dry-mixed geopolymer pastes

Paste ID	Mixed solids		Alkaline solution	
	GGBS	SSA	Na_2O content (wt. %)	Modulus
GeoP-N3.5-M0.60	0.5	0.5	3.5	0.60
GeoP-N3.5-M0.95	0.5	0.5	3.5	0.95
GeoP-N3.5-M1.30	0.5	0.5	3.5	1.30
GeoP-N4.0-M0.60	0.5	0.5	4.0	0.60
GeoP-N4.0-M0.95	0.5	0.5	4.0	0.95
GeoP-N4.0-M1.30	0.5	0.5	4.0	1.30
GeoP-N4.5-M0.60	0.5	0.5	4.5	0.60
GeoP-N4.5-M0.95	0.5	0.5	4.5	0.95
GeoP-N4.5-M1.30	0.5	0.5	4.5	1.30

3.4.3 Experimental Methods

The experimental methods for conducting the XRF, laser size diffraction, SEM, EDX, XRD and QXRD in the study of geopolymer pastes were the same as the aforementioned in section 3.2.3. The TCLP test was carried out by the same method as aforementioned in section 3.3.3.

Compressive strength was tested by using a universal testing machine with a maximum capacity of 3000 kN. The loading rate was set at 0.6 MPa/sec. For each mix twelve specimens at ages of 7 days and 28 days were tested, and the average results were reported.

Fragments from the central part of the broken specimens after measurement of the compressive strength were vacuum dried for carrying out microstructural analyses. The fractured specimens of 28 days in age were ground to powder passing the 45 μm sieve for the XRD, QXRD and Fourier transform infraRed spectroscopy (FTIR) analyses. For the SEM and EDX analyses, the broken pieces at the ages of 1, 3 and 28 days were gold coated after vacuum dried and observed by SEM.

The FTIR analyses were performed using a Bio Rad FTS 6000 Spectrometer. The spectra were collected in the range between 4000 and 400 cm^{-1} with a spectral resolution of 1 cm^{-1}. Specimens in powder form passing the 45 μm sieve were prepared by thoroughly mixing 1 mg of the powder with 200 mg of KBr (potassium bromide) and then pressed into transparent disks for the FTIR analyses.

CHAPTER 4 – COMPARATIVE STUDIES ON THE EFFECTS OF SSA AND PFA ON CEMENT HYDRATION AND PROPERTIES OF CEMENT MORTARS

4.1 Introduction

There are clear and well-established environmental, economic and technical advantages to using SCMs. The main SCMs include PFA, GGBS, silica fume, natural pozzolan (e.g., volcanic ash) and natural calcined pozzolan (e.g., MK). From a technical perspective, different SCMs exhibit different advantages and disadvantages. As one may expect, comparative studies of SSA and other SCM using the same equipment and applying the same conditions would help evaluate the effectiveness of SSA used in blending with cement and identify any unusual effects from SSA. As the size of SSA particles may also affect its properties, it is important to repeat tests on FSSA of corresponding amounts for comparison. FSSA was obtained from grinding the SSA in a ball mill for 3 hours.

While many studies have been conducted on the physical properties of SSA blended cement products, relatively little attention has been paid to the effect of SSA on cement hydration. The effect on early hydration of cement needs to be evaluated when part of cement is substituted by SCM. Simple studies using pure SSA and

blended with cement pastes may help explain better some of the results observed. Published literature mentioned that mortars of comparable strength could be produced using a small amount of SSA to replace cement. However, information on how SSA affected the properties of cement mortars was limited given the pozzolanic activities of most SSA being modest. Other factors can also affect strength development in mortars, including porosity, which will vary due to changes in w/c ratio caused by the presence of SCM. Additionally, very few studies have been performed to assess the effects of SSA on the volume stability of mortars due to drying shrinkage and the associated mechanisms. It is hoped that this study will provide more information on using SSA for partial replacement of cement for producing cement mortars with emphasis on filling the above knowledge gaps.

This study aimed to identify the mechanisms behind some beneficial effects of the SSA on the strength developments of mortars through a comparison study with FSSA and PFA. The physical and chemical properties of these materials and their influences on the mechanical performance and volume stability of cement pastes and mortars were studied. Tests were conducted to examine such properties and performance including heat of cement hydration, pozzolanic activity, workability, flexural and compressive strength, pore structure, qualitative and semi-quantitative phase composition, morphology and drying shrinkage. The results of these tests are given below.

4.2 Isothermal Calorimetry

It can be seen from Fig. 4.1a that there was no heat release from the paste containing only PFA, SSA or FSSA except in the initial 1-2 minutes of wetting, indicating that these materials did not undergo any hydration reactions. For SSA, one previous study using XRD analysis (Cyr et al., 2007) found that there were no phase changes except for the dissolution of gypsum in the pure SSA paste cast for several weeks and concluded that the SSA had no hydration activity itself. For PFA, it is believed to be non-hydraulic at the early stages (Maltais and Marchand, 1997; Langan et al., 2002).

Fig. 4.1b-d show the hydration heat liberation rates per gram of cement of the pastes with PFA, SSA or FSSA added to replace OPC. It can be seen that FSSA at all replacing levels achieved the highest peak heat liberation rate followed by SSA and then PFA. The peak rates of the pastes containing SSA or FSSA were higher than that of the cement only control mix. Higher SSA or FSSA content resulted in greater peak heat liberation rates. One previous study also found an increase of the peak heat evolution rate of cement hydration by replacing 25% and 50% of cement with SSA (Cyr et al., 2007), but the mechanisms were not further studied. On the other hand, PFA, of low or high content did not affect the peak heat evolution rate expressed as thermal power per gram of cement. It should be noticed that if the rate were expressed

in grams of binder, it would be lower than that of neat cement paste, and the more incorporated PFA, the lower the heat liberation rate.

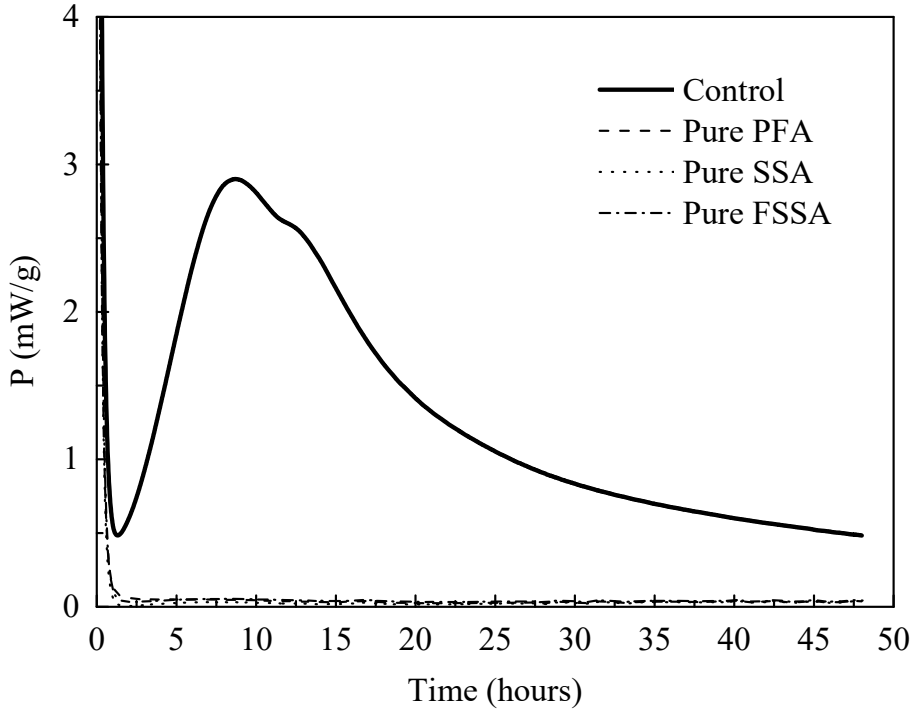

(a)

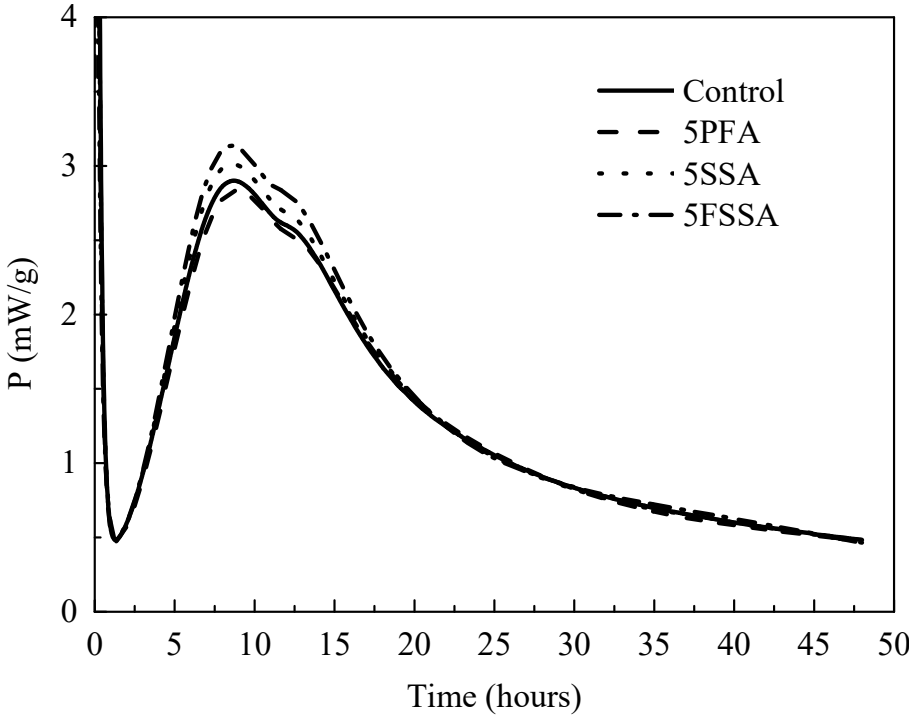
Control
5PFA
5SSA
5FSSA
P (mW/g)
Time (hours)
0
1
2
3
4
0
5
10
15
20
25
30
35
40
45
50

(b)

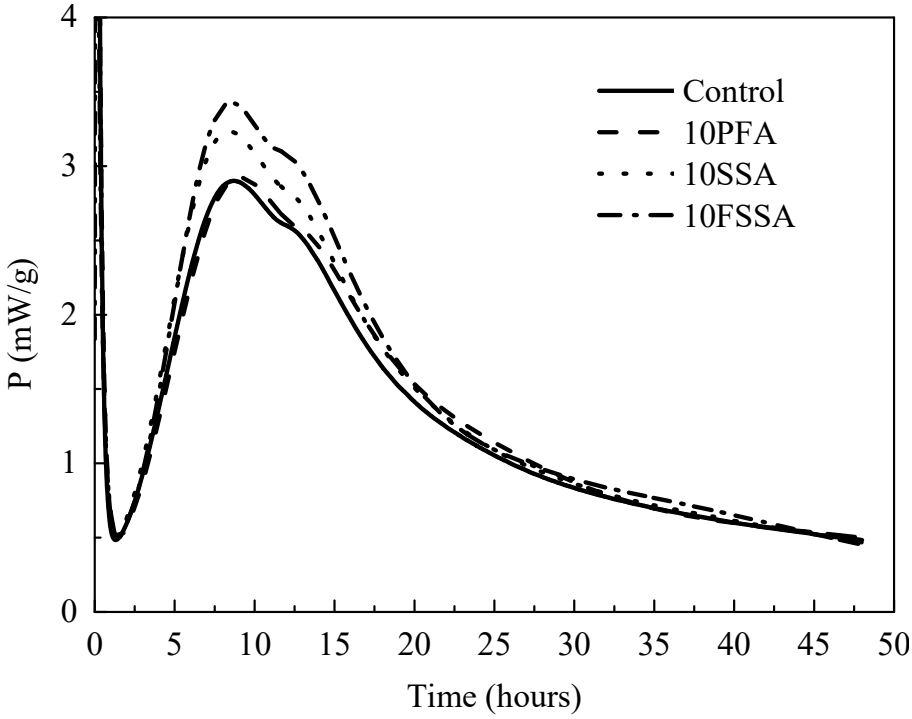
Control
10PFA
10SSA
10FSSA
P (mW/g)
Time (hours)
0
1
2
3
4
0
5
10
15
20
25
30
35
40
45
50

(c)

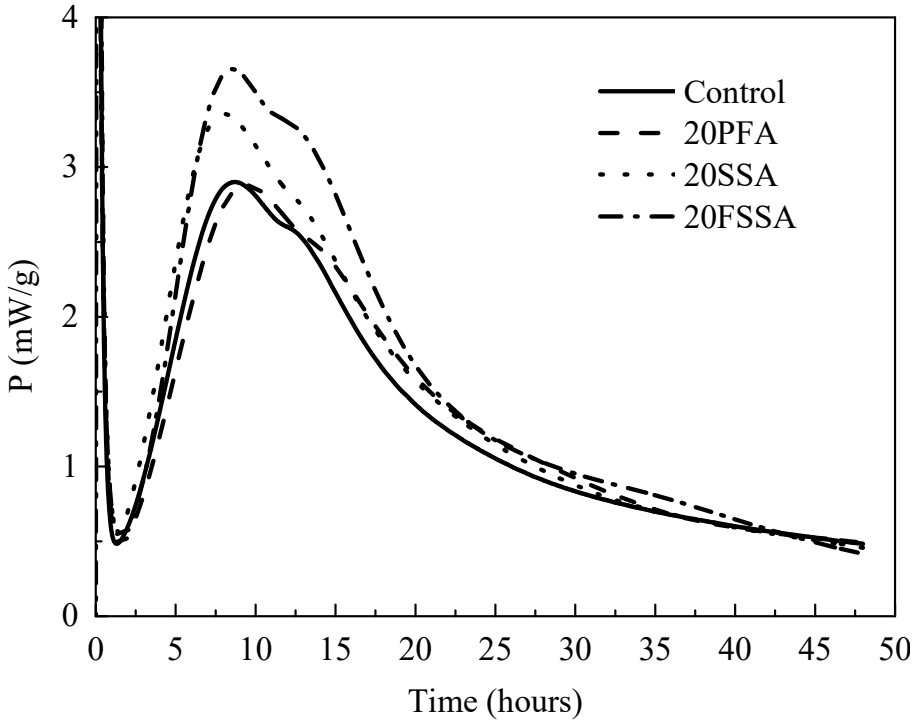

(d)

Fig. 4.1. Heat liberation rate of pastes in mW per gram of cement

When a certain amount of cement is replaced by other materials, less quantity of cement is present in the same amount of water implying less hydrated cement and less heat evolved (Lawrence et al., 2003; Cyr et al., 2007). This is a natural dilution effect. The enhancement effects of SSA and FSSA in the mix should most likely come from the porous nature of SSA and FSSA particles which entrap a significant amount of water in the pores, leading to a higher concentration of cement particles in water. Dhir et al. (2017) reported that the average absorption value of SSA is 18%. The water reduction effect generated from SSA or FSSA exceeds the cement dilution effect, resulting in a lower effective w/c ratio. According to the study of Hu et. al

(2014), a lower w/c ratio would lead to a higher rate of heat liberation in the cement hydration process. Furthermore, since FSSA is finer than SSA, it provides more nucleation sites for hydration product precipitation and thus speeds up cement hydration. The nucleation effect on cement hydration induced by very fine powder substitutes is due to the interfacial energy between two solids being smaller than that between a solid and a solution, and as such, finer particles with larger surface areas provide more nucleating sites and allow more hydraulic reaction to proceed (Stumm, 1992). Apparently, PFA has coarser particle sizes and smaller specific surface areas compared to FSSA, thus producing a smaller nucleation effect than FSSA. Besides, the narrow particle size distribution of PFA makes it less effective in dispersing cement particles. Therefore, during the early period, PFA has little effect on the hydration rate of cement as revealed by the rate of heat evolution.

4.3 Workability of Mortar with the same W/B Ratio

Fig. 4.2 gives the FTS results. A decrease in workability can be seen in the mortar containing SSA or FSSA. This result is reasonable due to the porous nature of SSA and FSSA which makes them hydroscopic. Increasing the content of SSA or FSSA naturally leads to a decrease in workability. It is interesting to note that although FSSA has a larger surface area compared to the original SSA, the former has a lesser effect on workability. This may be due to the effect of grinding which makes the ash

particles smoother and less porous, thus improving workability (Chen et al., 2013). The increase in workability of cement mortar containing PFA is due to the ball-bearing effect of PFA (Haleem et al., 2016; Zheng et al., 2016).

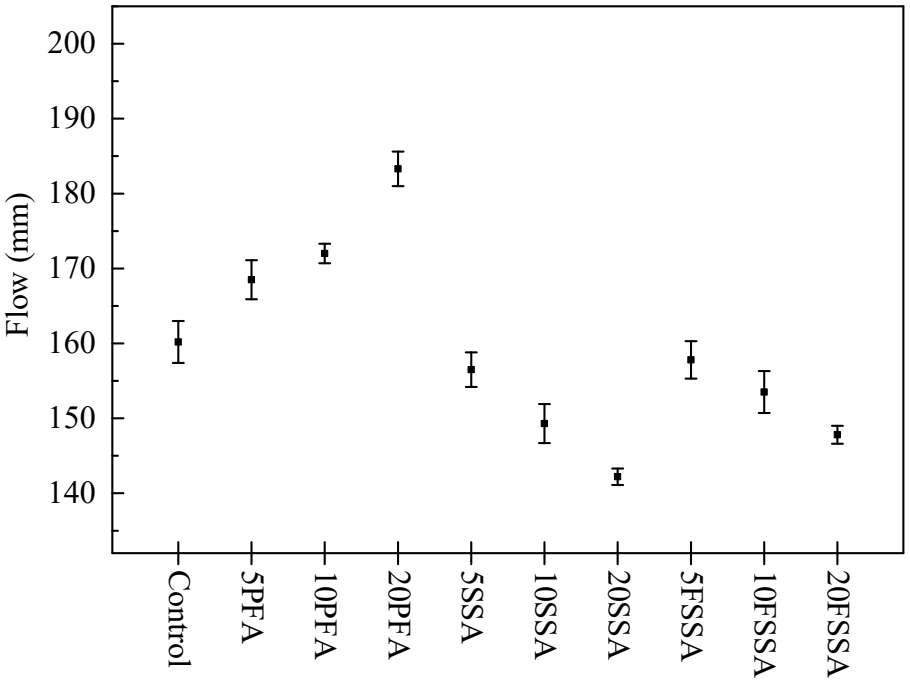

Fig. 4.2. Flow table values (workability) of mortars with the same w/b ratio

4.4 Pozzolanic Activities of PFA, SSA and FSSA

The pozzolanic activities of PFA, SSA and FSSA assessed by the Frattini test are presented in Fig. 4.3. The [Ca^{2+}] is expressed as equivalent [CaO]. According to EN 196-5 (2005), a material is regarded as pozzolanic when the test result lies beneath the lime saturation isotherm at 40°C. A result lying on or above the lime saturation

isotherm indicates no pozzolanic reaction. It is clear from Fig. 4.3 that all test results for PFA, SSA and FSSA lie below the lime saturation isotherm, indicating that PFA, SSA and FSSA are pozzolans under the Frattini standard. The degree of pozzolanic activity can also be assessed by checking the degree of reduction of the [CaO]. A higher pozzolanic activity was revealed in the PFA from the higher lime removal rate of 60.2%. As the FSSA consumed more lime than SSA did during the test, it reflects some positive effects of grinding on the pozzolanic activity of SSA.

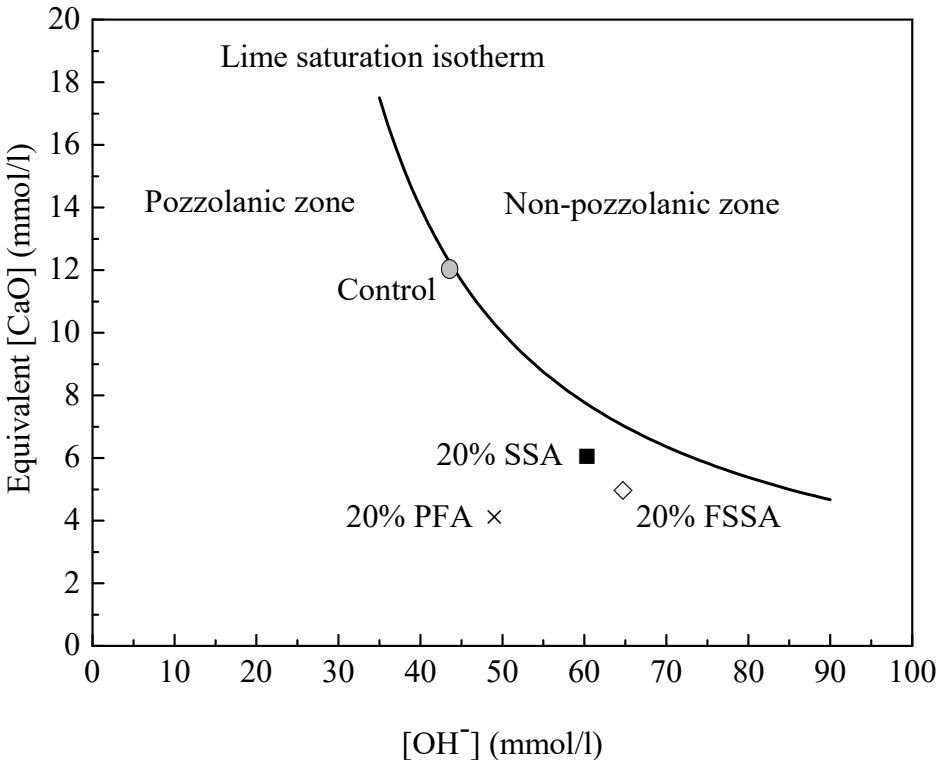

Consumption of [CaO] after 8 days of curing

Specimen	[OH] (mmol/l)	[CaO] (mmol/l)		[CaO] reduction (%)
		Saturation	Test	
Control	43.60	12.20	12.10	1.13
20% PFA	49.00	10.29	4.10	60.17
20% SSA	60.30	7.73	6.00	22.34
20% FSSA	64.60	7.06	4.90	30.56

Fig. 4.3. Pozzolanic activities of PFA, SSA and FSSA assessed by the Frattini test

The results of the SAI tests are given in Fig. 4.4. According to the results, the PFA can be regarded as a good pozzolan but not the SSA and FSSA using 75% as the reference. However, the test procedures might have distorted the results due to the need for adding more water to achieve the workability requirement due to the porous

nature of the SSA. Donatello et al. (2010) expressed the same view and remarked that the pozzolanic activity of a highly water absorbing material might be underestimated using the SAI test. Noting from Fig. 4.4 that the indices of the SSA and FSSA increased with time and considering the results from the Frattini test, it can be concluded that the SSA and FSSA did possess moderate pozzolanic activities. The degree of pozzolanic activity of the PFA, SSA and FSSA correlated with the contents of reactive amorphous phases in the materials. Relatively, being finer in size, the FSSA was a better pozzolan than the SSA (Kiattikomol et al., 2001; Shannag and Yeginobali, 1995; Shi and Zheng, 2007).

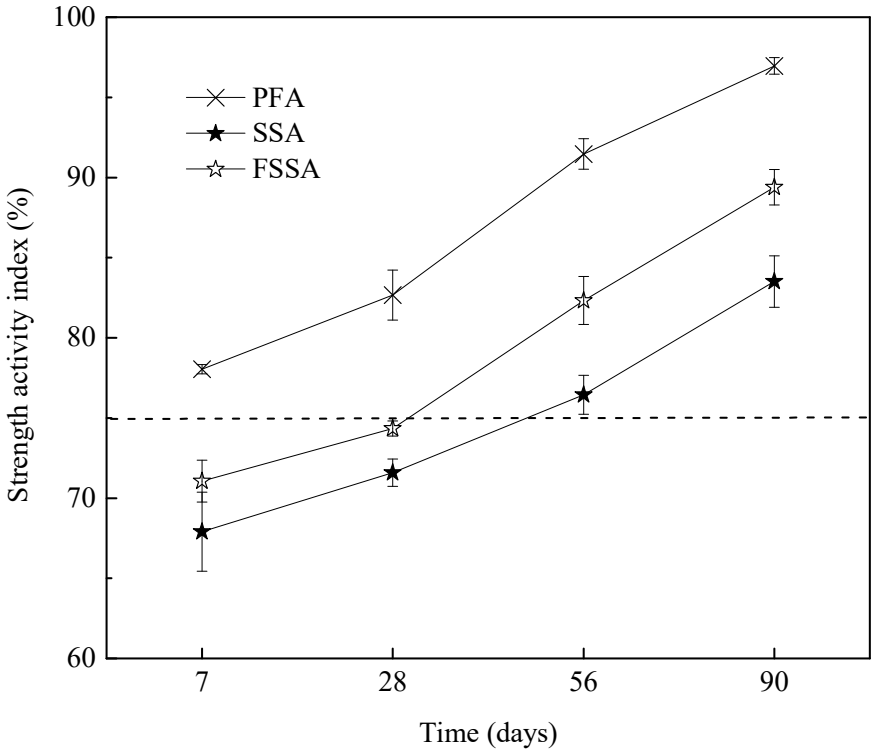

		Control	PFA	SSA	FSSA
7 days	Strength (MPa)	35.78	27.93	24.30	25.43
	SAI (%)		78.04	67.91	71.06
	Strength loss (%)		21.96	32.09	28.94
28 days	Strength (MPa)	45.68	37.76	32.70	33.96
	SAI (%)		82.66	71.58	74.34
	Strength loss (%)		17.34	28.42	25.66
56 days	Strength (MPa)	48.66	44.50	37.20	40.06
	SAI (%)		91.46	76.45	82.33
	Strength loss (%)		8.54	23.55	17.67
90 days	Strength (MPa)	50.54	49.00	42.20	45.17
	SAI (%)		96.96	83.51	89.39
	Strength loss (%)		3.04	16.49	10.61

Fig. 4.4. SAI test on PFA, SSA and FSSA

4.5 Flexural and Compressive Strength Development

The results of compressive and flexural strength tests are presented in Fig. 4.5. The influence of PFA, SSA or FSSA on the flexural strength of cement mortar was found to be similar to that on compressive strength. It can be noticed from these results that the compressive strength of the mortar containing PFA dropped noticeably at the early curing ages due to the cement dilution effect but gradually picked up after a longer curing time due to the stronger pozzolanic reaction between the reactive silica and alumina in the PFA and calcium hydroxide generated from cement hydration producing additional calcium silicate and aluminum silicate hydrates. The strength values of the mortars containing SSA or FSSA at replacement levels of up to 10% were comparable to those of the control mortar taking account of the measurement variability. The strength values marginally decreased when 20% SSA or FSSA was used in the binder. Although SSA or FSSA has lower pozzolanic activity compared to PFA, they are not inferior in regard to strength development. When OPC was replaced at up to 20%, the flexural strength of PFA, SSA, FSSA cement mortars reached 8.08 MPa, 8.21 MPa and 8.47 MPa respectively while the compressive strength reached 45.81 MPa, 46.74 MPa and 46.85 MPa respectively at 90 days. This encouraging phenomenon of strength development of SSA and FSSA cement mortars may be due to the following reasons. First, the initial absorption of water into the

pores of SSA and FSSA particles reduces the effective w/b ratio which counterbalances the dilution effect. Second, the release of water gradually from the pores at a later time allows hydration of the remaining cement (see analysis of the MIP test). Besides, the modest pozzolanic activities of SSA and FSSA provide additional strength. The angular shape of unreacted SSA and FSSA particles also enhances the interlocking among molecules and grains, thus contributing to the overall strength. This beneficial effect was also reported in trials of soil stabilization using SSA which enhanced the shear strength of the soil (Lin et al., 2007; Chen and Lin, 2009). Furthermore, XRD analysis for identifying the crystalline phase can provide additional information to explain the strength developments of SSA and FSSA cement mortars. It is also noted that finer SSA gave higher compressive and flexural strength values at all curing ages.

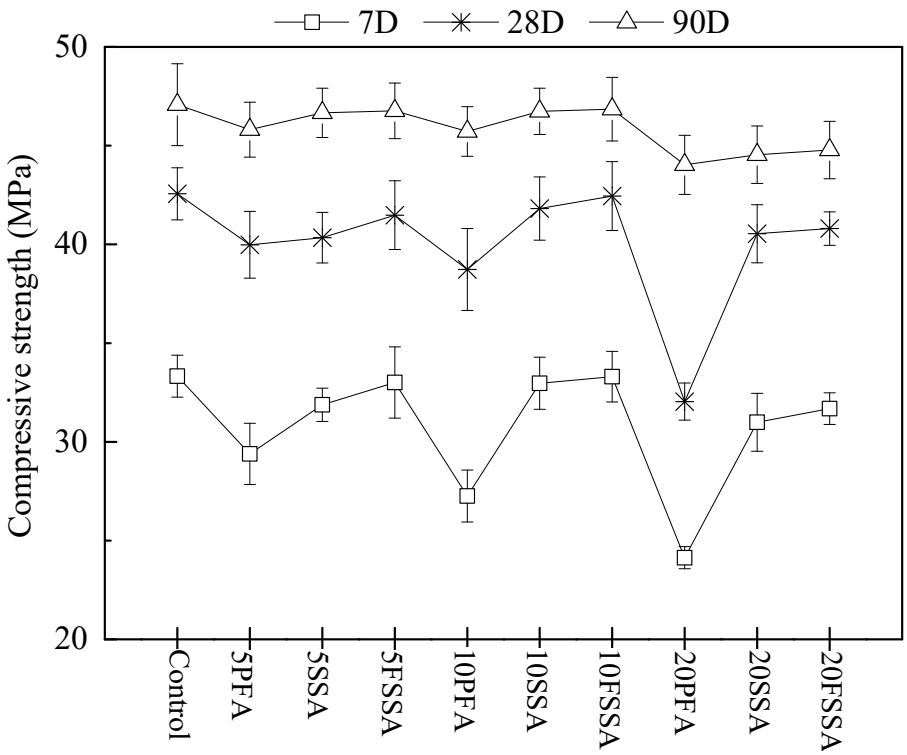

(a)

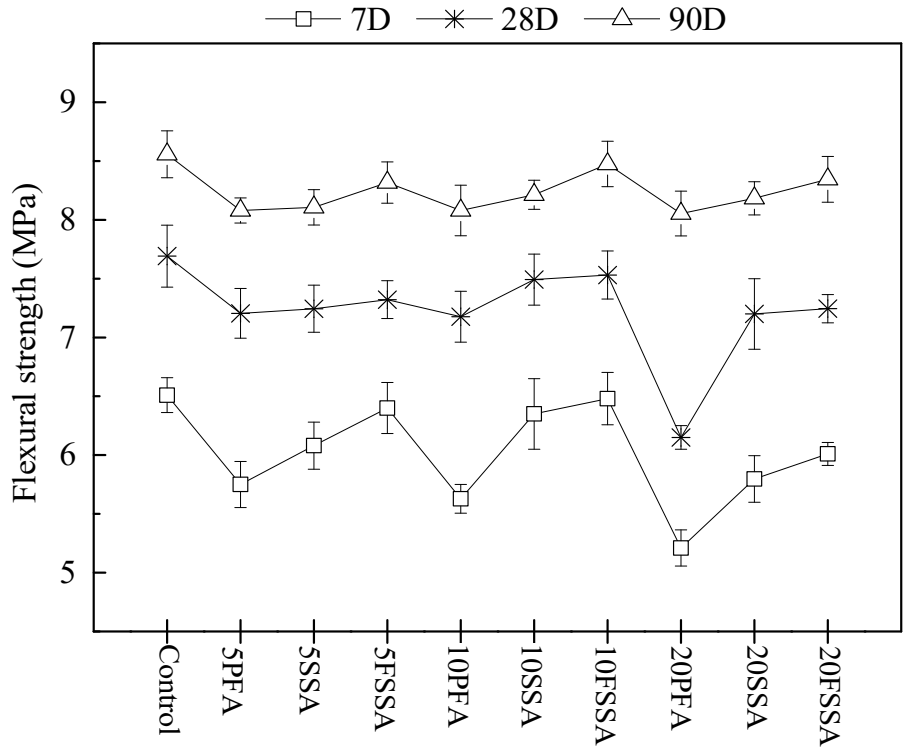

(b)

Fig. 4.5. Compressive (a) and flexural (b) strength of mortars containing different amounts of PFA, SSA and FSSA in the binder

4.6 MIP Tests

The results of the MIP analyses of the paste specimens cured for 28 days are shown in Fig. 4.6 and Fig. 4.7. Fig. 4.6a and Fig. 4.6b indicate that with the incorporation of up to 10% SSA or FSSA in the binder, the pore structures of the paste specimens exhibited little change in comparison to the control. As SSA and FSSA are themselves porous materials, this result could imply that the pores of SSA and FSSA particles might be partially or totally filled by the hydration products (Kaufmann et al., 2009; Zhou et al., 2010). In addition, the water inside or expulsed from the pores allows further hydration of the cement particles around it. The pore structures of SSA or FSSA blended cement paste varied with replacement level. Increasing the content of SSA or FSSA to 20% led to a shift of the distribution curve to the right, i.e., an increase in pore size. According to these findings, it can be concluded that blending with 10% or less SSA or FSSA balances the effects of the high porosity of SSA or FSSA in the cement paste with improved hydration of cement using the water absorbed into the pores, resulting in a similar compactness of cement paste. The MIP results are consistent with the strength results and further substantiate the beneficial effect of SSA and FSSA on strength development despite their weak pozzolanic activity.

The cumulative intrusion curves for the pastes prepared with 10% and 20% PFA, SSA or FSSA are shown in Fig. 4.6c and Fig. 4.6d respectively. The pastes containing PFA had larger pore size distributions compared with those containing SSA and FSSA at the same replacement levels. Furthermore, the FSSA cement pastes had smaller pore size distributions than those of the SSA cement pastes.

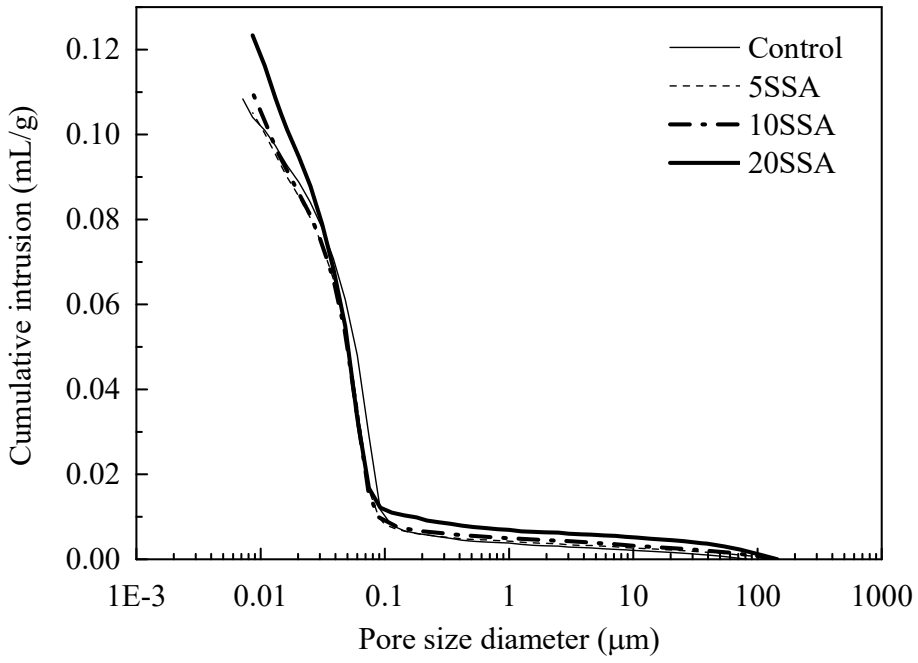

(a)

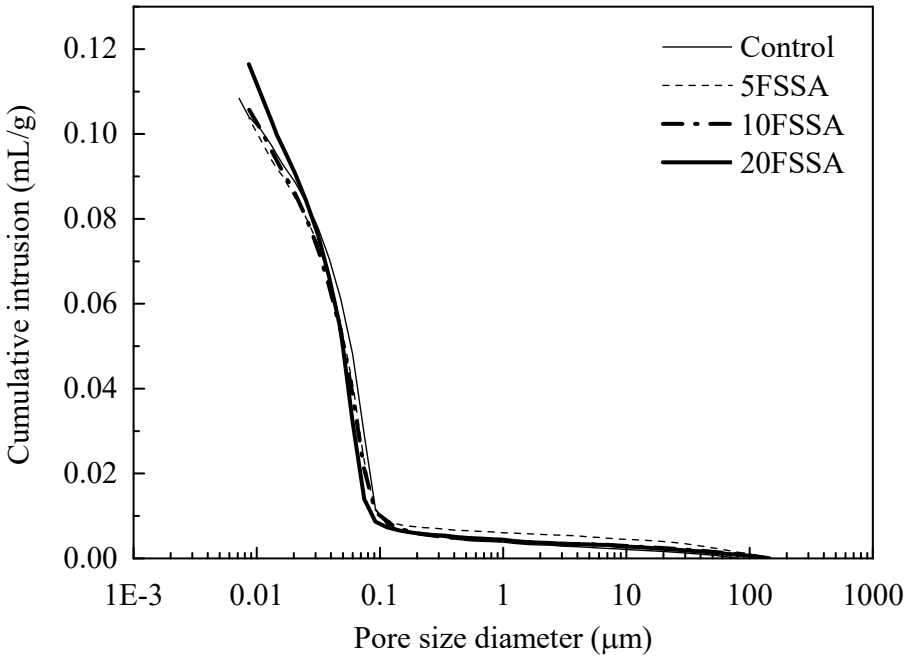
Control
5FSSA
10FSSA
20FSSA
Cumulative intrusion (mL/g)
0.12
0.10
0.08
0.06
0.04
0.02
0.00
1E-3
0.01
0.1
1
10
100
1000
Pore size diameter (μm)

(b)

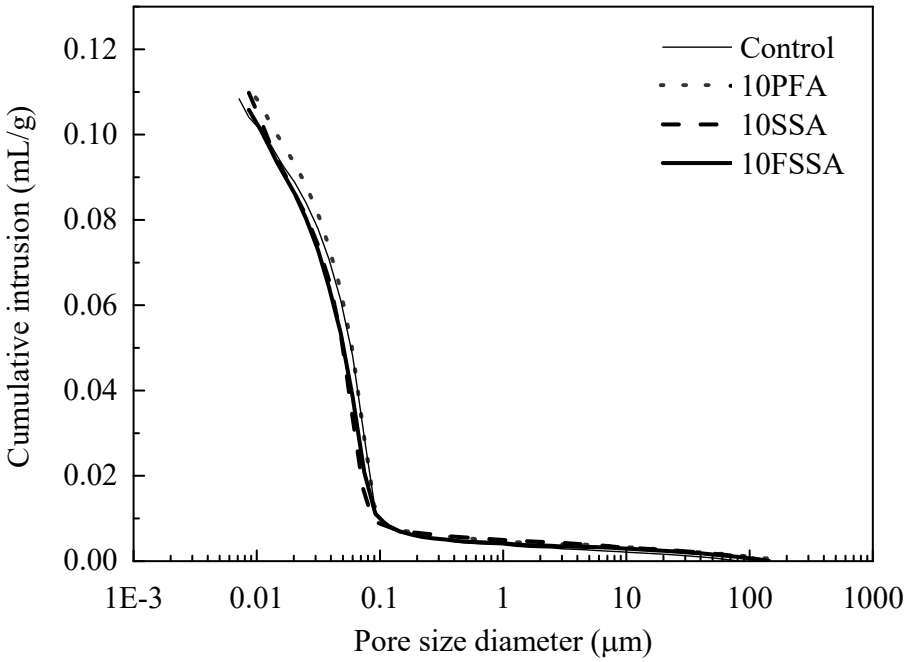
Control
10PFA
10SSA
10FSSA
Cumulative intrusion (mL/g)
0.12
0.10
0.08
0.06
0.04
0.02
0.00
1E-3
0.01
0.1
1
10
100
1000
Pore size diameter (μm)

(c)

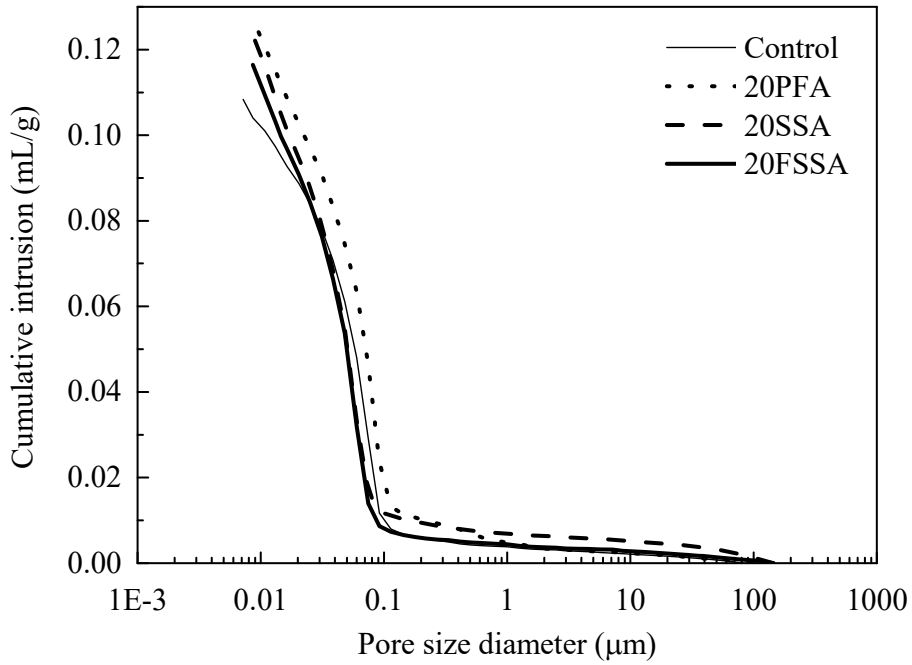

(d)

Fig. 4.6. Pore size distributions of pastes containing different amounts of PFA, SSA and FSSA

By comparing the curves of the log differential intrusion of the specimens, it can be found from Fig. 4.7a and Fig. 4.7b that the amounts of mesopores with less than 0.025 μm increased with an increase in replacement level of OPC by SSA or FSSA. The classification of mesopore is described in the International Union of Pure and Applied Chemistry system (Everett, 1972). From Fig. 4.7c and Fig. 4.7d, the amounts of mesopores in the cement pastes using FSSA were apparently greater than those in the cement pastes using SSA, while the amounts of mesopores were least in the PFA pastes. It should be noticed here that the mesopores do not affect the mechanical

properties but have a critical influence on the drying shrinkage of mortar (Collins and Sanjayan, 2000; Jiang et al., 2005; Vaitkevičius et al., 2014; Zhang et al., 2015).

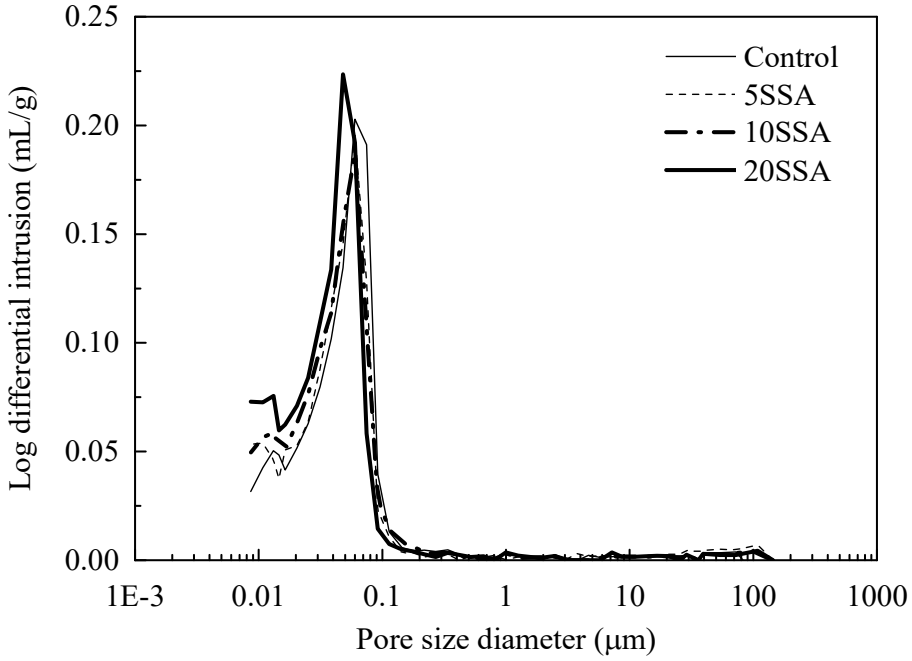

(a)

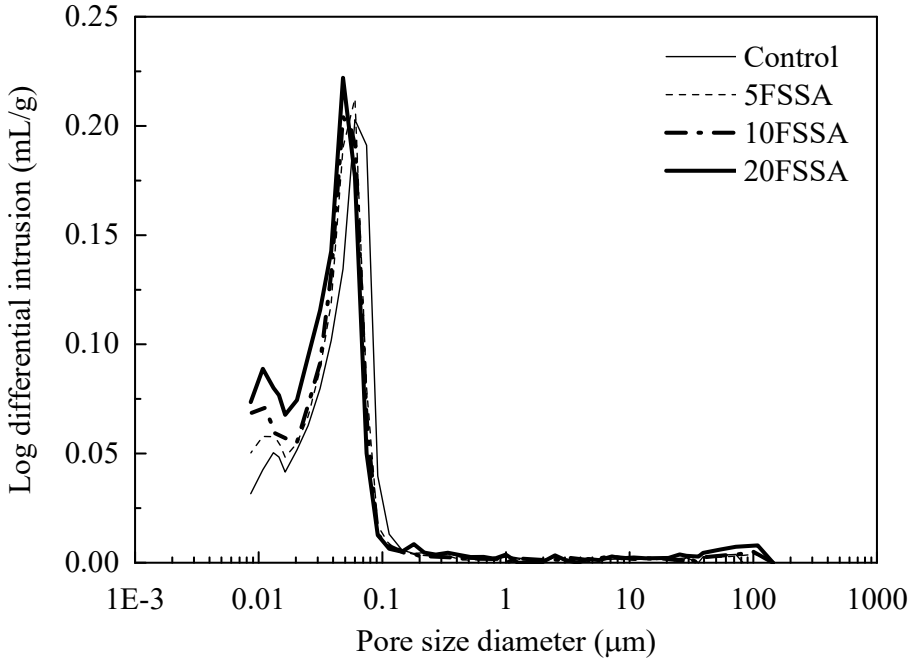

(b)

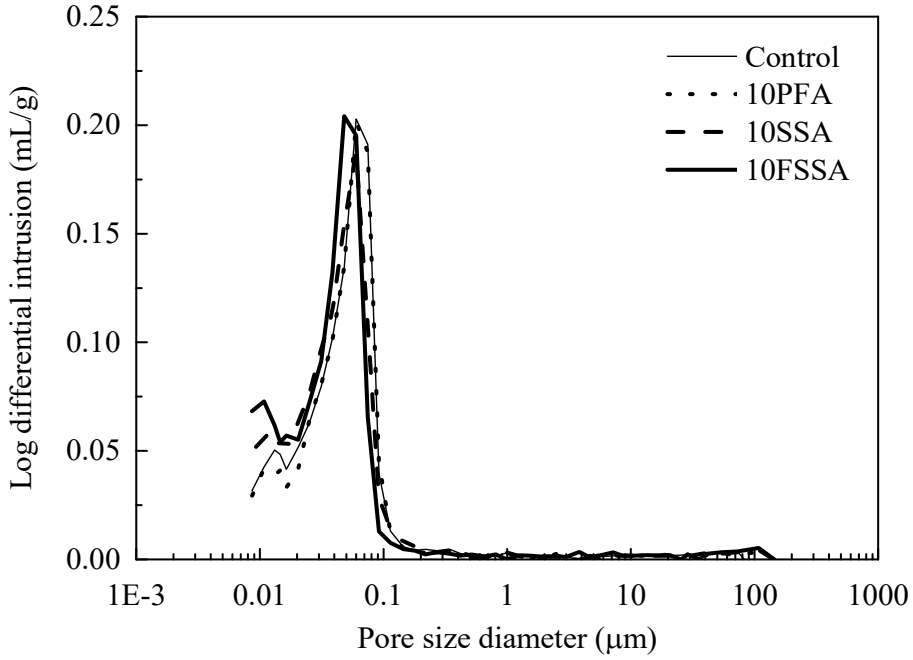

(c)

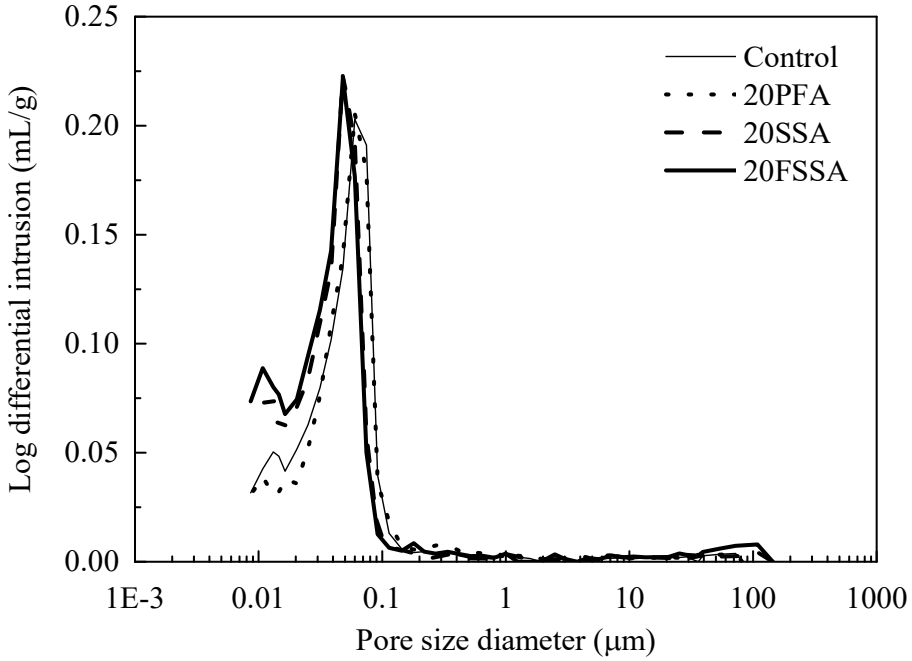

(d)

Fig. 4.7. Log differential intrusion of pastes containing different amounts of PFA, SSA and FSSA

4.7 XRD Analysis

XRD analysis was used to detect changes in the crystalline phases of cement pastes incorporating PFA, SSA or FSSA. At curing ages of 6 hours, 12 hours, 1 day and 2 days, cement pastes blended with PFA, SSA or FSSA exhibited similar phases to pure hydrated cement. The major components in the pastes were $Ca(OH)_2$, AFt, C_3S and C_2S. The peak positions and ICDD PDF card numbers corresponding to these components are given in Table 4.1. The quality of all the diffraction data are marked as "Star Patterns".

Table 4.1 XRD peaks of crystalline components in hydrated pastes at early ages

Component	d-spacing (angstrom)	2-theta angle (degree)	PDF #
$Ca(OH)_2$	2.627, 4.906, 1.926, 1.796, 3.111	34.10, 18.07, 47.14, 50.80, 28.68	01-076-0571
AFt	3.881, 9.721, 5.614	22.90, 9.09, 15.77	00-037-1476
C_3S	2.781, 2.756, 1.765	32.13, 32.46, 51.75	00-049-0442
C_2S	2.731, 3.013, 2.752	32.77, 29.63, 32.51	01-086-0397

Fig. 4.8 shows that a new crystalline compound $CaHPO_4 \cdot 2H_2O$, brushite (ICDD PDF card number 01-075-4370) weakly appeared after 28 days of curing and became

distinct after 90 days of curing in the cement pastes with incorporation of SSA or FSSA. However, no such phase was detected in the control and the PFA cement pastes. A previous study also found the formation of an amorphous or poorly crystalline hydroxyapatite $Ca_5(PO_4)_3OH$ in cement paste containing SSA (Dyer et al., 2011). Hydroxyapatite, which is considered to be a derivative of brushite (Neuman et al., 1962; Pak et al., 1971), found in that study was likely to be generated from the reaction between amorphous iron phosphate in SSA and calcium hydroxide produced from cement hydration. The average weight percentages of Fe_2O_3 and P_2O_5 in the raw materials (SSA) were 9.6% and 14.0% respectively. Brushite has been widely used as a biochemical material for the production of calcium phosphate cement. Because of its cementing ability, it is used as coating materials, dental cement and bone adhesives (Theiss et al., 2005; Ajaxon et al., 2015; Blanda et al., 2016; Sopcak et al., 2016). Brushite may therefore contribute to the development of strength in the late age of SSA or FSSA blended mortar.

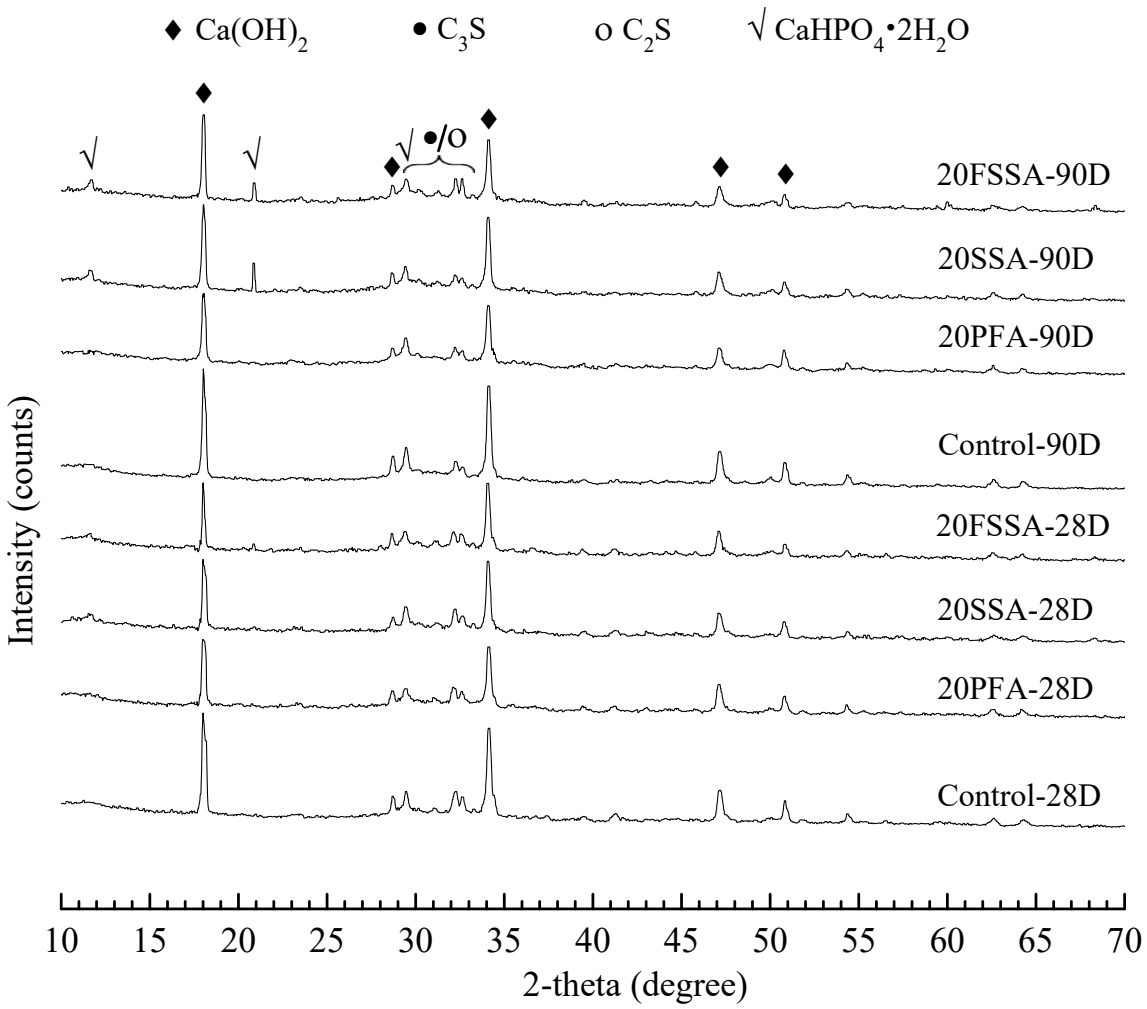

Fig. 4.8. XRD spectra of pastes at late ages

4.8 SEM and EDX Analyses

Fig. 4.9 shows SEM images together with EDX results obtained from cement paste with 20% SSA after 90 days of curing. The SEM images show the formation of plate-like crystals in the hydrates, which match the micrographs of brushite crystals reported in the literature (Han et al., 2007; Gashti et al., 2013; Bakhsheshi-Rad et al.,

2014). According to the corresponding EDX spectra, the elements detected were mainly Ca, O and P. The molar ratios of Ca to P (Ca/P) calculated from the weight percentages obtained from the EDX semi-quantitative chemical analyses ranged from 0.87 to 1.41. This is in agreement with the theoretical Ca/P ratio of brushite (1.00) (Miller et al., 2012; Parvinzadeh Gashti et al., 2013).

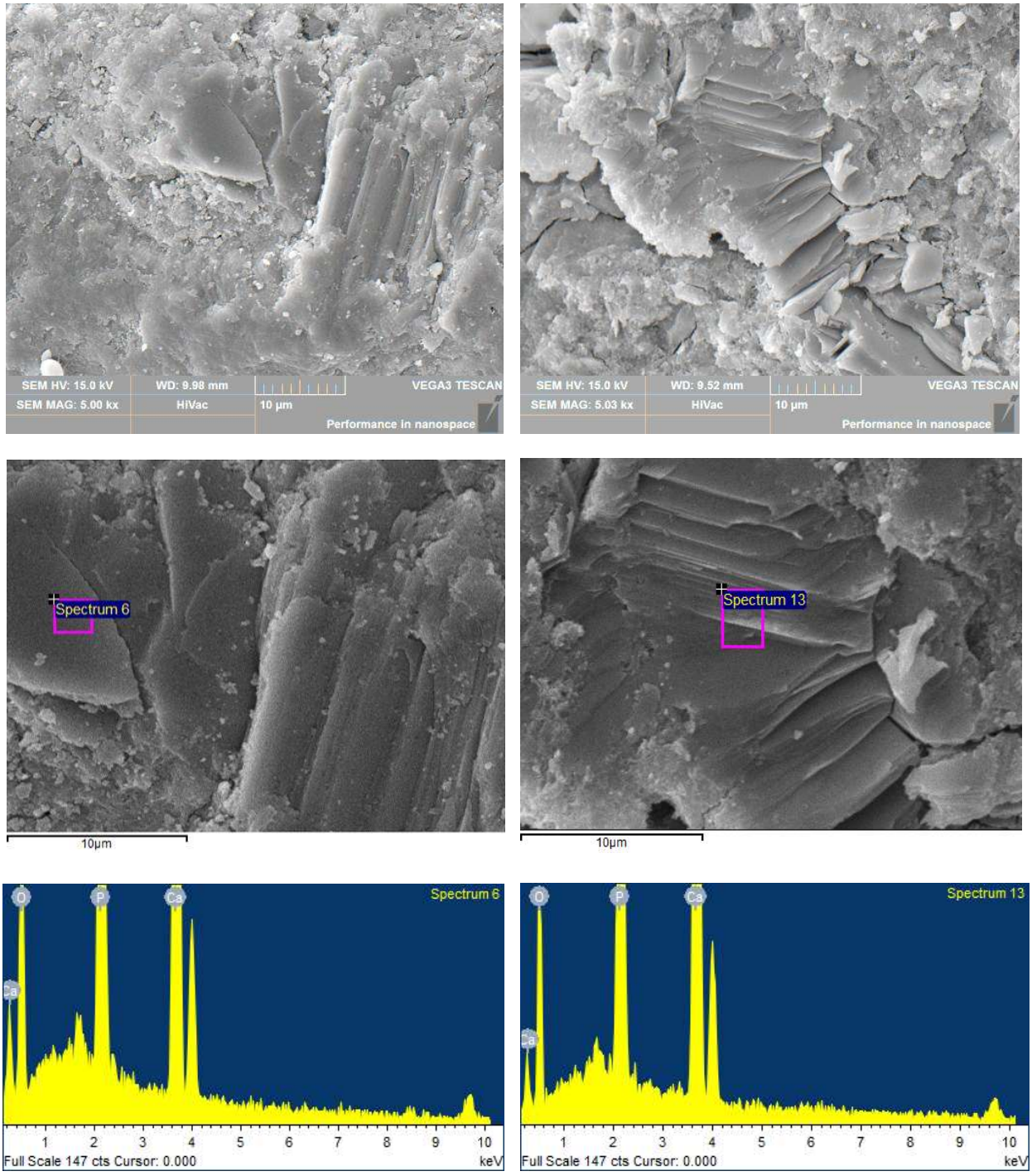

Fig. 4.9. Representative SEM images and corresponding EDX spectra of plate-like crystals

4.9 Drying Shrinkage

The results of the drying shrinkage tests for different mortar mixes up to 112 days are shown in Fig. 4.10. It can be seen from Fig. 4.10a-b that with the inclusion of SSA or FSSA, the drying shrinkage of mortar increased when compared to the control mortar. Sasaoka et al. (2006) also reported that the drying shrinkage of concrete containing 10% SSA in the binder was higher than that of the control. The increase in drying shrinkage may be related to the increase in free water content in the mortar (Pittman and Ragan, 1998; Zhang et al., 2013; Farzadnia et al., 2015). Water absorbed by the pores of SSA or FSSA particles creates additional free water in addition to the water in the cement paste. Upon drying, the free water in the pores of SSA and FSSA particles might evaporate before being consumed by the cement hydration. The deleterious effect of FSSA on drying shrinkage was greater than that of SSA due to the larger surface area and smaller pore size of FSSA. Furthermore, the larger amounts of mesopores in FSSA cement mortar also cause a greater degree of drying shrinkage.

PFA mortar exhibited the lowest shrinkage value which was even smaller than that of the neat cement mortar (Fig. 4.10c-d). The shrinkage reduction effect was more apparent with a higher content of PFA and at later ages. This phenomenon can be explained mainly by the pozzolanic activity of PFA. The stronger structure of the

mortar as a result of the pozzolanic reaction could resist higher shrinkage stress caused by water evaporation. Many previous studies have reported the positive effect of the pozzolanic reaction on drying shrinkage (Chindaprasirt et al., 2004; Güneyisi et al., 2008; Itim et al., 2011; Nunes et al., 2016). Moreover, smaller amounts of mesopores in PFA mortar also effectively reduce shrinkage.

The drying shrinkage of mortars containing 20% SSA, FSSA and PFA was 0.0909%, 0.1011% and 0.0652% of the initial length respectively at the end of 56 days. The length changes of mortar incorporating SSA or FSSA did not meet the requirement of BS ISO 1920-8 (2009) which specifies a drying shrinkage limit of 0.075% at 56 days.

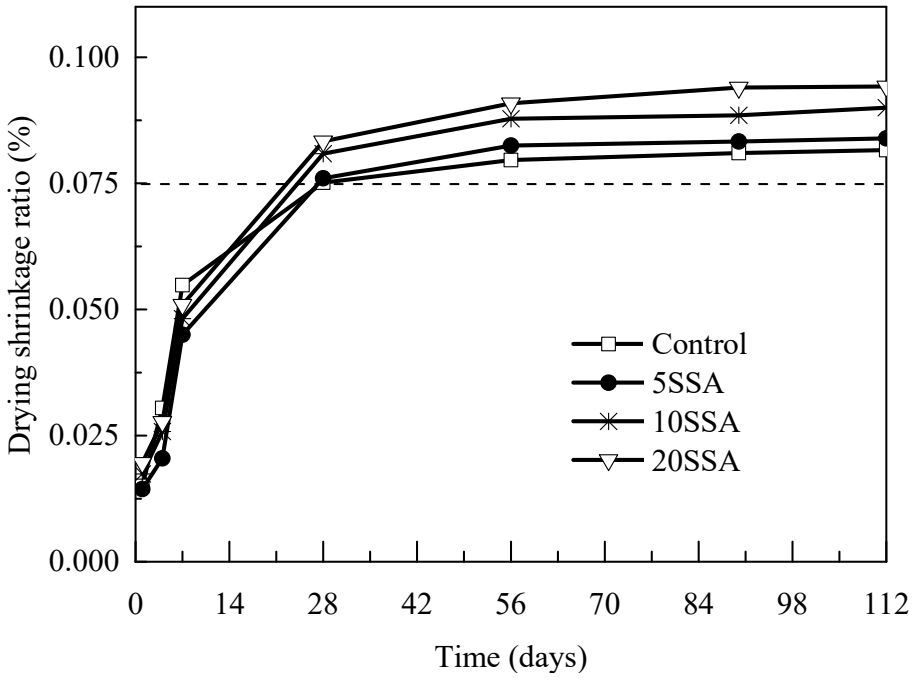

(a)

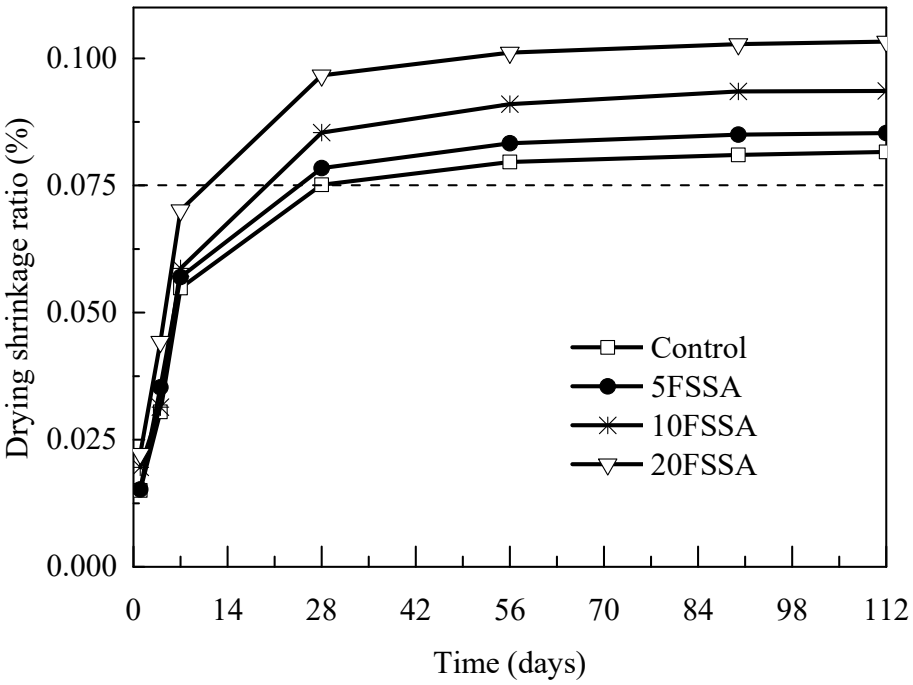
Drying shrinkage ratio (%)
0.100
0.075
0.050
0.025
0.000
0
14
28
42
56
70
84
98
112
Time (days)
Control
5FSSA
10FSSA
20FSSA

(b)

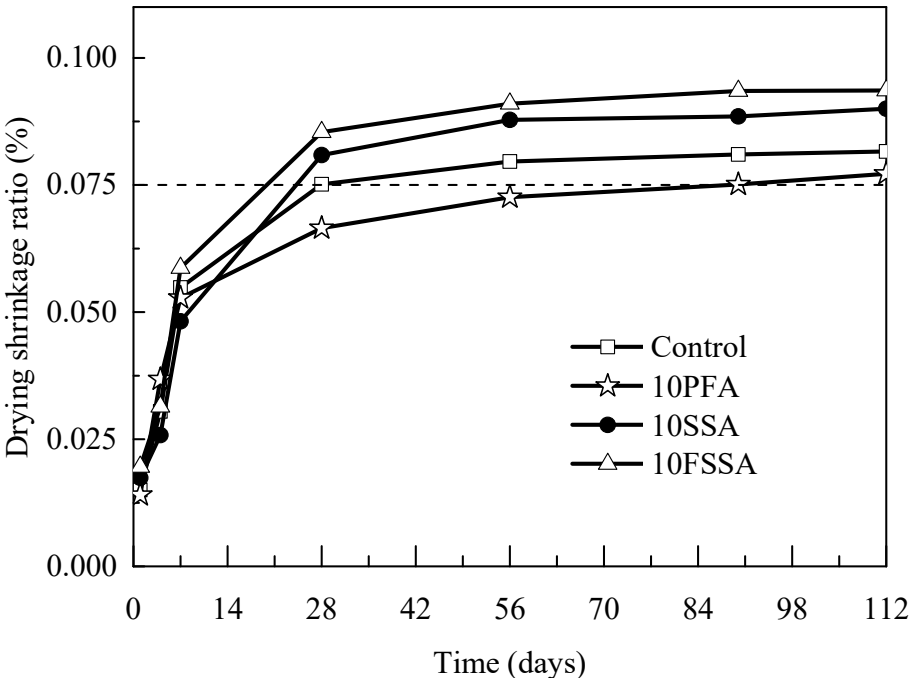
Drying shrinkage ratio (%)
0.100
0.075
0.050
0.025
0.000
0
14
28
42
56
70
84
98
112
Time (days)
Control
10PFA
10SSA
10FSSA

(c)

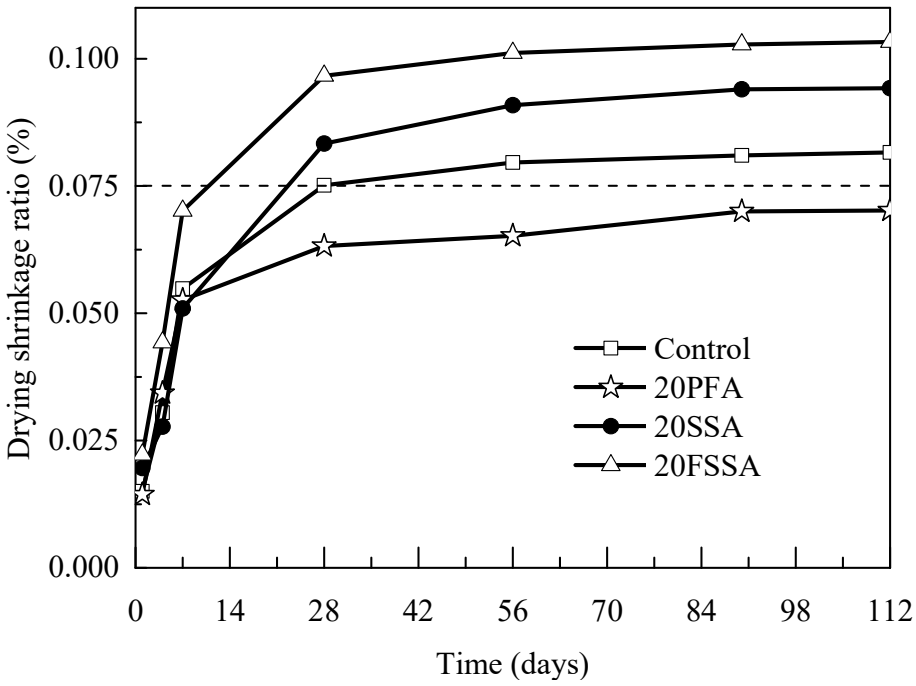

(d)

Fig. 4.10. Drying shrinkage values of mortars containing different amounts of PFA, SSA and FSSA in the binder

4.10 Summary

In this chapter, the mechanical and durability properties of cement pastes and mortars containing the SSA of two different size ranges were evaluated and compared to those containing PFA. A summary of the test results can be drawn as follows:

(1) The main oxide components in the SSA were SiO_2, Al_2O_3 and CaO. The oxide compositions indicated that the SSA could be used as a SCM.

(2) The specific gravity of the SSA was smaller than that of OPC. The particle sizes of the SSA were slightly larger than those of OPC but both were at the micron scale.

(3) The SSA particles were irregular in shape, rough on surface and contained many isolated and open pores making the SSA hydrophilic. More water was required to achieve similar workability of cement mortar as content of the SSA increased in the binder.

(4) Both the SSA and PFA contained crystalline minerals of quartz, hematite and magnetite. The contents of non-crystalline (amorphous and semi-crystalline) phases in the SSA and PFA were 53.11% and 82.97% respectively which correlated well with the relative pozzolanic activity of the SSA and PFA.

(5) SSA met the criterion under the Frattini standard to be a pozzolan.

(6) The specific gravity, fineness and specific surface area of the SSA increased with the grinding time. The pozzolanic activity of the SSA increased after grinding. However, finer SSA led to larger drying shrinkage.

(7) SSA did not undergo hydration itself, but the presence of SSA could promote the early stage hydration of cement. The peak heat liberation rate, expressed as thermal power per gram of cement, of the cement paste containing SSA was higher than that of the neat cement paste. Higher SSA content resulted in greater peak heat liberation rate.

(8) XRD analysis revealed the production of a new crystalline compound $CaHPO_4 \cdot 2H_2O$, brushite, slowly and becoming distinct after 90 days of curing in the

cement pastes containing the SSA. SEM together with EDX analysis also found the formation of plate-like brushite crystals in the cement pastes.

(9) The compressive and flexural strength of mortars containing SSA were comparable to those containing PFA at the same cement replacement level of up to 20% despite the lower pozzolanic activity of the SSA compared to PFA.

(10) The pore structures of the cement pastes with the incorporation of up to 10% SSA in the binder exhibited little change in comparison with the neat cement paste although the SSA was itself a porous material. The pores of the SSA particles might be partially or totally filled by the hydration products.

(11) The amounts of mesopores in the cement pastes with less than 0.025 μm increased with the replacement level of OPC by the SSA. The amounts of mesopores were apparently greater with the incorporation of the fine SSA. The drying shrinkage of cement mortars increased with the mesopore content.

CHAPTER 5 – COMBINED USE OF SSA AND RECYCLED GC FOR THE PRODUCTION OF CONCRETE BLOCKS

5.1 Introduction

Concrete paving blocks are widely used in many parts of the world because of their flexibility in construction and low maintenance costs. New generations of the blocks have already incorporated some types of wastes for achieving waste recycling. SSA could be used to partially replace cement for construction. One disadvantage of using SSA in cement mortar or concrete is the reduction in workability due to the porous nature of the SSA particles. Although the reduction in workability can be compensated by adding superplasticizers, this incurs additional costs. The application of SSA in making precast concrete blocks may be more suitable for the recycling of the waste because only a small quantity of water is needed to give a dry but cohesive mix suitable for the production of concrete blocks by the compression method. However, little effort has been devoted to the research of using SSA as a cement substitute in the production of precast concrete blocks. Besides, previous studies did not assess the durability performance of the blocks such as drying shrinkage and alkali-silica expansion if reactive aggregates were used. Furthermore, data on leachability of metal(loid)s from concrete blocks containing SSA was also absent.

Aggregates are major constituents in making concrete blocks. Normally, NA such as river sand and crushed stones are used. In Hong Kong, it has been demonstrated that concrete blocks made with C&D and GC aggregates comply with local standards for civil engineering works and are being commercialized. This study aimed to evaluate the effects brought from the combined use of SSA as a cement replacement and recycled C&D aggregates or GC as a partial substitution of NA in concrete blocks. The evaluation was more meaningful when some complementary effects among wastes were demonstrated.

For these purposes, this study investigated the properties of concrete blocks using SSA as a cement replacement together with recycled C&D aggregates or GC as a partial substitution of NA for producing concrete blocks by the dry-mixed (zero slump) compression method. No research in published literature has been conducted on the complementary effects from the utilization of SSA as a cement substitute and some recycled materials as aggregates in producing concrete blocks. Assessments of technical benefits and leaching risks were made with a view to encouraging recycling of waste materials and enhancing conservation of natural resources. A series of tests were conducted to determine the properties of the blocks with different constituents of waste materials. The control mix was made with OPC and NA. Recycled aggregates derived from C&D waste and crushed beverage GC were incorporated

separately for replacing NA. SSA was used to partially replace cement as a binder. FSSA obtained from grinding SSA and PFA were also used at the same replacement levels for comparison of performance. Tests were carried out to assess the pozzolanic activities of PFA, SSA and FSSA. The density, water absorption, compressive strength and drying shrinkage of the blocks were also tested. As glass contains a high level of reactive silica, the potential ASR in the blocks was also examined. The total and leachable metal(loid) contents in SSA and the blocks were also determined. Laboratory test results are discussed in the following sections.

5.2 Concrete Blocks Made with Recycled C&D Aggregates and Binder Containing 20% of SSA

For assessing the effects of recycled C&D aggregates on properties of the concrete blocks, the composition of the binder was fixed at 80% OPC and 20% SSA. The results of compressive strength of concrete blocks incorporating different amounts of recycled aggregates are presented in Fig. 5.1a. It can be observed that the specimens made with 100% NA gave the highest compressive strength. The strength decreased by 11.8% and 21.6% as the amount of recycled aggregates increased to 20% and 50% respectively.

The values of drying shrinkage of block specimens made with different amounts of recycled aggregates are shown in Fig. 5.1b. It can be seen that the drying shrinkage of all the specimens increased with time due to loss of free water. The drying shrinkage also increased significantly with the increasing content of recycled aggregates. This can be explained by the high water absorption value of the recycled aggregates which led to great volume change in the drying condition.

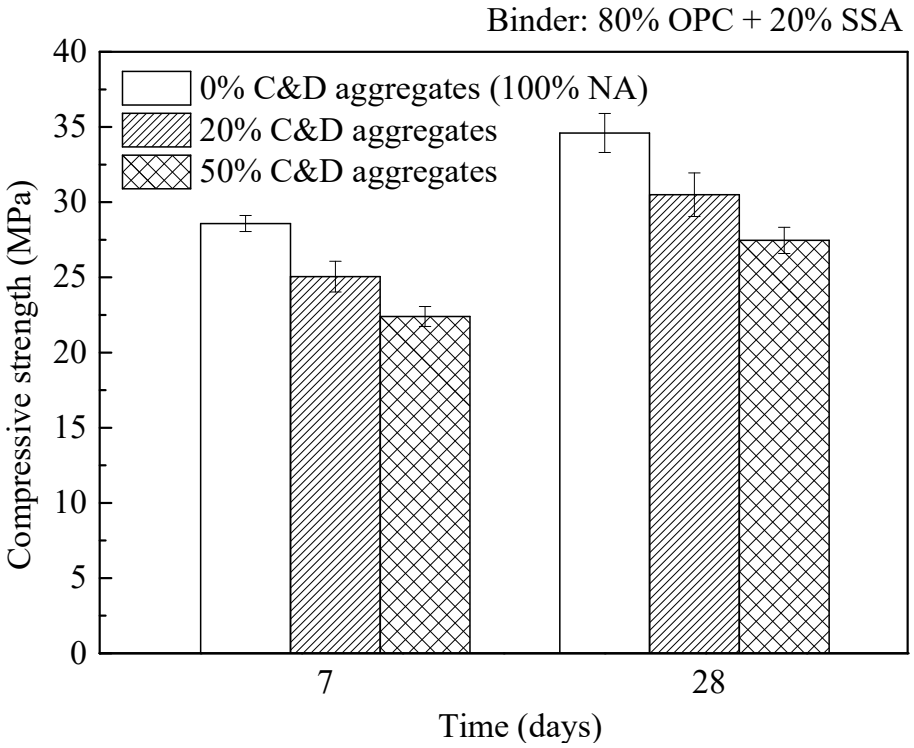

(a)

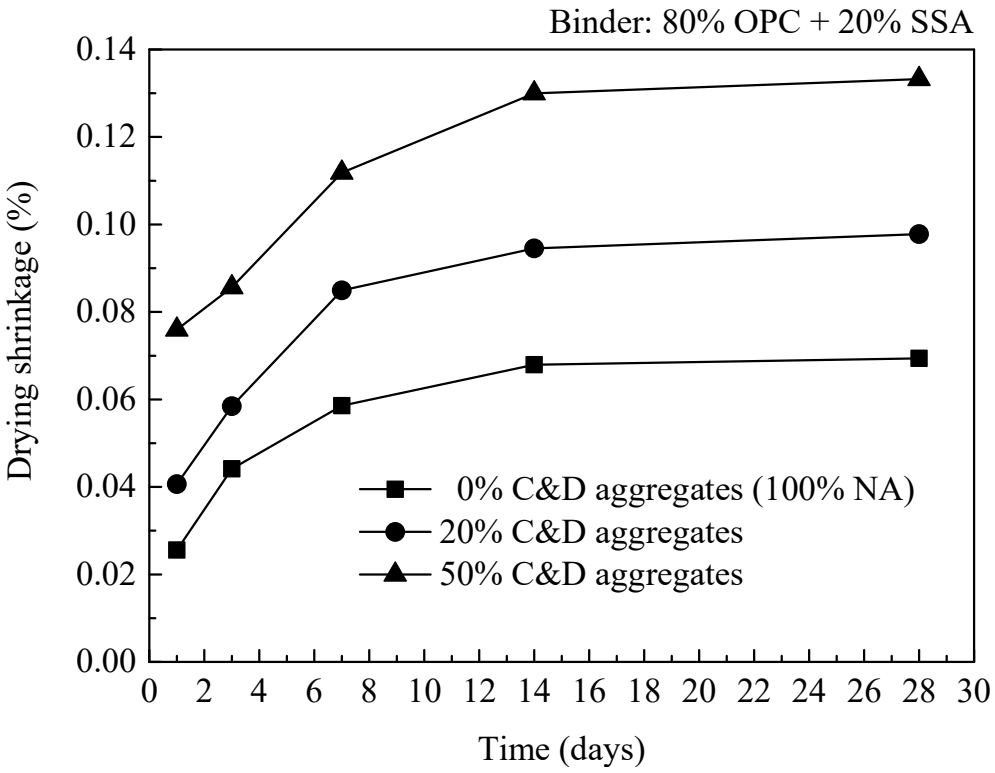

(b)

Fig. 5.1. Effects of using C&D aggregates on compressive strength and drying shrinkage of blocks with 20% SSA in binder

5.3 Concrete Blocks Made with Recycled GC

5.3.1 W/B Ratios for Preparation of the Concrete Blocks

As the block specimens were produced using just sufficient water to achieve similar consistency, the amount of water required for producing the blocks varied depending

on different constituents in the blocks. Fig. 5.2 shows the changes of w/b ratio in different mixtures containing GC. It can be seen that at higher GC contents, less water was required. This is due to the much lower water absorption value and the smooth surface of the GC.

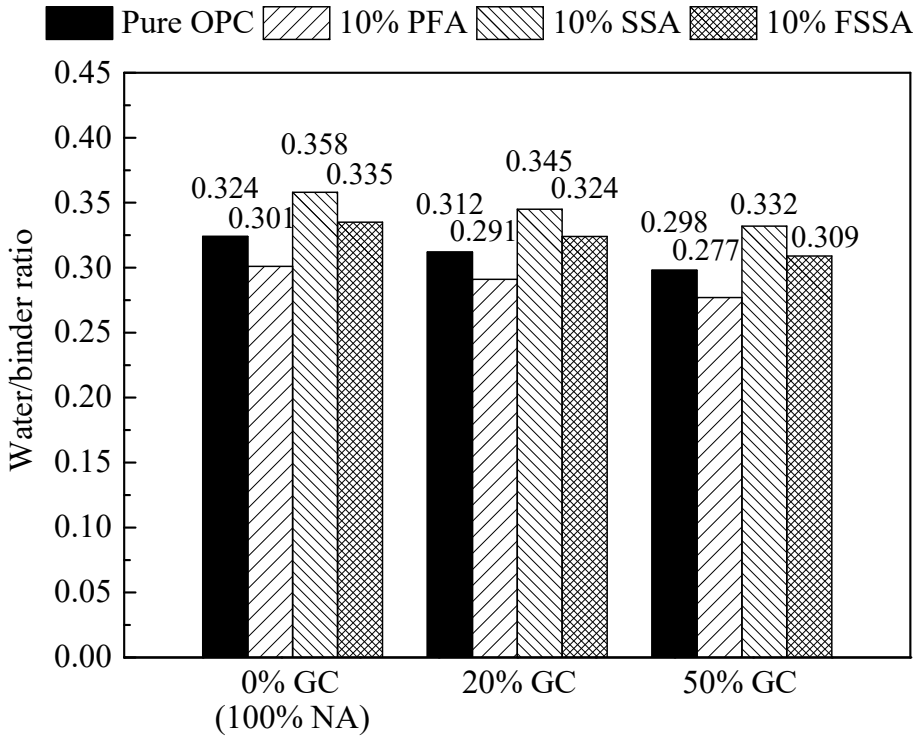

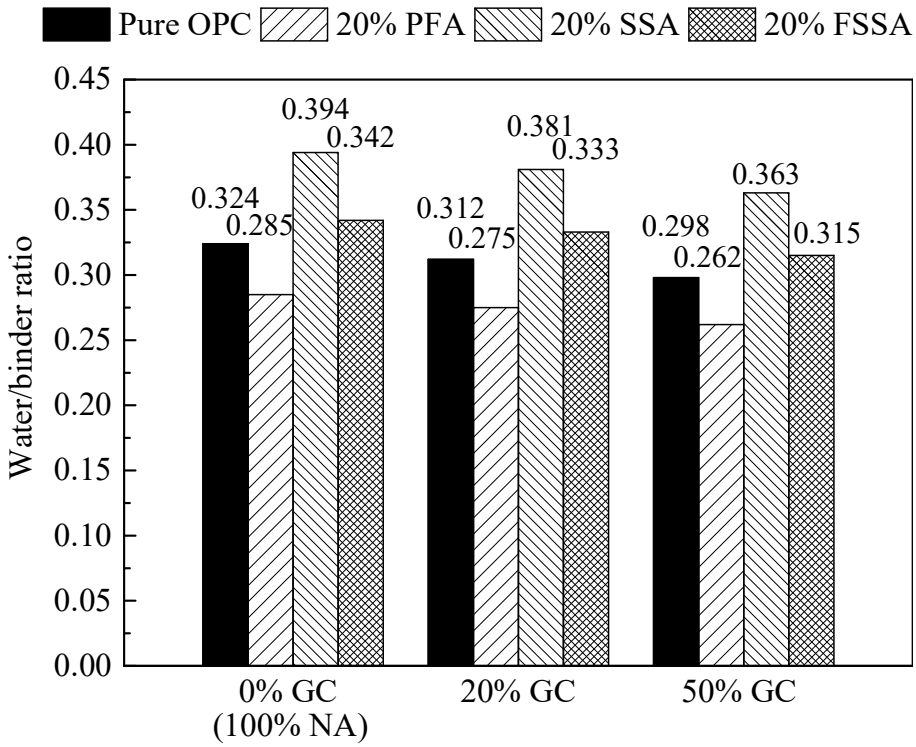

Fig. 5.2. W/B ratios for producing blocks with different contents of GC and different binder compositions

Disregarding the effects from aggregates, less water was required in blending the FSSA in the binder than the SSA of the same content to achieve the same consistency because after grinding SSA particles became smoother and less porous (Chen et al., 2013). The least amount of water was required in the case of PFA due to the ball-bearing effect of the PFA particles (Haleem et al., 2016; Zheng et al., 2016). The higher water requirements of SSA and FSSA blocks compared to PFA blocks were due to the porous characteristic of the SSA and FSSA particles which took up more water.

5.3.2 Hardened Density

Fig. 5.3 shows the hardened densities of different concrete blocks. The results show that the density decreased with the incorporation of more GC to replace the NA. This is due to the density of GC is lower than that of the NA.

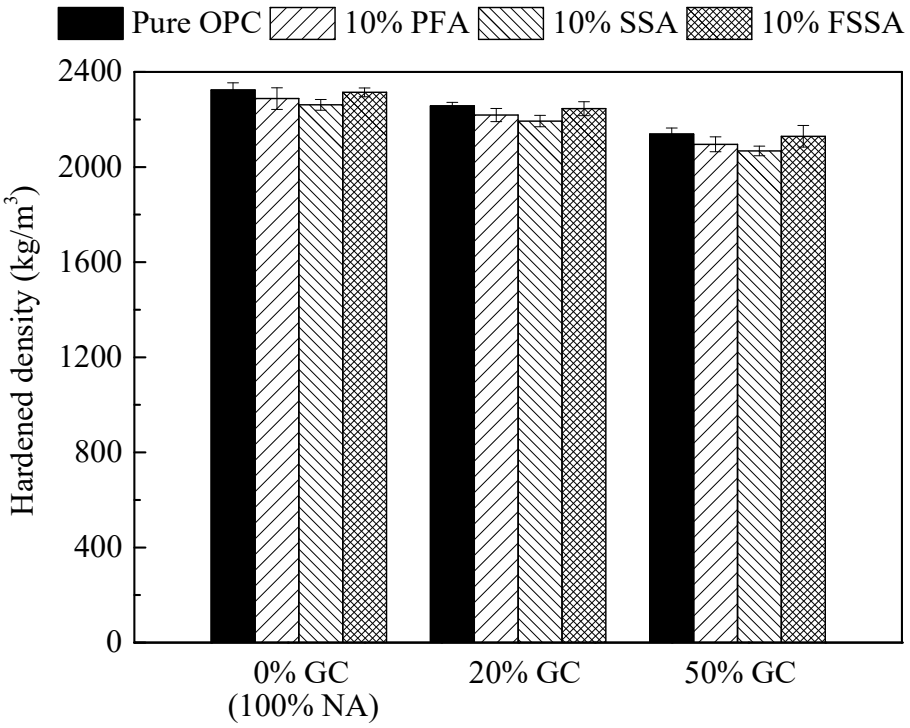

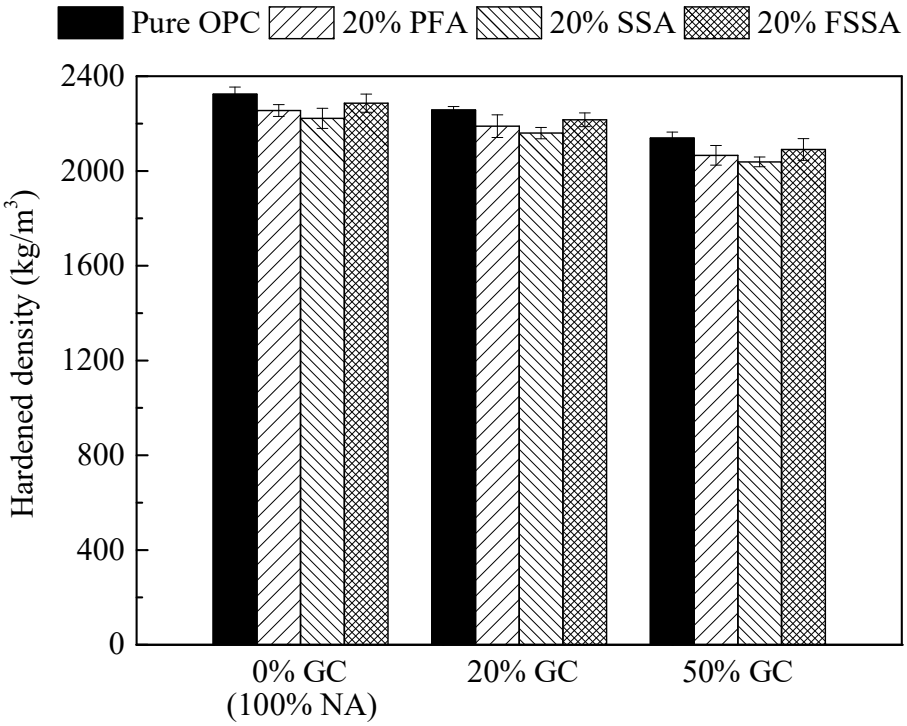

Fig. 5.3. Hardened densities of blocks with different contents of GC and different binder compositions

In terms of the binder, the densities of the blocks did not change too much with the incorporation of more PFA, SSA or FSSA to replace cement considering variabilities in experimental results. The order of block densities, ranked from high to low is FSSA blocks followed by the PFA blocks and then the SSA blocks. This order matches with the order of their specific gravity from high to low and also their fineness. It is believed that finer particles may fill more voids within the mixes leading to slightly higher density of the blocks.

5.3.3 Compressive Strength

The compressive strength of the different block specimens after curing for 28 days are presented in Fig. 5.4. It can be observed that the compressive strength decreased with the incorporation of more GC to replace the NA. However, it was evident that GC performed better than the recycled aggregates in contributing to compressive strength (Fig. 5.1). With the binder containing 20% SSA, the compressive strength of the blocks made with 20% and 50% GC only reduced by 6.4% and 13.0% respectively, whereas reductions of 11.8% and 21.6% occurred using 20% and 50% recycled aggregates in the blocks. The irregular shape of the GC might reduce the compactness of the blocks and their compressive strength (Park et al., 2004). Besides, the weaker bond between the GC and cement paste might also cause further decrease in the compressive strength (Topçu and Canbaz, 2004). However, the blocks prepared with GC showed higher compressive strength than similar blocks prepared with C&D aggregates. This phenomenon might be due to the higher individual particle strength of GC compared to C&D aggregates (Arulrajah et al., 2014).

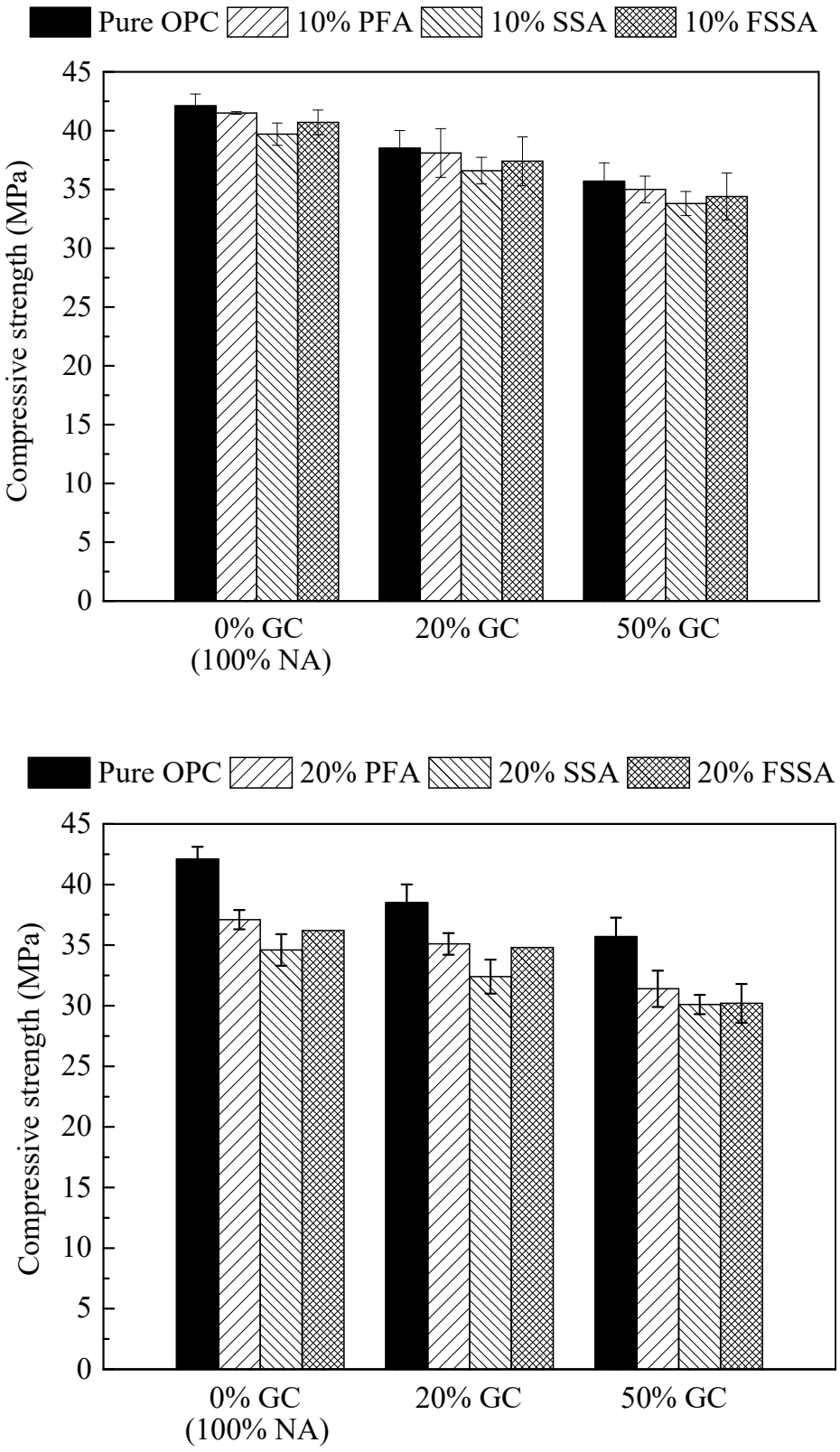

Fig. 5.4. 28-day compressive strength of blocks with different contents of GC and different binder compositions

Excluding the effects of aggregates, 10% replacement of OPC with SSA or FSSA caused little effect on the strength of the blocks. However, increasing the content of SSA or FSSA in the binder to 20% resulted in some reduction in the strength. Nevertheless, at the replacement level of 20%, the SSA concrete blocks could still achieve 28-day compressive strength of 34.6 MPa, 32.4 MPa and 30.1 MPa with using 0% GC (100% NA), 20% GC and 50% GC as aggregates respectively. The strength would further increase by up to 12% after two more months of curing due to slow pozzolanic activity of the SSA (results not shown here). Higher compressive strength could be achieved in the PFA blocks at the same cement replacement levels due to its higher pozzolanic activity. Slightly higher strengths could be achieved by using the FSSA than SSA due to the better pozzolanic activity. The strength development therefore depended mainly on the pozzolanic activities of PFA, SSA and FSSA.

5.3.4 Water Absorption

Fig. 5.5 shows the water absorption values of the block specimens. It can be seen that the water absorption reduced with increasing content of GC in the blocks. This benefit obviously came from the non-hydrophilic nature of the GC.

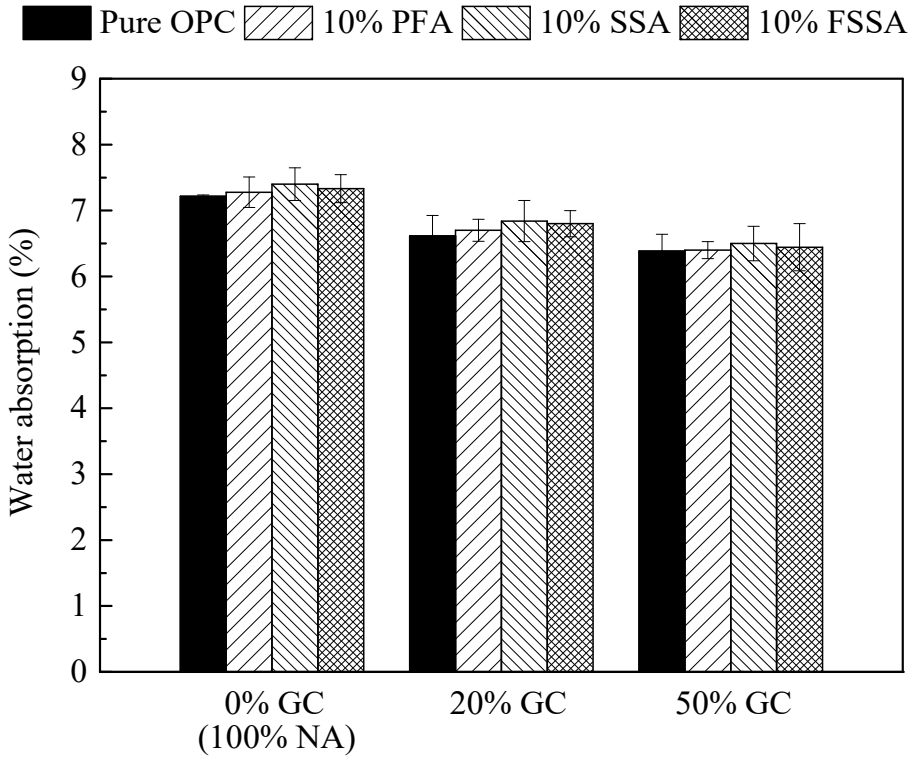

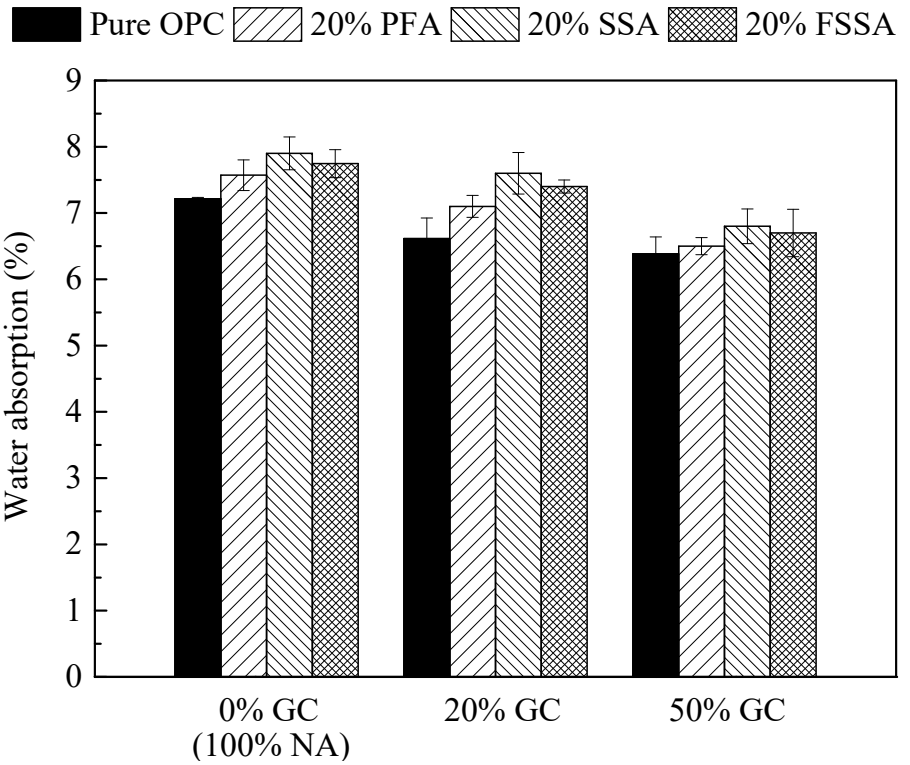

Fig. 5.5. Water absorption of blocks with different contents of GC and different binder compositions

With the same composition of aggregates, the blocks produced with 20% of PFA, SSA or FSSA blended in the binder all showed higher water absorption compared with blocks made with the pure cement binder. The highest being the SSA blocks, followed by the FSSA and the PFA blocks. This phenomenon correlated with the strength development of these blocks which reflected the degree of porosity and water absorptivity (Farhana et al., 2015; Prahara, 2014). As discussed earlier, the PFA blocks exhibited the highest strength, followed by the FSSA and the SSA blocks.

5.3.5 Drying Shrinkage

The results of the drying shrinkage tests of the block specimens containing GC are shown in Fig. 5.6. As the GC did not absorb water and the zero absorption characteristic restricted water migration, the shrinkage value reduced with increasing amount of GC in the blocks.

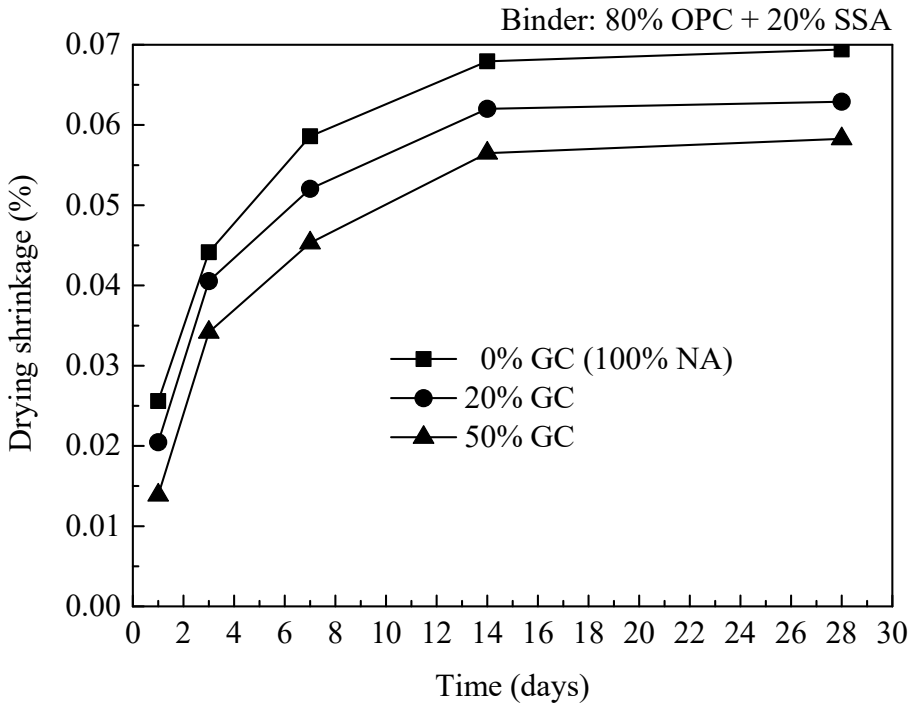
Binder: 80% OPC + 20% SSA
Drying shrinkage (%)
Time (days)
0% GC (100% NA)
20% GC
50% GC

(a)

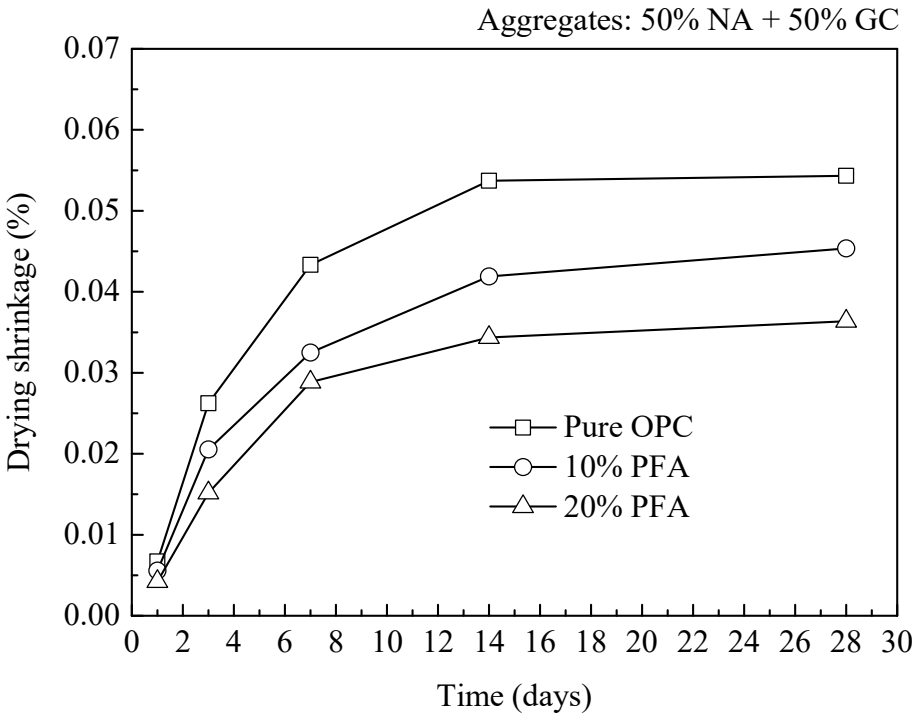
Aggregates: 50% NA + 50% GC
Drying shrinkage (%)
Time (days)
Pure OPC
10% PFA
20% PFA

(b)

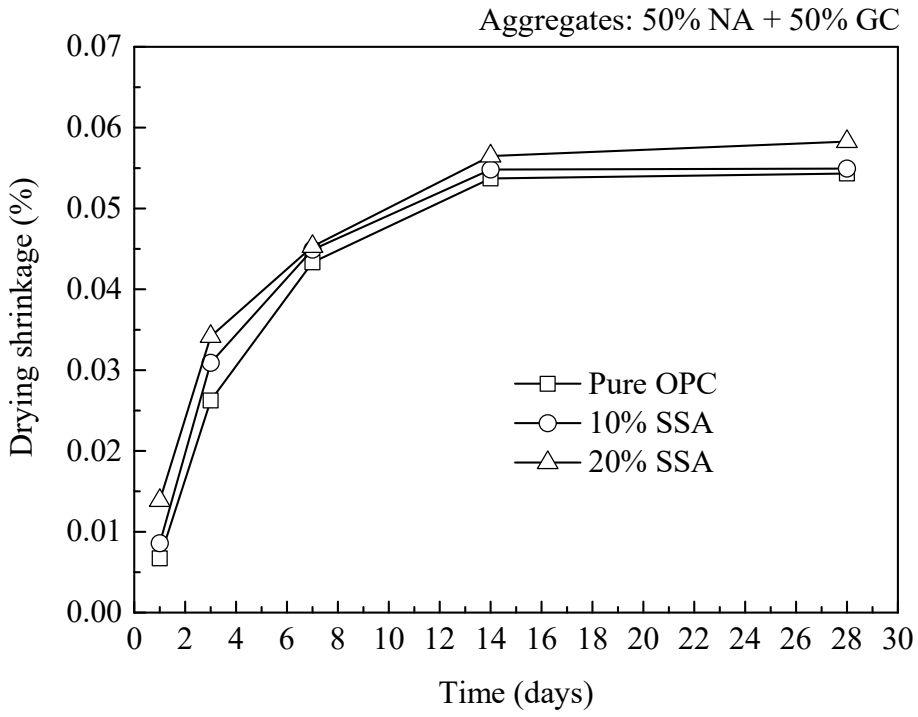
Aggregates: 50% NA + 50% GC
Drying shrinkage (%)
Time (days)
Pure OPC
10% SSA
20% SSA

(c)

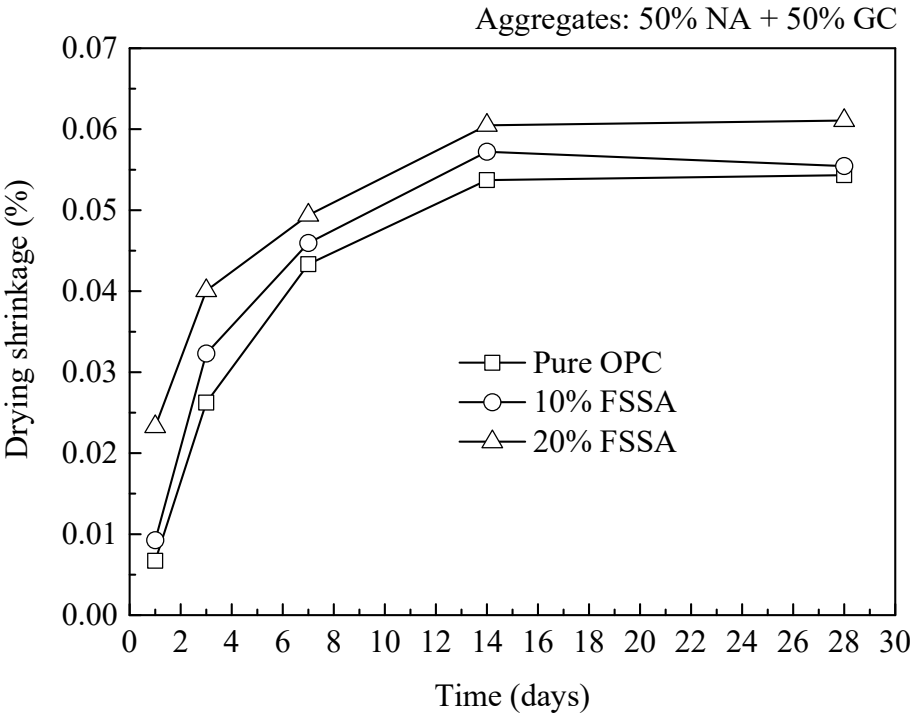
Aggregates: 50% NA + 50% GC
Drying shrinkage (%)
Time (days)
Pure OPC
10% FSSA
20% FSSA

(d)

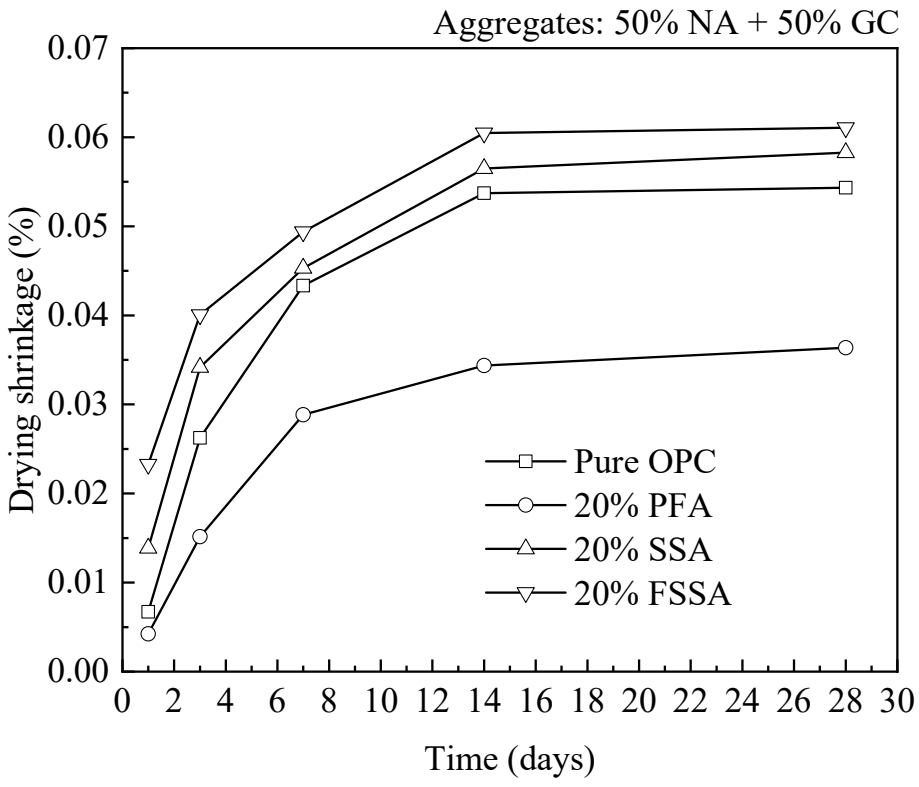

(e)

Fig. 5.6. Drying shrinkage of blocks with different contents of GC (a) and different binder compositions (b)-(e)

On the other hand, the blending of SSA or FSSA in the binder increased the drying shrinkage. This occurred because the SSA and FSSA are porous and absorbed more water during casting which led to subsequent higher shrinkage. The problem was worse with FSSA due to its finer particle size and larger surface area making it easier for water to dry out. But this problem could be alleviated through the combined use of GC in the aggregates because GC could reduce the drying shrinkage.

5.3.6 ASR

The potential ASR problem of the blocks containing GC was examined on blocks made with 100% GC as aggregates. The average expansion results are shown in Fig. 5.7. The expansion of the control specimen without the use of PFA, SSA or FSSA was found to be higher than the deleterious limit of 0.1% at 14 days set by ASTM C1567 (2013). However, the ASR expansion decreased with increasing contents of PFA, SSA or FSSA in the binder. The expansion was reduced to below the deleterious limit when the content of SSA or FSSA was increased to 20%. The results show that the SSA and FSSA were very effective in reducing ASR expansion caused by the GC. It is believed that the mechanism was similar to those of other pozzolans suppressing ASR expansion (Idir et al., 2010; Taha and Nounu, 2008; Venkatanarayanan and Rangaraju, 2013). It is therefore feasible to produce concrete blocks with high contents of GC as aggregates with appropriate amounts of SSA to control ASR.

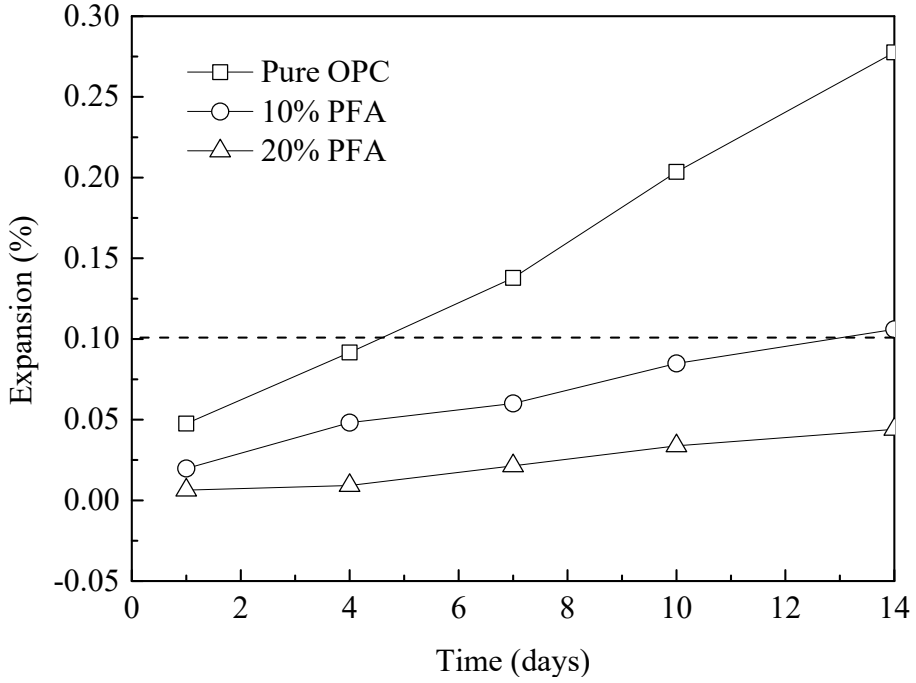
Pure OPC
10% PFA
20% PFA
Expansion (%)
Time (days)
0.30
0.25
0.20
0.15
0.10
0.05
0.00
-0.05
0
2
4
6
8
10
12
14

(a)

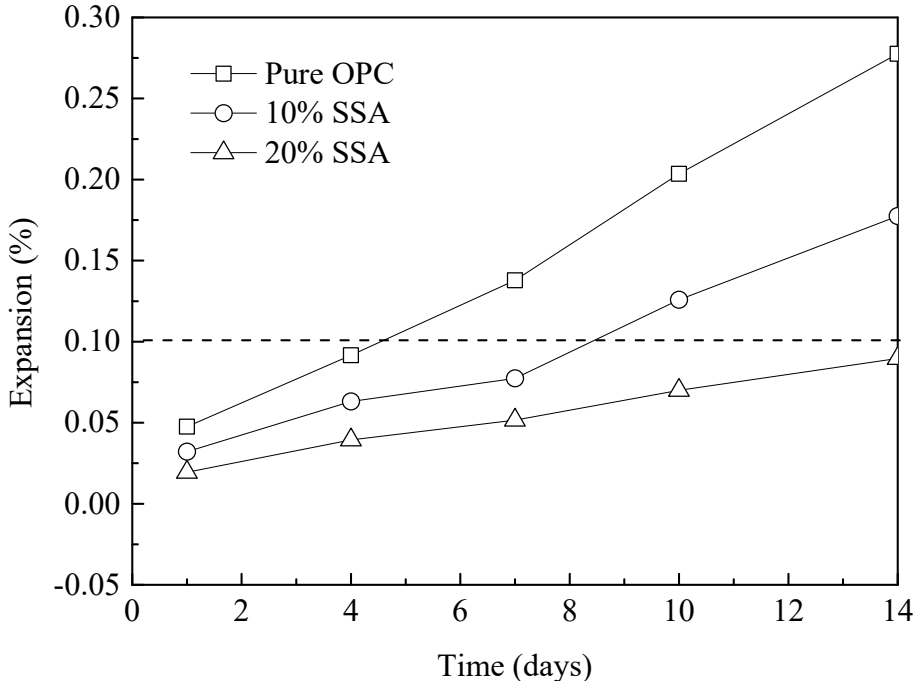
Pure OPC
10% SSA
20% SSA
Expansion (%)
Time (days)
0.30
0.25
0.20
0.15
0.10
0.05
0.00
-0.05
0
2
4
6
8
10
12
14

(b)

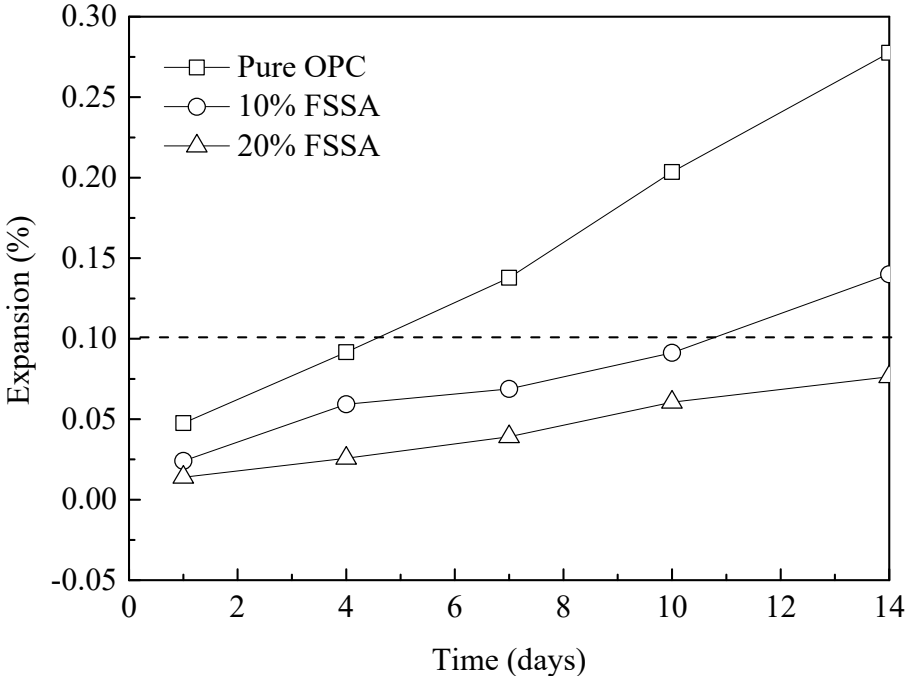

(c)

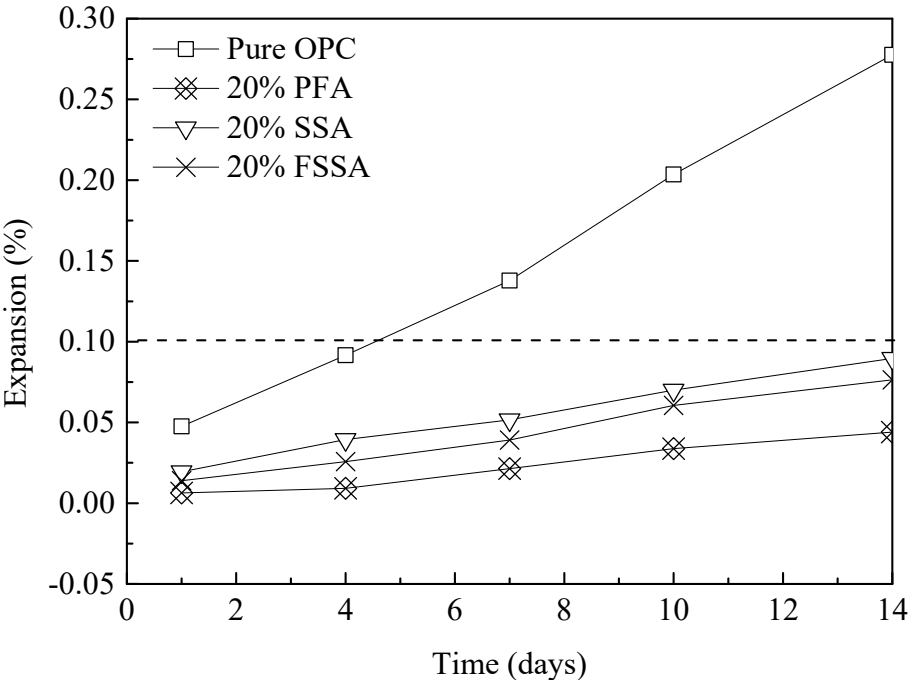

(d)

Fig. 5.7. Alkali-silica expansion from GC with different binder compositions

5.4 Leaching of Metal(loid)s from Blocks

The test results shown in Table 5.1 reveal that leaching of metal(loid)s from the ash-containing blocks were well below the specified limits, indicating that the SSA can be safely used as a substitution of OPC at 20%. It is noted that the leaching of some metal(loid) concentrations were higher from the blocks than the SSA alone. This may be due to the amphoteric behavior of some metal(loid)s and the metal(loid)s were present in the GC (Komonweeraket et al., 2015; Li and Poon, 2017). Nonetheless, all the leachate concentrations were below the stipulated TCLP limits.

Table 5.1 Leachable metal(loid) concentrations from blocks with 20% FSSA in binder and GC as aggregates

Element	Leachate (mg/L)	Element	Leachate (mg/L)	Element	Leachate (mg/L)
Sb	0.005	As	< DL	Ba	0.2985
Cd	< DL	Cr	0.0815	Cu	< DL
Pb	0.068	Ni	0.022	Co	0.003
Se	0.0425	Sr	2.5695	Ag	< DL
Zn	< DL				

5.5 Factory trial production of blocks

Trials on factory production of the concrete blocks were conducted at TIOSTONE Holdings Ltd. in Hong Kong after the laboratory studies. Based on the experimental results and existing guidance RD/GN/044A (2017) which recommends GC in paving blocks constitute only 20 to 25% by weight of the total aggregates, SSA was used to replace 10% of OPC and GC was used to replace 25% of NA. The materials were mixed in a drum mixer (Fig. 5.8). The blocks were moulded with an automatic block-making machine, under both vibration and compressive force of 80 psi for 12 seconds. The shape of the 60 mm thick concrete blocks is shown in Fig. 5.8. The blocks were then cured in air and the compressive strength were tested at the ages of 7, 28 and 60 days.

(a) Block-making machine

(b) Produced blocks

Fig. 5.8. Photos of factory production of blocks

Table 5.2 shows the compressive strength of concrete blocks with or without the incorporation of SSA at different ages. The compressive strength of the blocks satisfies the requirements for paving units on public footways and cycle tracks specified by Highways Department in Hong Kong (RD/GN/044A, 2017).

Table 5.2 Compressive strength of concrete blocks produced in factory

	7 days	28 days	60 days
Control	62.2	65.3	71.4
SSA block	46.3	55.4	62

Agreement has been made with an organization to lay the SSA blocks on about 300 sq meters of open ground. Blocks have been produced and the performance of the blocks on site will be monitored.

5.6 Summary

The experimental work produced the following results:

(1) Higher SSA content in the binder demanded more water to achieve similar consistency in the wet mixes due to the hydrophilic nature of the SSA.

(2) The SSA did not satisfy the reference criterion of a good pozzolan according to the SAI test. However, the index of the SSA increased with time. A combination of both results of Frattini and SAI tests, the SSA was considered to possess moderate pozzolanic activity.

(3) The blending of up to 20% SSA or FSSA in the binder increased the water absorption values of the concrete blocks but the effects on hardened densities were not obvious.

(4) With no more than 20% of the SSA in the binder and with 50% of NA replaced by GC, the 28-day compressive strength of concrete blocks could exceed 30 MPa.

(5) The use of recycled GC as aggregates generated the lowest drying shrinkage, followed by NA, and the recycled C&D aggregates generated the highest drying shrinkage.

(6) The drying shrinkage of concrete blocks increased with the SSA content, which limited the use of the SSA in concrete block production. Using recycled GC as fine aggregates together with SSA in concrete blocks production may reduce the drying shrinkage due to the impermeable nature of recycled GC.

(7) The SSA was very effective in reducing ASR expansion caused by the recycled GC aggregates. Around 20% of the SSA in the binder could assure the control of ASR expansion if all aggregates were recycled GC.

(8) The SSA contained some harmful metal(loid) elements, but the leachate amounts were very small and well below the specified US EPA limits for hazardous waste identification. Therefore, the SSA could be considered as a nonhazardous waste. Furthermore, blending the SSA in concrete blocks could effectively immobilize the metal(loid)s making the blocks totally safe to humans and the environment.

(9) It is feasible to produce concrete blocks with a high content of recycled GC as aggregates and the SSA as a SCM in view of their complimentary effects. The optimal content of the SSA in the binder was 20% for producing concrete blocks with satisfactory strength and low ASR risk.

(10) In the trial study, the compressive strength of concrete blocks met the requirement for paving units in footways and cycle tracks and further long-term properties are being monitored.

CHAPTER 6 – COMPRESSIVE STRENGTH AND MICROSTRUCTURAL PROPERTIES OF DRY-MIXED GEOPOLYMER PASTES SYNTHESIZED FROM GGBS AND SSA

6.1 Introduction

Geopolymers are promising materials to replace cement as alternative binder materials in construction works. The synthetization of geopolymers is an environmental-friendly process in which three-dimensional aluminosilicate materials are synthesized. SSA is rich in SiO_2, Al_2O_3 and CaO, which are the most active compounds for geopolymerization. It is a potential source material of geopolymer. The use of GGBS to produce geopolymers has been successful but knowledge on geopolymerization of SSA or its effects on other geopolymers remain limited. This study aimed at examining geopolymerization of mixtures of GGBS and SSA in equal weight further with binary alkaline activators, namely, NaOH and Na_2SiO_3. Focus was made on the effects of weight percentage of alkali to the mixed solids, i.e., Na_2O content, and molar ratio of SiO_2 to Na_2O in the mixed alkaline activator, i.e. modulus, on the compressive strength of geopolymer pastes, and the microstructural characteristics of the geopolymer pastes. The dry-mixed compression method was applied to prepare specimens to overcome molding problem due to the poor workability of the mixtures. Compressive strength of the hardened geopolymer

pastes were tested and their microstructure and composition were analyzed by XRD, QXRD, FTIR, SEM and EDX. Since long term shrinkage is a major durability concern and drying shrinkage generally accounts for most of the overall long-term shrinkage (Wallah and Hardjito, 2014), this study also provided preliminary results of drying shrinkage tests for reference in further durability study and supporting the practical value of recycling GGBS and SSA as dry-mixed geopolymers. As sewage sludge is a residue from wastewater treatment in which metal(loid)s accumulate and such metal(loid)s may remain in the ash after thermal treatment of sewage sludge, the leaching of metal(loid)s is also a concern in recycling SSA (Fang et al., 2016; Li and Poon, 2017; Li et al., 2017). Therefore, the leachability of metal(loid)s from the raw mixed solids and the geopolymer products were tested. Test results are provided in the following sections.

6.2 Compressive Strength

Fig. 6.1 shows the variation of compressive strength with different Na_2O contents and moduli in the geopolymer pastes. Raising Na_2O content could enhance the compressive strength of the geopolymer pastes until the percentage reached about 4.0%. The increase in compressive strength was possibly due to the availability of more alkali to attack the precursors generating more dissolved species which enhanced geopolymerization of the pastes (Wang et al., 2005). However, the strength

dropped when the Na_2O content was above 4.0%. This can be explained by early precipitation of some geopolymer gel due to elevated reaction blocking potential precipitation of more gel (Lee and Van Deventer, 2002).

Similarly, the compressive strength increased initially with the modulus but dropped after an optimal value. Higher modulus means higher Si concentration which enhanced the reaction with calcium (Ca) to form C-S-H gel and aluminosilicate components to from T-O-Si (T = Si or Al) (Krizan and Zivanovic, 2002). However, the beneficial effect only appeared up to a certain level. Strength increased with the modulus up to about 0.95 and dropped thereafter. The drop may be due to too much Na_2SiO_3 hindering the release of air bubbles, evaporation of water, and formation of geopolymers by blocking the contact between the precursors and the alkaline solution (Cheng and Chiu, 2003).

Therefore, at Na_2O content of 4.0% and modulus of 0.95, an optimal condition was reached which was most favorable for strength development. A maximum strength of 32.81 MPa at 28 days of the pastes could be attained.

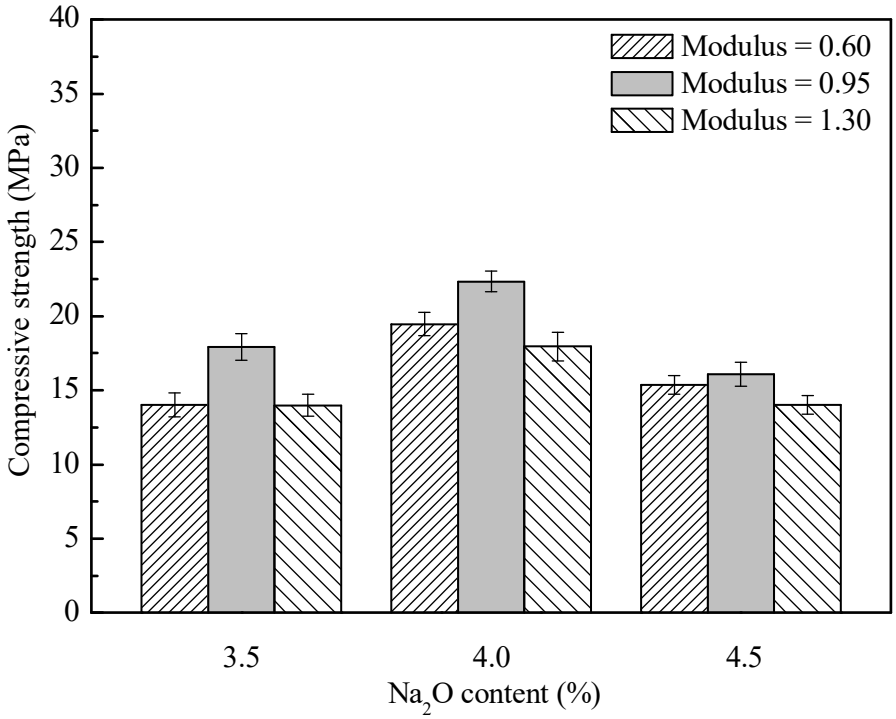

(a)

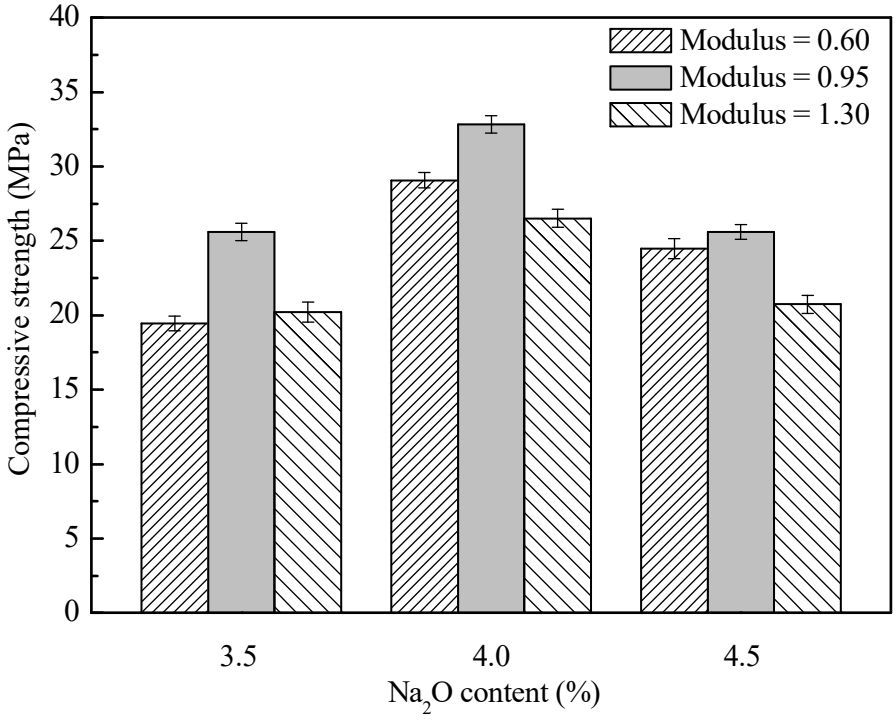

(b)

Fig. 6.1. Effects of Na_2O content and modulus on the compressive strength of geopolymer pastes aged of (a) 7 days and (b) 28 days

6.3 XRD Analysis

Fig. 6.2 shows the XRD patterns of GGBS and SSA. Very different from SSA, GGBS exhibited a broad amorphous hump with no distinct crystalline peaks.

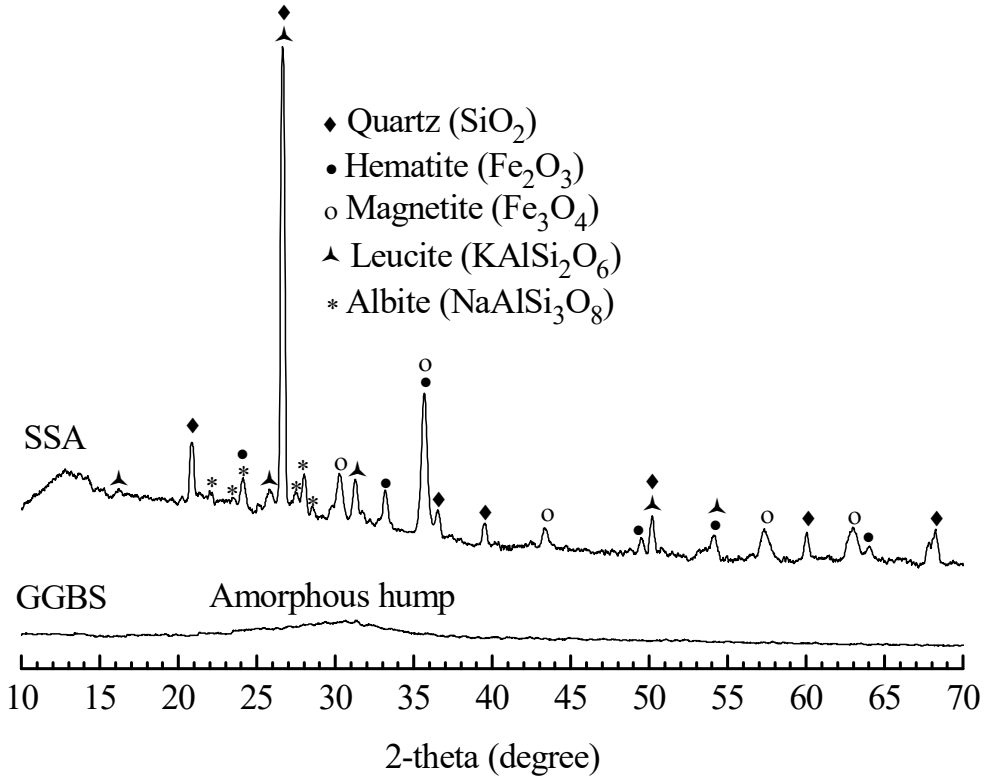

Fig. 6.2. XRD patterns of GGBS and SSA

Fig. 6.3 shows the XRD patterns of the raw mixed solids and geopolymer pastes synthesized from different Na_2O contents. Fig. 6.4 shows the XRD patterns of the

raw mixed solids and geopolymer pastes synthesized from different moduli. The pattern of the raw mixed solids was the combined patterns of GGBS and SSA. The crystalline peaks in the pattern were mainly associated with the SSA. The geopolymer pastes contained crystalline phases similar to those in the raw mixed solids. However, the XRD patterns exhibited sharp reduction in the intensities of crystalline peaks indicating the occurrence of geopolymerization reactions. The intensities associated with quartz were reduced. Hematite which existed in the raw mixed solids was not found. No new crystalline phase was discovered. The results of XRD tests indicated crystalline minerals in the SSA being integrated into the geopolymerization products. The intensities of peaks in the paste formed with Na_2O content of 4.0% and modulus of 0.95 were the lowest indicating the greatest amount of geopolymer gels formed in this paste (see Fig. 6.3c and Fig. 6.4c). It is worth recalling that the highest strength was obtained from the same paste. At 28 days of age, except for gaining the greatest compressive strength in geopolymer pastes using Na2O content of 4.0% as shown in Fig. 6.1b, the crystallinity content in the specimen was the lowest as shown in Fig. 6.3 (XRD of pastes at 28 days). Similarly, the highest compressive strength was obtained at the modulus of 0.95 as shown in Fig. 6.1b and the degree of crystallinity in the specimen was the lowest as shown in Fig. 6.4 (XRD of pastes at 28 days). It should be pointed out that trace minerals are not always present in XRD, so the use of QXRD is required to provide complimentary information on the mineral quantity (Ruffell and Wiltshire, 2004; Wiskel et al., 2018).

Besides, broad diffuse scattering humps extending from 20^{o} to 40^{o} 2θ appeared in all the geopolymer pastes. These humps were reported as amorphous aluminosilicate gels and known as finger print area of geopolymerization (Yaseri et al., 2017). It was reported that the Ca-O bond was much weaker than the Si-O and Al-O bonds, more Ca dissolved in water and reacted with the Si to form C-S-H (Rajaokarivony-Andriambololona et al., 1990). In the presence of Al, the C-S-H gel transformed C-S-H → C-(A)-S-H → C-A-S-H (calcium aluminate silicate hydrate), and if Ca was present, it would likely be adsorbed preferentially and N-A-S-H (sodium aluminate silicate hydrate) would exist if there was insufficient Ca (Garcia-Lodeiro et al., 2011 and 2013). Therefore in the present study, the aluminosilicate gel formed was likely to be C-A-S-H or a combination of both C-A-S-H and N-A-S-H gels.

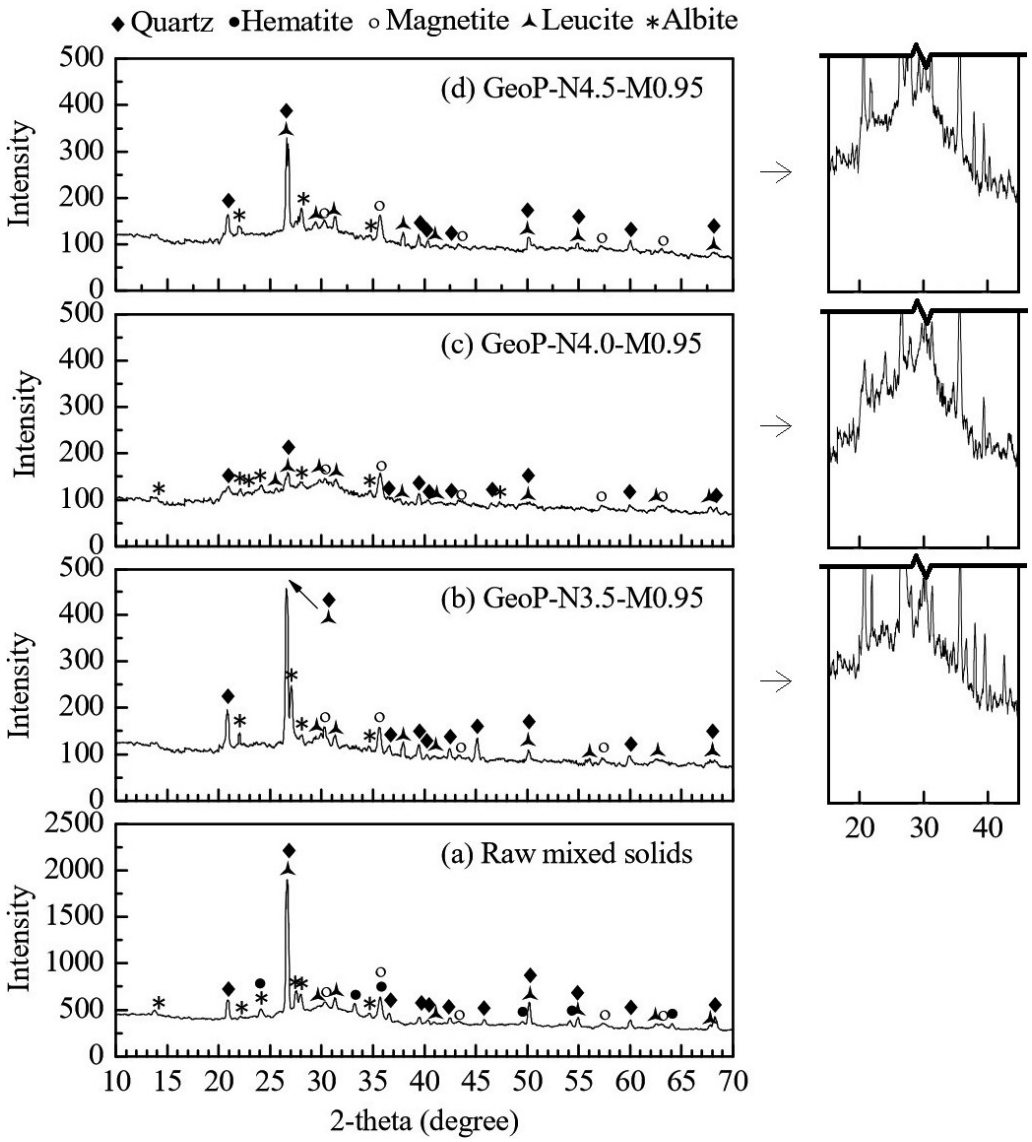

Fig. 6.3. XRD patterns of raw mixed solids and geopolymer pastes synthesized from different Na_2O contents

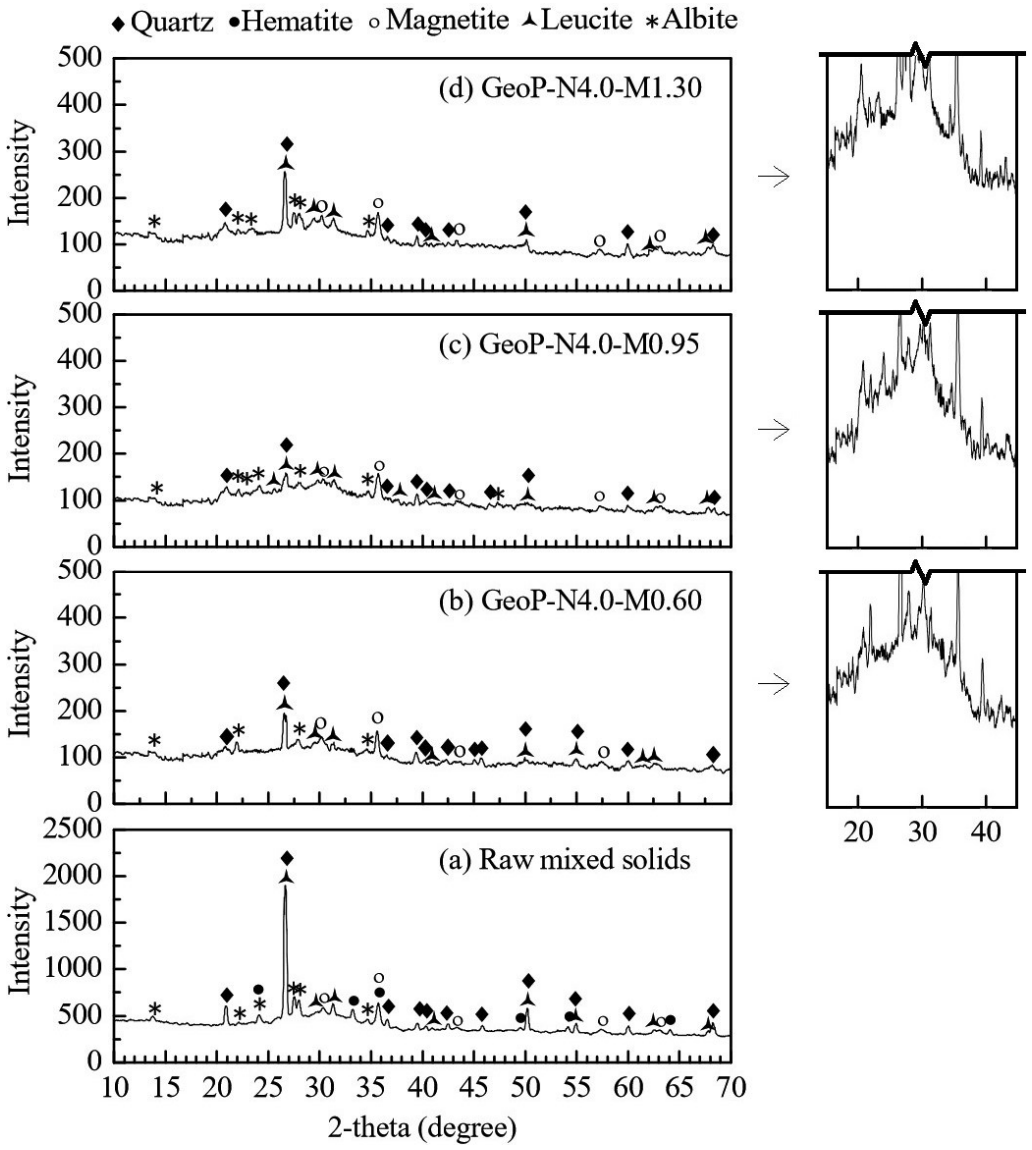

Fig. 6.4. XRD patterns of raw mixed solids and geopolymer pastes synthesized from different moduli

6.4 QXRD Analysis

The results of QXRD analyses on the formation of non-crystalline phases, i.e., amorphous and semi-crystalline phases, are presented in Fig. 6.5. The overall

contents of the non-crystalline phases in the specimens before and after geopolymerization were both very high although there were changes in the compositions of the non-crystalline phases. Considering the margin of errors, very little changes in the quantities of albite, leucite and magnetite were noted before and after geopolymerization indicating that these minerals had not participated in the geopolymerization. Hematite and quartz contents decreased in the geopolymer pastes indicating changes from crystalline phases to amorphous or semi-crystalline phases with dissolution. Crystalline silica was found to be structurally deformed and partially dissolved by weak alkaline solutions but at a much slower rate compared with amorphous silica (Baltakys et al., 2007). The transformation of hematite crystal into amorphous or semi-crystalline phase indicated that iron (Fe) in the SSA may be involved in the geopolymerization. Specimens prepared with Na_2O content of 4.0% and modulus of 0.95 contained the highest proportion of all non-crystalline phases. The QXRD analyses confirmed the findings in the XRD.

Comparing the total contents of non-crystalline phases after geopolymerization with the compressive strength, it can be found that geopolymer paste synthesized from the optimal Na_2O content of 4.0% and modulus of 0.95 in the alkaline activator contained the largest quantity of non-crystalline phases and gave the highest compressive strength. The increase in non-crystalline content seemed to be correlated with the increase in compressive strength. This relationship was also noted in the specimens

of GeoP-N3.5-M0.95 and GeoP-N4.5-M0.95. It can be seen from Fig. 6.5 (QXRD of pastes at 28 days) that these two specimens contained similar total amounts of non-crystalline phases and showed similar compressive strength as shown in Fig. 6.1b. However, this relationship was not always valid as seen from results of other specimens. Previous studies indicated that only the amorphous reaction product (geopolymer gel) influenced the compressive strength (Bhagath Singh and Subramaniam, 2016; Ziolkowski and Kovtun, 2018). That is, higher geopolymer gel contents gave rise to higher compressive strength of geopolymer paste. In view of the high compressive strength in the optimal specimen GeoP-N4.0-M0.95, it was expected that the non-crystalline phases in the specimen mostly consisted of geopolymer gel phases and the raw materials should have undergone high degree of reaction during the geopolymerization. This result can be identified in SEM photographs of fracture surfaces on the specimen which will be discussed in the following sections.

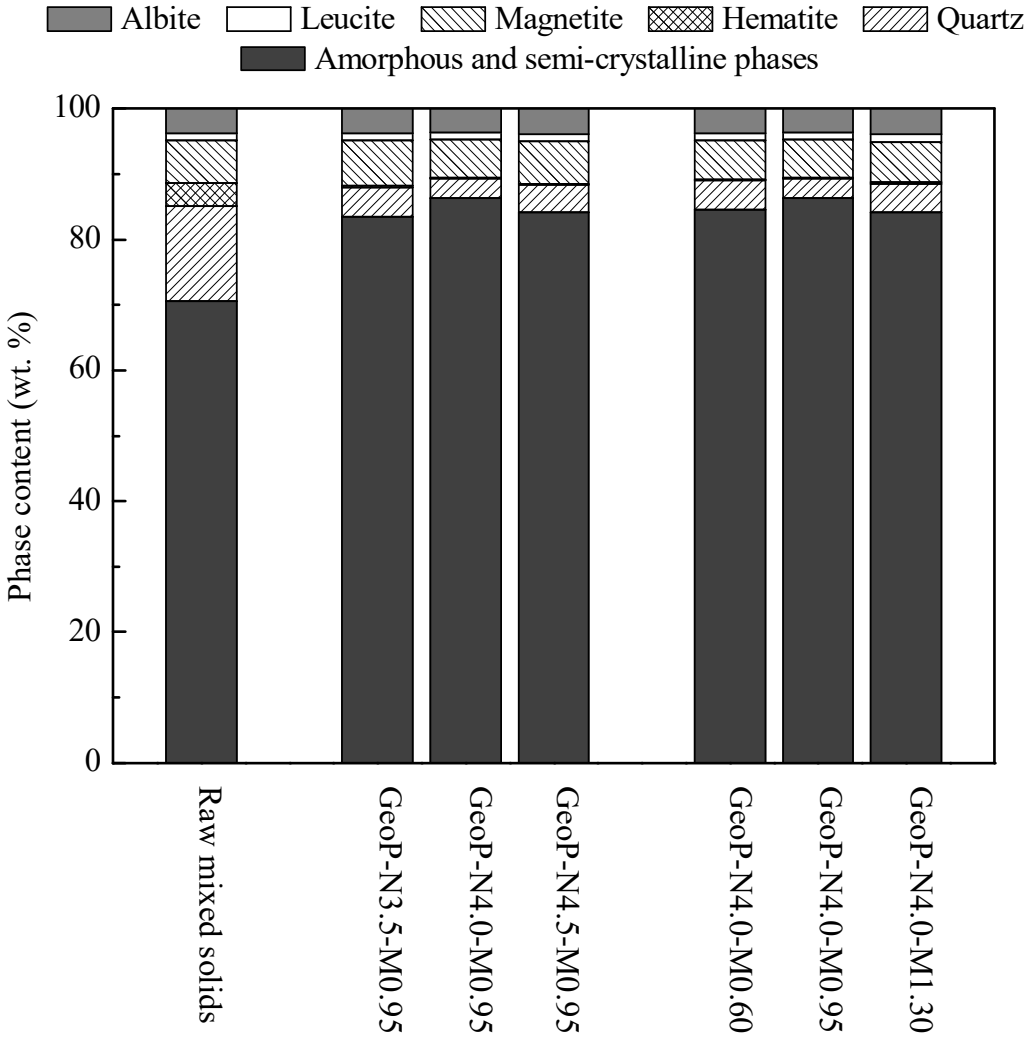

Fig. 6.5. Phase contents of raw mixed solids and geopolymer pastes

6.5 FTIR Analysis

FTIR analysis can yield information about the organization of molecular chains regardless of the phase of the substance. Fig. 6.6 illustrates the FTIR spectra of GGBS and SSA. In the spectrum of GGBS, weak bands centered at 1437 cm^{-1} are associated with the asymmetric stretching of O-C-O bonds of carbonate groups (Yu et al.,, 2017) which may come from the carbonation of GGBS in the environment.

The vibrations at around 970 cm^{-1} are associated with the asymmetric stretching vibrations of T-O-Si (El-Gamal and Selim, 2017). The weak peak at 671 cm^{-1} is due to the symmetric stretching vibrations of the T-O-Si bonds (El-Didamony et al., 2012). The bands at around 503 cm^{-1} are originated from the in-plane O-T-O bending vibrations (Gu et al., 2015). SSA exhibited characteristic bands centered at 3544 cm^{-1} (Frost et al., 2011) and 3475 cm^{-1} (De Ligny et al., 2013) corresponding to the stretching vibrations of structural Al-OH groups and the band at 3414 cm^{-1} to the O-H stretching vibration under hydrogen bonded association inside molecules (Lin et al., 2017). Adsorption bands centered at 1638 cm^{-1} (Bai et al., 2012) and 1620 cm^{-1} (Litke et al., 2017) are due to the O-H bending of adsorbed H_2O molecules. Adsorption bands with peak located at 1124 cm^{-1} are the Si-O stretching vibrations (Kawano and Tomita, 1991). The peak occurring at 1097 cm^{-1} is associated with the sulphate ion existed in seawater (Petrone et al., 2011) which is widely used in Hong Kong for flushing. The peak at 1035 cm^{-1} is related to the stretching vibrations of Si-O-Si bonds (Ma et al., 2013). The peaks at 600 cm^{-1} (Schmitt and Flemming, 1998), 560 cm^{-1} (Toderaş et al., 2006) and 450 cm^{-1} (Lemougna et al., 2017) correspond to the Fe-O stretching vibrations of the hematite structure.

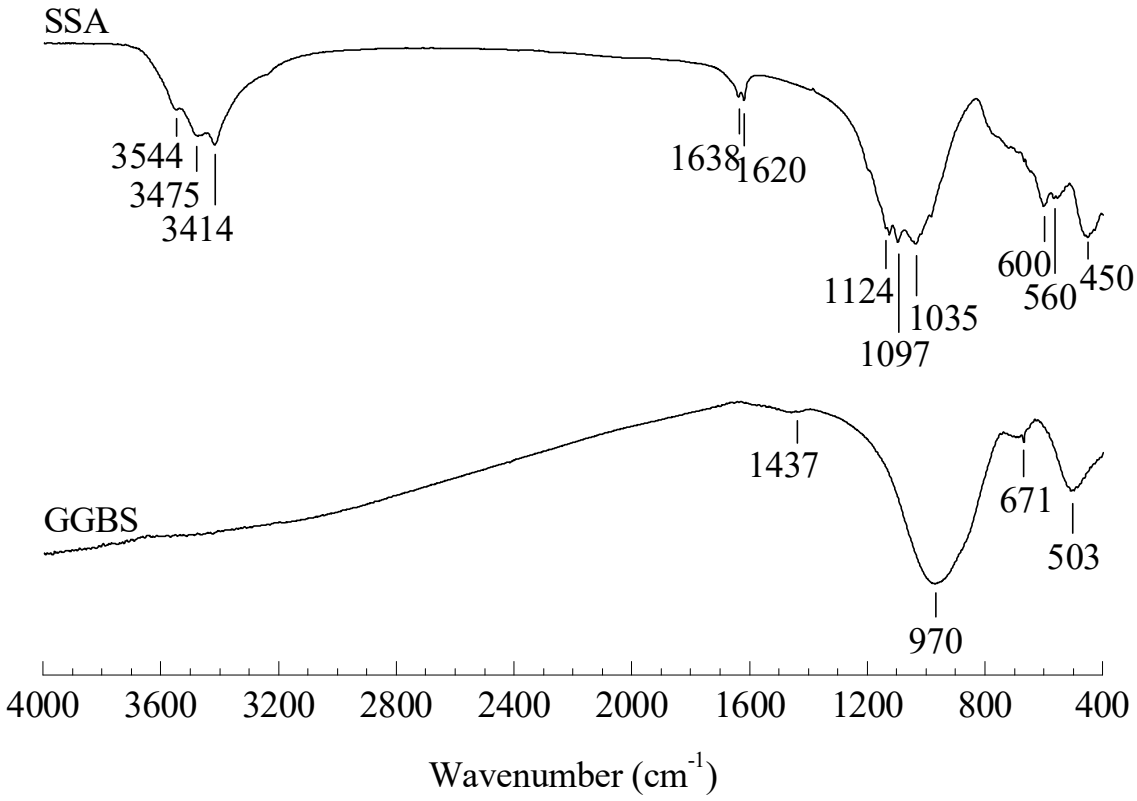

Fig. 6.6. FTIR spectra of GGBS and SSA

Fig. 6.7 shows the FTIR spectra of the raw mixed solid (Fig. 6.7a), geopolymer pastes synthesized from different Na_2O contents (Figs. 6.7b-d) and geopolymer pastes synthesized from different moduli (Figs. 6.7e-g). The raw mixed solids exhibits five specific spectral regions: (i) the overlapping bands at 3660 - 3120 cm^{-1} correspond to the stretching vibrations of Al-OH groups and O-H stretching under hydrogen bonded groups; (ii) the bands from 1708 to 1576 cm^{-1} correspond to the O-H bending of H_2O molecules; (iii) the absorption characteristic of sulphate ions in combination with stretching vibrations of Si-O and T-O-Si bonds appear in the zone 1281 - 841 cm^{-1}; (iv) stretching vibrations of Fe-O bonds appear in the zone 648 - 515 cm^{-1}, and,

(v) the in-plane O-T-O bending and Fe-O stretching vibrations appear from 515 to 400 cm^{-1}.

The FTIR spectra of the geopolymer pastes show clear differences with the spectrum of the raw mixed solids indicating structural changes in the geopolymerization. It shifted vibrations in the spectral region of 3660 - 3120 cm^{-1} to higher wavenumbers. With reference to the vibrations mentioned above, the Al-OH groups give sharp peaks at wavenumbers of 3544 cm^{-1} and 3475 cm^{-1}. Besides, from reports of previous researches, the bonds of hydrogen bonded silanol (SiO-H) having adjacent pairs of Si-OH groups with hydrogen bonded to each other appear at 3700 - 3200 cm^{-1} (Smidt et al., 2011) and the bands of H_2O molecules associated with silanol groups are normally peaked at 3450 cm^{-1} (Pimraksa et al., 2011). The results suggested that there may exist certain amounts of uncondensed Al and Si species. The adsorptions at around 1708 - 1576 cm^{-1} may be due to the weak bands of moisture present. The adsorptions at around 1000 cm^{-1} is related to the T-O-Si bonds formed after geopolymerization accounting for the development of compressive strength in the geopolymer pastes (Liu et al., 2016). It should be noted that the adsorptions at around 1034 cm^{-1} are related to the Si-O-Si stretching in SSA and the adsorptions at around 1000 cm^{-1} are related to the tetrahedral species formed after geopolymerization accounting for the strength development in the geopolymer pastes. Geopolymerization shifted the vibrations centered around 1034 to around 1000 cm^{-1}

indicating participation of SSA in the geopolymerization. According to Beer-Lambert law mentioned in the same article, stronger adsorbance corresponds to larger quantity of the products. Comparing the adsorbance in the region of 1281 - 841 cm^{-1}, the highest absorbances are found in geopolymer pastes synthesized from mixes with 4.0% Na_2O content (see Figs. 6.7b-d) and modulus of 0.95 (see Figs. 6.7e-g). With these proportions, larger quantities of reaction products were produced leading to increased compressive strength. Moreover, geopolymerization shifted the vibrations in this region to lower wavenumbers, which is correlated to the decreased number of Si-O-Al bonds (N-A-S-H gel) and the increased number of Si-O-Si bonds (C-A-S-H gel) due to more cross-linked N-A-S-H and C-S-H type gels which caused the compressive strength to increase (Mijarsh et al., 2014; Yang et al., 2017). Unlike alkaline activation of GGBS alone, showing vibration band typically associated with C-A-S-H gels in the product (Ariffin et al., 2013), this study indicated possible coexistence of C-A-S-H and N-A-S-H gels in the geopolymers synthesized from GGBS and SSA. In all geopolymer pastes, no adsorption peaks occurred in the region of 648 - 515 cm^{-1} which are characteristic adsorptions of the Fe-O stretching vibrations of the hematite structure. This indicates the dissolution of hematite in the geopolymerization reactions. This finding is in agreement with the analyses in XRD. The shifting of O-T-O bonds localized from 515 to 400 cm^{-1} toward lower wavenumbers after geopolymerization indicated the formation of more condensed tetrahedral species (Fernández-Jiménez et al., 2003).

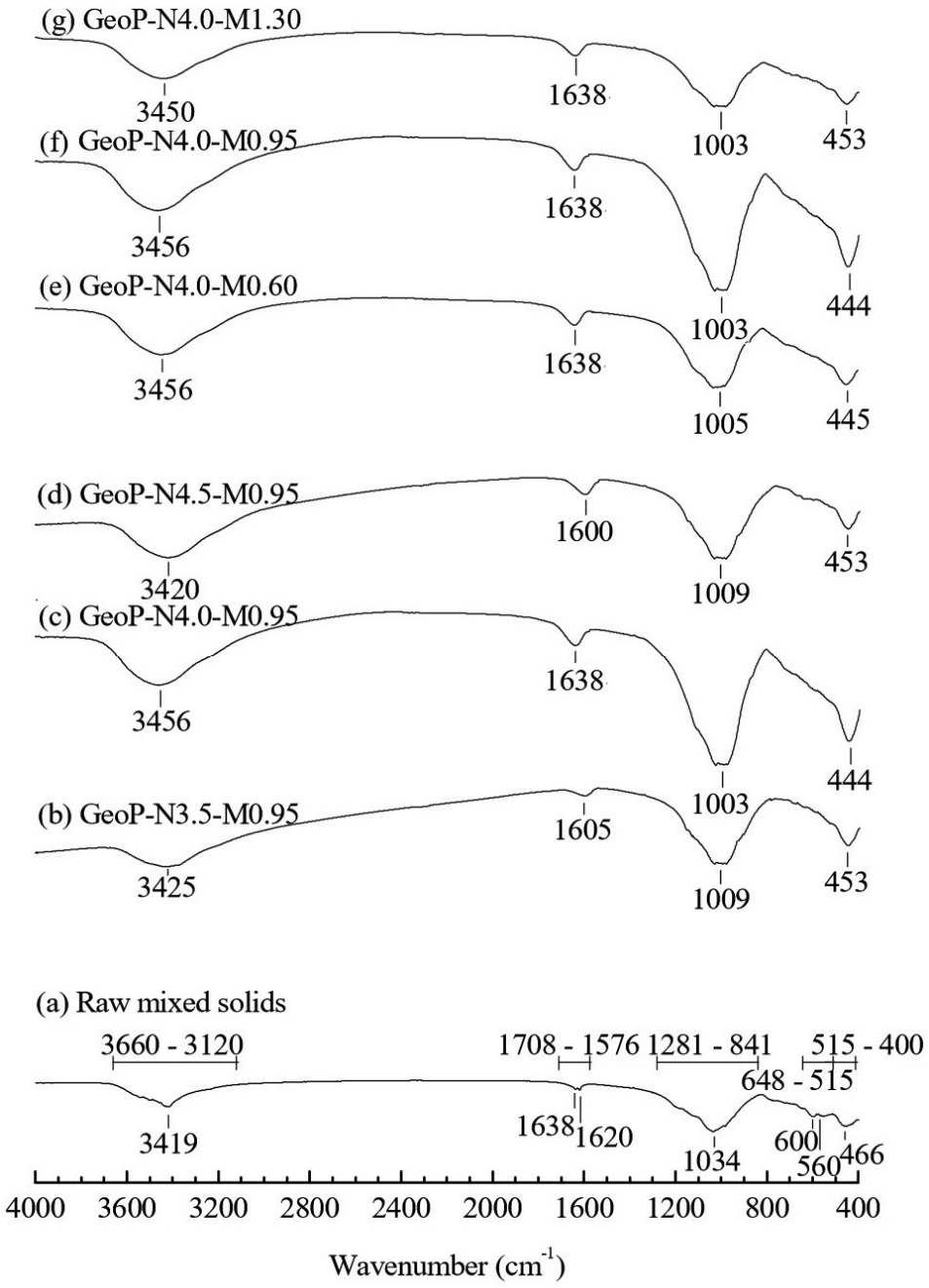

Fig. 6.7. FTIR spectra of (a) raw mixed solids, (b-d) geopolymer pastes synthesized from different Na_2O contents and (e-g) geopolymer pastes synthesized from different moduli

6.6 SEM and EDX Analyses

The SEM morphology of GGBS is shown in Fig. 6.8a. GGBS granules were predominately in angular shape with sharp edges. Figs. 8b-d present the morphologies of pastes synthesized from 4.0% Na_2O content and modulus of 0.95 cured for 1, 3 and 28 days respectively. The geopolymer matrixes only contained GGBS and SSA solids, as well as geopolymer gels formed after their contact with the alkaline activators. Therefore, the analyses of the morphologies of the geopolymer pastes could confirm the attack of GGBS and SSA particles by the alkaline activators, leading to the formation of the geopolymer gels. From Fig. 6.8b, partially dissolved surface of the SSA particle can be observed, indicating participation of SSA in the geopolymerization. Fig. 6.8c shows further evidence of such participation. The SSA particle was largely transformed into the reaction products and the inner parts of the particle seemed to be filled substantially with the reaction products. These morphological views clearly support the finding of dissolution of SSA in the XRD analyses. After curing for 28 days, as can be seen in Fig. 6.8d, the matrix exhibited a dense and compacted microstructure due to the formation of thick layers of gel phases covering the remaining partially reacted particles, which can hardly be observed.

Elemental identification and quantification based on the average of fifteen individual EDX performed at different locations revealed that the most abundant elements in the gel phases were Si and Al (see Fig. 6.8e). The resultant Si/Al atomic ratio was 2.16 on average. The high contents of Si and Al could enhance the compressive strength of the geopolymer pastes through the development of cross-linked SiO4 and AlO4 tetrahedra. The average ratio of Ca/Si atoms was 0.32. The availability of Ca in the gel phases could also contribute to an increase in compressive strength through the formation of C-S-H type gel (Yip et al., 2005) and as a charge-balancing agent (Lecomte et al., 2006). The average Na/Si atomic ratio was 0.23. However, it was reported that Na did not contribute to the gel strength (Salih et al., 2014). Hitherto, the elemental compositions generally lay within the region associated with the C-(N)-A-S-H type gel resulting from the compatibility and reaction between the C-A-S-H and N-A-S-H gels as reported from a previous study (Garcia-Lodeiro et al., 2011). The EDX test also detected the presence of Fe with an average Fe/Si ratio of 0.09 in the phases. Previous researches have reported the positive effects of Fe^{3+} on the compressive strength of geopolymer concretes due to the substitution of some Al atoms by Fe atoms in the geopolymer structure (Lemougna et al., 2013; Reddy et al., 2016).

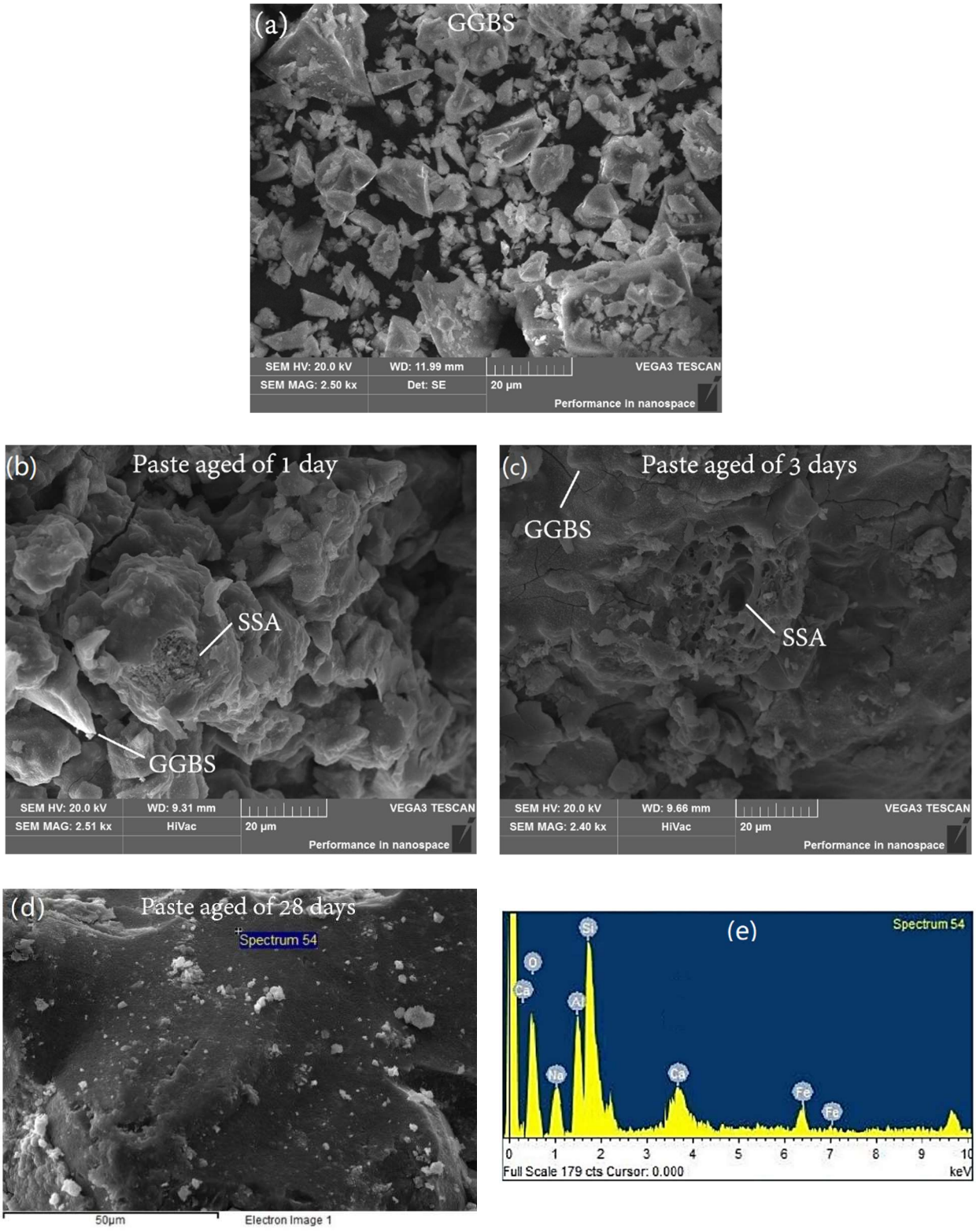

Fig. 6.8. SEM images of (a) GGBS, (b)-(d) geopolymer pastes at different curing ages and (e) EDX result of geopolymer paste at age of 28 days

6.7. Drying shrinkage

Fig. 6.9 shows the drying shrinkage of the geopolymer pastes under the standard drying process. Fig. 6.9a depicts the drying shrinkage of specimens synthesized from different Na_2O contents, namely, 3.5%, 4.0% and 4.5%. Fig. 6.9b depicts the drying shrinkage of specimens synthesized from different moduli, namely, 0.60, 0.95 and 1.30. It can be observed from both Fig. 6.9a and Fig. 6.9b that the drying shrinkage of all geopolymer pastes increased rapidly in the first 7 days. Thereafter, the drying shrinkage only increased gently and further increase was very small after 28 days. Besides, it is worth noting that the 14-day drying shrinkage of all the geopolymer pastes were below the limit of 0.06% as specified in BS 6073 (1981) for dry-mixed specimens. The low water precursors ratio, i.e., 0.2, led to low drying shrinkage of geopolymer pastes (Wallah and Hardjito, 2014). When aggregates are added to the pastes to make geopolymer concrete, the drying shrinkage of the product would be further reduced since aggregates are highly volumetric stable (Dougla et al., 1992; Bissonnette et al., 1999).

It can be seen from Fig. 6.9a that the drying shrinkage reduced with lower Na_2O contents in the geopolymer pastes. This result is in agreement with the findings reported by Allahverdi et al. (2010) and Jiao et al. (2018). However, it should be

noted that, the study by Aydın and Baradan (2014) showed that Na_2O contents would only affect the drying shrinkage of alkali-activated slag mortars when the activator modulus reached 0.4 and above. At the same Na_2O content of 4.0%, as observed from Fig. 6.9b, pastes synthesized from lower activator moduli showed lower shrinkage values. This result is also supported by previous findings (Krizan and Zivanovic, 2002; Gao et al., 2016). Many previous studies indicated that the drying shrinkage depended on the amount of mesopores smaller than 25 nm in geopolymer paste rather than moisture loss (Collins and Sanjayan, 2000; Brough and Atkinson, 2002; Zhu et al., 2018). Geopolymer paste with a higher volume of mesopores exhibited a higher degree of drying shrinkage due to the development of water meniscus which significantly increased the capillary stress (Zhang et al., 2015). In fact, Shi (1996) reported that the inclusion of silica in the alkaline activator would produce finer pore structure in alkaline activated slag pastes, and the compressive strength of the pastes generally decreased with the increase in total porosity with pores larger than 5 nm. Moreover, Kumarappa et al. (2018) found that larger amounts of Na_2O and higher activator modulus led to greater capillary stress. Therefore, it is believed that Na_2O contents and moduli may affect the volume of mesopores in geopolymer pastes which influence the drying shrinkage. To check such effects, the relationship between pore structures of geopolymer pastes and different Na_2O contents and activator moduli should be further studied.

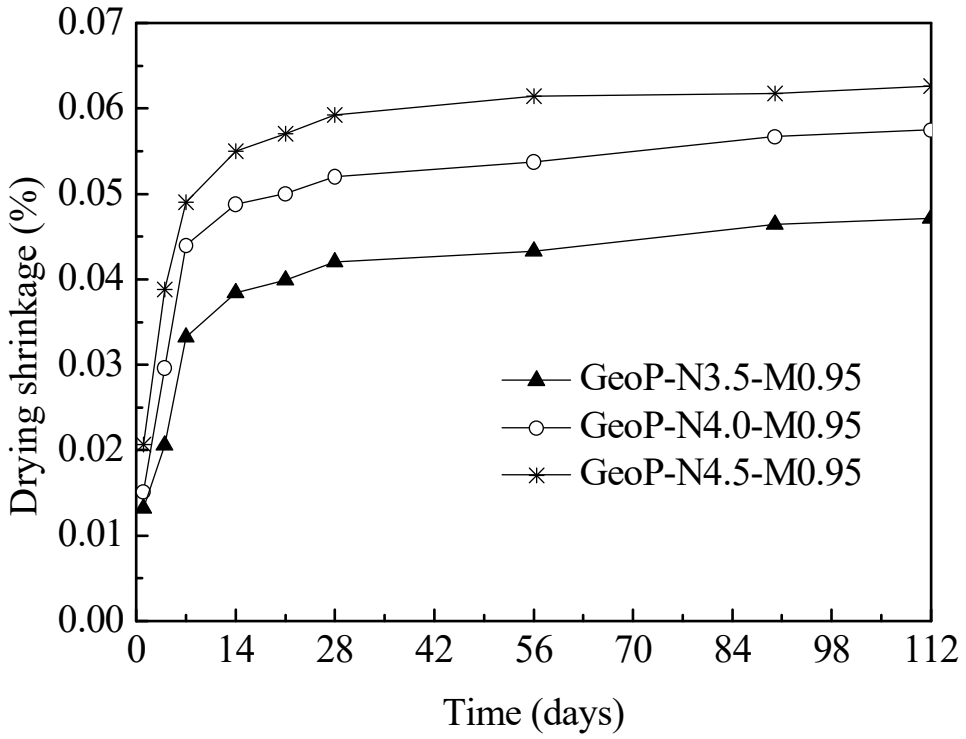

(a)

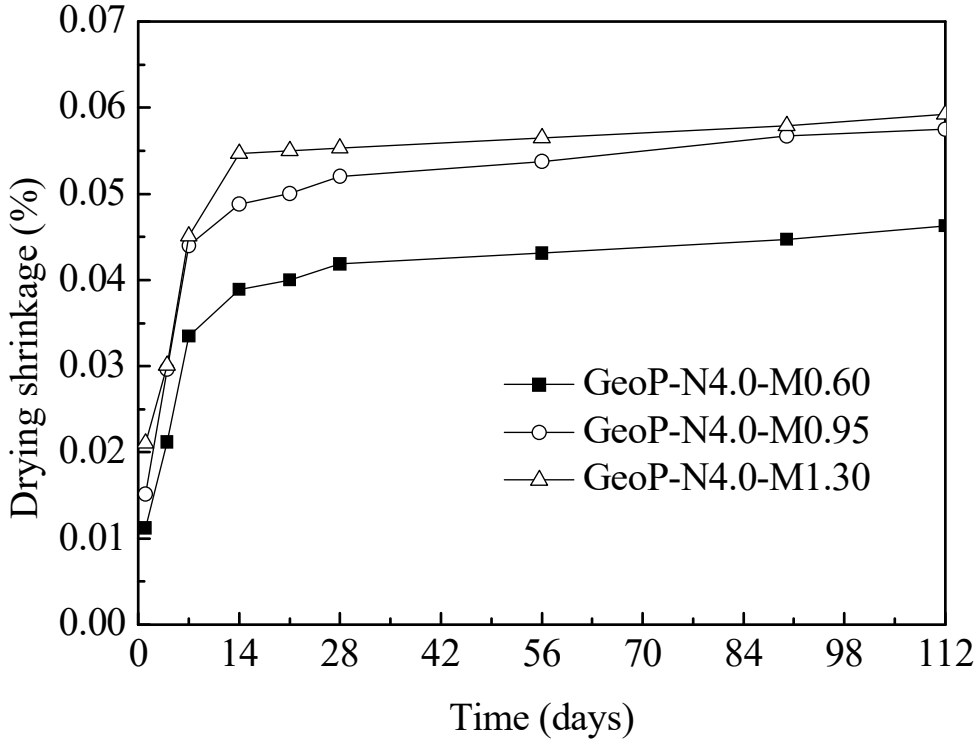

(b)

Fig. 6.9. Drying shrinkage of geopolymer pastes synthesized from (a) different Na2O contents and (b) different moduli

6.8 Leaching of Metal(loid)s

The total metal(loid) contents and leachable metal(loid) concentrations from the raw SSA used in this study have been reported in our previous research on this material (Chen et al., 2018). Table 6.1 shows the leachable metal(loid) concentrations from the raw mixed solids and the geopolymer pastes synthesized from Na_2O content of 4.0% and modulus of 0.95. The concentrations of different metal(loid)s leached from the raw mixed solids were below the stipulated TCLP limits. The concentrations from the paste were even lower, indicating that metal(loid)s had been bonded tightly after geopolymerization posing little hazard to the ambient environment. It can be concluded that the SSA can be safely used with GGBS half to half by weight as precursors for geopolymerization.

Table 6.1 TCLP leaching concentrations from the raw mixed solids and geopolymer pastes

Metal(loid)	Leachate from the raw mixed solids (mg/L)	Leachate from the paste GeoP-N4.0-M0.95 (mg/L)	TCLP limit (mg/L)
Sb	0.0031	< DL	–
As	0.025	< DL	5
Ba	0.0166	< DL	100
Cd	0.007	< DL	1
Cr	< DL	< DL	5
Cu	1.203	0.069	–
Pb	0.014	< DL	5
Ni	0.0421	0.011	–
Co	0.002	< DL	–
Se	0.071	< DL	1
Sr	2.003	< DL	–
Ag	< DL	< DL	5
Zn	1.453	1.300	–

DL: detection limit

6.9 Summary

The geopolymer pastes were synthesized through activation of GGBS and SSA mixed in 1:1 by weight in a binary alkaline activators, namely, NaOH and Na_2SiO_3, and then moulded by compression method. The variables studied were Na_2O to the mixed solids (precursors) weight ratio and modulus of the mixed alkaline solution. Compressive strength and microstructural properties of the geopolymer pastes were studied. The experimental results were summarized below:

(1) The infrared microspectroscopy showed the SSA contained characteristic adsorption bands corresponding to the stretching vibrations of Al-OH groups, O-H bonds under hydrogen bonded association inside molecules, Si-O bonds, Si-O-Si bonds and Fe-O bonds in the crystal structure of hematite, as well as the characteristic vibrations of the simple sulphate ion.

(2) The Fe_2O_3 compound existed in the SSA had very profound influence on the properties and final compositions of the SSA blended GGBS geopolymer pastes.

(3) In the synthesis of the geopolymer pastes, SSA was found to be a candidate precursor material for geopolymerization. The transformation of crystalline phase of hematite in the SSA to amorphous form after geopolymerization was confirmed by XRD, QXRD, FTIR and EDX analyses.

(4) Variation in compressive strength development indicated that the alkaline medium played important roles in the geopolymerization. Too high or too low alkali

content and modulus had detrimental effects on the compressive strength. Geopolymer pastes of adequate strength could be synthesized by using SSA as a precursor. The highest compressive strength was obtained with an optimal alkali content, i.e., weight percentage of Na_2O to the mixed precursors, of 4.0%, and modulus, i.e., molar ratio of SiO_2 to Na_2O in the mixed sodium hydroxide and sodium silicate alkaline solution, of 0.95.

(5) A C-(N)-A-S-H type gel with Fe substitutions was formed in the geopolymerization of mixes of GGBS and SSA in 1:1 by weight moulded by compression method. Its microstructure was dense and compact.

(6) Drying shrinkage tests indicated that using activators with lower Na_2O contents and activator moduli can reduce the drying shrinkage of dry-mixed geopolymer pastes cured at room temperature.

(7) Geopolymers could effectively immobilize metal(loid)s and reduce leachate concentrations well below limits specified by US EPA for hazardous material identification. Geopolymers synthesized from the mixed precursors of GGBS and SSA in 1:1 by weight posed no harmful effects to the environment.

CHAPTER 7 – CONCLUSIONS AND RECOMMENDATIONS

7.1 Introduction

Given the main oxide compositions of the SSA, research studies were directed to the use of the SSA as a SCM in paste and mortar applications and as an aluminosilicate precursor in geopolymer application. Considering the negative impact on workability due to high porosity of the SSA, the dry-mixed method was applied to produce blocks by compression into moulds in contrast to the wet-mixed method which relied on superplasticizer to achieve workability for good compaction by vibration. The following conclusions can be drawn based on the results of the laboratory experiments presented in the fourth, fifth and sixth chapters of this thesis:

7.2 Conclusions

The pozzolanic activity of SSA was weak. However, at the same replacement level of cement up to 20%, the compressive and flexural strength of mortars containing PFA or SSA were comparable. Apart from pozzolanic activity, several interacting factors contributed to the strength development in cement-SSA products including lowering of the effective w/b ratio, enhancement in the rate and degree of cement hydration and the formation of brushite crystals by the incorporation of the SSA.

The concrete blocks containing 20% SSA in the binder and 50% GC in the aggregates could achieve compressive strength of not less than 30 MPa at the age of 28 days. The drying shrinkage values of the blocks increased with a higher content of SSA in the binder but the combined use of recycled GC as aggregates could alleviate the detrimental effect due to its extremely low water absorptivity of GC. On the other hand, the blending of the SSA in the binder could effectively suppress ASR expansion caused by the reactive glass aggregates. It is recommended that 20% of the SSA should be added in the binder for assuring the control of ASR expansion even if all the aggregates are GC. Given that the benefits and drawbacks of GC and SSA are "complimentary" to each other, it is feasible to produce concrete blocks with a high content of GC as aggregates and the SSA as a SCM. This combined usage can significantly reduce the disposal of both types of wastes at landfills.

The SSA was a candidate source material for geopolymerization as evident from the transformation of crystalline phases of quartz and hematite in the SSA into amorphous forms in the reaction. The highest compressive strength of 32.81 MPa at 28 days was attained in the geopolymer pastes generated from GGBS and SSA mixed in 1:1 by weight with the optimal Na_2O content of 4.0% and a modulus of 0.95. The main product formed from the optimum mixture was a C-(N)-A-S-H type gel with Fe substitutions having a dense and compacted microstructure.

7.3 Recommendations

It is clear that the SSA can be used as a SCM and a geopolymer precursor in the light of its chemical composition. In order to explore the wider use of the SSA in cement-based materials and geopolymers, more studies are needed. The following experimental approaches are recommended for future work based on the experience gained in this study.

The high porosity of the SSA leads to reduction in workability of the mortar. Dry-mixed compression method may be adopted to cope with the problem thus opening greater opportunity for recycling of the material. However, applications would be limited to the production of blocks using this placing method.

Cement mortar and concrete blocks containing the SSA have shown high drying shrinkage. This problem is more serious with fine FSSA. Therefore, grinding of the SSA to finer particles is not recommended although this may slightly improve the pozzolanic activity of the SSA.

The use of non-hydroscopic aggregates, such as glass cullet, in the concrete mixes with the incorporation of SSA can balance the high water absorption and large drying shrinkage caused by the SSA.

The use of SSA for synthesizing geopolymers is a promising way for recycling SSA in view of the high usage of SSA in this application. Apparently, mixing SSA with another precursors has high potential of accomplishing geopolymerization of the material.

Some future work on the study of recycling SSA is recommended. As SSA would increase the drying shrinkage of cement-based products, means of controlling the drying shrinkage should be found. Besides, the variation of pore structures of geopolymer pastes with different Na_2O contents or activator moduli should be evaluated. In addition, the effects of varying mix proportions of GGBS and SSA and different curing conditions on geopolymerization should be evaluated. Furthermore, the feasibility of geopolymerization of SSA with other precursors should be studied.

REFERENCES

Adam, C., Peplinski, B., Michaelis, M., Kley, G., Simon, F. G., 2009. Thermochemical treatment of sewage sludge ashes for phosphorus recovery. Waste Management 29(3), 1122-1128.

Ajaxon, I., Öhman, C., Persson, C., 2015. Long-term in vitro degradation of a high-strength brushite cement in water, PBS, and serum solution. BioMed Research International 2015, 1-17.

Akasaki, J.L., Reig, L., Moraes, J.C.B., Santini Jr., M., Payá J., Borrachero, M.V., Tashima, M.M., 2015. Alkali activation of sewage sludge ash/slag blends. The ninth International Conference on the Environmental and Technical Implications of Construction with Alternative Materials, Santander, Cantabria, Spain.

Allahverdi, A., Shaverdi, B., Najafi Kani, E., 2010. Influence of sodium oxide on properties of fresh and hardened paste of alkali-activated blast-furnace slag. International Journal of Civil Engineering 8 (4), 304-314.

Al Sayed, M.H., Madany, I.M., Buali, A.R.M., 1995. Use of sewage sludge ash in asphaltic paving mixes in hot regions. Construction and Building Materials 9(1), 19-23.

Alsubari, B., Shafigh, P., Jumaat, M.Z., 2016. Utilization of high-volume treated palm oil fuel ash to produce sustainable self-compacting concrete. Journal of

Cleaner Production 137, 982-996.

Anderson, M., 2002. Encouraging prospects for recycling incinerated sewage sludge ash (ISSA) into clay-based building products. Journal of Chemical Technology and Biotechnology 77, 352-360.

Ariffin, M., Bhutta, M., Hussin, M., Tahir, M.M., Aziah, N., 2013. Sulfuric acid resistance of blended ash geopolymer concrete. Construction and Building Materials 43, 80-86.

Arulrajah, A., Disfani, M.M., Horpibulsuk, S., Suksiripattanapong, C., 2014. Physical properties and shear strength responses of recycled construction and demolition materials in unbound pavement base/subbase applications. Construction and Building Materials 58, 245-257.

Arvaniti, C., Juenger, C.G., Bernal, A., Duchesne, J., Courard, L., Leroy, S., Provis, L., Klemm, A., Belie, N.D., 2015. Determination of particle size, surface area, and shape of supplementary cementitious materials by different techniques. Materials and Structures 48 (11), 3687-3701.

AS/NZS 4456, 2003. Masonry Units and Segmental Pavers and Flags. Methods of Test. Determining Water Absorption Properties. Australian/New Zealand Standard.

ASTM C348-97, 2002. Standard test method for flexural strength of hydraulic-cement mortars. American Society for Testing and Materials International, West Conshohocken, Pennsylvania.

ASTM C349, 2008. Standard test method for compressive strength of hydraulic cement mortars (using portions of prisms broken in flexure). American Society for Testing and Materials International, West Conshohocken, Pennsylvania.

ASTM C1679-09, 2009. Standard practice for measuring hydration kinetics of hydraulic cementitious mixtures using isothermal calorimetry. American Society for Testing and Materials International, West Conshohocken, Pennsylvania.

ASTM C596-01, 2009. Standard Test Method for Drying Shrinkage of Mortar Containing Hydraulic Cement. American Society for Testing and Materials International, West Conshohocken, Pennsylvania.

ASTM C311, 2012. Standard Test Methods for Sampling and Testing Fly Ash or Natural Pozzolans for Use as a Mineral Admixture in Portland-Cement Concrete. American Society for Testing and Materials International, West Conshohocken, Pennsylvania.

ASTM C618, 2012. Standard Specification for Coal Fly Ash and Raw or Calcined Natural Pozzolan for Use in Concrete. American Society for Testing and Materials International, West Conshohocken, Pennsylvania.

ASTM C109, 2013. Standard test method for compressive strength of hydraulic cement mortars (Using 2-in. or [50-mm] cube specimens). American Society for Testing and Materials International, West Conshohocken, Pennsylvania.

ASTM C1567, 2013. Standard Test Method for Determining the Potential Alkali-silica Reactivity of Combinations of Cementitious Materials and Aggregate (Accelerated Mortar-bar Method). American Society for Testing and Materials International, West Conshohocken, Pennsylvania.

ASTM C33/C33M, 2016. Standard specification for concrete aggregates. American Society for Testing and Materials International, West Conshohocken, Pennsylvania.

Aydın, S., Baradan, B., 2014. Effect of activator type and content on properties of alkali-activated slag mortars. Composites Part B: Engineering 57, 166-172.

Baeyens, J., Puyvelde F.V., 1994. Fluidized bed incineration of sewage sludge: a strategy for the desigh of the incinerator and the future for incinerator ash utilization. Journal of Hazardous Materials 37, 179-190.

Baeza-Brotons, F., Garcés, P., Payá, J., Saval, J.M., 2014. Portland cement systems with addition of sewage sludge ash. Application in concretes for the manufacture of blocks. Journal of Cleaner Production 82, 112-124.

Bai, Z.M., Wang, Z.Y., Zhang, T.G., Fu, F., Yang, N., 2012. Synthesis and characterization of Co-Al-CO_3 layered double-metal hydroxides and assessment of their friction performances. Applied Clay Science 59, 36-41.

Bakharev, T., 2005. Durability of geopolymer materials in sodium and magnesium sulfate solutions. Cement and Concrete Research 35(6), 1233-1246.

Bakhsheshi-Rad, H., Hamzah, E., Daroonparvar, M., Ebrahimi-Kahrizsangi, R.,

Medraj, M., 2014. In-vitro corrosion inhibition mechanism of fluorine-doped hydroxyapatite and brushite coated Mg-Ca alloys for biomedical applications. Ceramics International 40(6), 7971-7982.

Baltakys, K., Jauberthie, R., Siauciunas, R., Kaminskas, R., 2007. Influence of modification of SiO2 on the formation of calcium silicate hydrate. Journal of Materials Science 25(3), 663-670.

Bhagath Singh, G.V.P., Subramaniam, V.L., 2016. Quantitative XRD study of amorphous phase in alkali activated low calcium siliceous fly ash. Construction and Building Materials 124, 139-147.

Bissonnette, B., Pierre, P., Pigeon, M., 1999. Influence of key parameters on drying shrinkage of cementitious materials. Cement and Concrete Research 29 (10), 1655-1662.

Blanda, G., Brucato, V., Pavia, F.C., Greco, S., Piazza, S., Sunseri, C., Inguanta, R., 2016. Galvanic deposition and characterization of brushite/hydroxyapatite coatings on 316L stainless steel. Materials Science and Engineering C 64, 93-101.

Brough, A.R., Atkinson, A., 2002. Sodium silicate-based, alkali-activated slag mortars: Part I. Strength, hydration and microstructure. Cement and Concrete Research 32 (6), 865-879.

BS 6073, 1981. Precast Concrete Masonry Units. Part 1: Specification for Precast Concrete Mansonry Units. British Standard Institution, London.

BS 1881-114, 1983. Testing Concrete. Methods for Determination of Density of Hardened Concrete. British Standard Institution, London.

BS 7591-1, 1992. Porosity and pore size distribution of materials, Method of evaluation by mercury porosimetry. British Standard Institution, London.

BS 812, 1995. Testing Aggregates. Part 2: Methods of Determination of Density. British Standard Institution, London.

BS EN 1015, 1999. Methods of test for mortar for masonry Part 3: Determination of consistence of fresh mortar (by flow table). British Standard Institution, London.

BS EN 13657, 2002. Characterization of Waste-digestion for Subsequent Determination of Aqua Regia Soluble Portion of Elements. British Standard Institution, London.

BS EN 196-6, 2010. Methods of Testing Cement. Determination of Fineness. British Standard Institution, London.

BS EN 197-1, 2011. Cement: Composition, specifications and conformity criteria for common cements. British Standard Institution, London.

BS ISO 1920-8, 2009. Determination of drying shrinkage of concrete for samples prepared in the field or in the laboratory. British Standard Institution, London.

Bullard, J.W., Jennings, H.M., Livingston, R.A., Nonat, A., Scherer, G.W., Schweitzer, J.S., Scrivener, K.L., Thomas, J.J., 2011. Mechanisms of cement hydration. Cement and Concrete Research 41, 1208-1223.

Chakraborty, S., Jo, B.W., Jo, J.H., Baloch, Z., 2017. Effectiveness of sewage sludge

ash combined with waste pozzolanic minerals in developing sustainable construction material: An alternative approach for waste management. Journal of Cleaner Production 153, 253-263.

Cheeseman, C.R., Virdi, G.S., 2005. Properties and microstructure of lightweight aggregate produced from sintered sewage sludge ash. Resources, Conservation and Recycling 45, 18-30.

Cheng, T., Chiu, J., 2003. Fire-resistant geopolymer produced by granulated blast furnace slag. Minerals Engineering 16(3), 205-210.

Chen, L., Lin, D.F., 2009. Stabilization treatment of soft subgrade soil by sewage sludge ash and cement. Journal of Hazardous Materials 162, 321-327.

Chen, L., Lin, D.F., 2009a. Applications of sewage sludge ash and nano-SiO_2 to manufacture tile as construction material. Construction and Building Materials 23, 3312-3320.

Chen, M.Z., Blanc, D., Gautier, M., Mehu, J., Gourdon, R., 2013. Environmental and technical assessments of the potential utilization of sewage sludge ashes (SSAs) as secondary raw materials in construction. Waste Management 1268-1275.

Chen, Z., Li, J.S., Poon, C.S., 2018. Combined use of sewage sludge ash and recycled glass cullet for the production of concrete blocks. Journal of Cleaner Production 171, 1447-1459.

Chhaiba, S., Blanco-Varela, M.T., Diouri, A., Boukhari, A., 2018. Experimental study of raw material from Moroccan oil shale and coal waste and their reuse in

cement industry. Journal of Materials and Environmental Sciences 9(4), 1128-1139.

Chindaprasirt, P., Homwuttiwong, S., Sirivivatnanon, V., 2004. Influence of fly ash fineness on strength, drying shrinkage and sulfate resistance of blended cement mortar. Cement and Concrete Research 34(7), 1087-1092.

Chiou, I.J., Wang, K.S., Chen, C.H., Lin, Y.T., 2006. Lightweight aggregate made from sewage sludge and incinerated ash. Waste Management 26, 1453-1461.

Collins, F., Sanjayan, J., 2000. Effect of pore size distribution on drying shrinking of alkali-activated slag concrete. Cement and Concrete Research 30(9), 1401-1406.

Cyr, M., Coutand, M., Clastres, P., 2007. Technological and environmental behavior of sewage sludge ash (SSA) in cement-based materials. Cement and Concrete Research 37, 1278-1289.

Cyr, M., Idir, R., Escadeillas, G., 2012. Use of metakaolin to stabilize sewage sludge ash and municipal solid waste incineration fly ash in cement-based materials. Journal of Hazardous Materials 243, 193-203.

Davidovits, J., 1994. Geopolymers: man-made rock geosynthesis and the resulting development of very early high strength cement. Journal of Materials Education 16(2), 91-139.

Day, R.L., Marsh, B.K., 1988. Measurement of porosity in blended cement pastes. Cement and Concrete Research 18(1), 63-73.

De Ligny, D., Guillaud, E., Gailhanou, H., Blanc, P., 2013. Raman spectroscopy of

adsorbed water in clays: first attempt at band assignment. Procedia Earth and Planetary Science 7, 203-206.

Dhir, R.K., Ghataora, G.S., Lynn, C.J., 2017. Sustainable Construction Materials: Sewage Sludge Ash. Woodhead Publishing, Birmingham.

Dhir, R.K., Limbachiya, M.C., McCarthy, M.J., 2001. Recycling and reuse of sewage sludge: proceedings of the international symposium. Thomas Telford.

Donatello, S., Tyrer, M., Cheeseman, C. R., 2010. Comparison of test methods to assess pozzolanic activity. Cement and Concrete Composites 32, 121-127.

Donatello, S., Cheeseman, C.R., 2013. Recycling and recovery routes for incinerated sewage sludge ash (ISSA): A review. Waste Management 33, 2328-2340.

Douglas, E., Bilodeau, A., Malhotra, V.M., 1992. Properties and durability of alkali-activated slag concrete. ACI Materials Journal 89 (5), 509-516.

Dyer, T.D., Halliday, J.E., Dhir, R.K., 2011. Hydration chemistry of sewage sludge ash used as a cement component. Journal of Materials in Civil Engineering 23(5), 648-655.

El-Didamony, H., Amer, A.A., Ela-ziz, H.A., 2012. Properties and durability of alkali-activated slag pastes immersed in sea water. Ceramics International 38(5), 3773-3780.

El-Gamal, S., Selim, F., 2017. Utilization of some industrial wastes for eco-friendly cement production. Sustainable Materials and Technologies 12, 9-17.

Environmental Protection Department, 2014. Letter to the editor of South China

Morning Post-Response to reader's letter relating to sludge treatment facility. http://www.epd.gov.hk/epd/english/news_events/letters/letters_140612a.html (accessed 17.03.18).

Environmental Protection Department, 2017. Monitoring of solid waste in Hong Kong, waste statistics for 2015. https://www.wastereduction.gov.hk/sites/default/files/msw2015.pdf (accessed 04.04.18).

EN 196-5, 2005. Methods of testing cement Part 5: pozzolanicity test for pozzolanic cement. The European Committee for Standardization, Brussels, Belgium.

EPA Method 1311, 1990. Toxicity Characteristic Leaching Procedure. Environmental Protection Agency, United States.

Everett, D.H., 1972. Manual of Symbols and Terminology for Physicochemical Quantities and Units. International Union of Pure and Applied Chemistry, Washington DC.

Fang, W., Wei, Y.H., Liu, J.G., 2016. Comparative characterization of sewage sludge compost and soil: heavy metal leaching characteristics. Journal of Hazardous Materials 310, 1-10.

Farhana, Z., Kamarudin, H., Rahmat, A., Al Bakri, A., 2015. The relationship between water absorption and porosity for geopolymer paste. Materials Science Forum, 166-172.

Farzadnia, N., Noorvand, H., Yasin, A.M., Aziz, F.N.A., 2015. The effect of nano

silica on short term drying shrinkage of POFA cement mortars. Construction and Building Materials 95, 636-646.

Fernández-Jiménez, A., Puertas, F., Sobrados, I., Sanz, J., 2003. Structure of calcium silicate hydrates formed in alkaline-activated slag: influence of the type of alkaline activator. Journal of the American Ceramic Society 86(8), 1389-1394.

Ferraris, C., Garboczi, E., 2013. Research results digest 382: Measuring cement particle size and surface area by laser diffraction. Transportation Research Board 2013 Annual Meeting, Washington DC.

Fontes, C., Barbosa, M., Toledo Filho, R., Goncalves, J., 2004. Potentiality of sewage sludge ash as mineral additive in cement mortar and high performance concrete. Proceedings of the International RILEM Conference on the Use of Recycled Materials in Buildings and Structures 8-11 November 2004, Barcelona, Spain.

Franz, M., 2008. Phosphate fertilizer from sewage sludge ash (SSA). Waste Management 28, 1809-1818.

Frías, M., Rodríguez, C., 2008. Effect of incorporating ferroalloy industry wastes as complementary cementing materials on the properties of blended cement matrices. Cement and Concrete Composites 30, 212-219.

Frost, R.L., Xi, Y., Palmer, S.J., Pogson, R., 2011. Vibrational spectroscopic analysis of the mineral crandallite $CaAl_3(PO_4)_2(OH)_5 \cdot (H_2O)$ from the Jenolan Caves, Australia. Spectrochimica Acta Part A: Molecular and Biomolecular Spectroscopy 82(1), 461-466.

Gao, X., Yu, Q.L., Brouwers, H.J.H., 2016. Assessing the porosity and shrinkage of alkali activated slag-fly ash composites designed applying a packing model. Construction and Building Materials 119, 175-184.

Garcia-Lodeiro, I., Fernández-Jiménez, A., Palomo, A., 2013. Variation in hybrid cements over time. Alkaline activation of fly ash-portland cement blends. Cement and Concrete Research 52, 112-122.

Garcia-Lodeiro, I., Palomo, A., Fernández-Jiménez, A., Macphee, D., 2011. Compatibility studies between NASH and CASH gels. Study in the ternary diagram Na_2O-CaO-Al_2O_3-SiO_2-H_2O. Cement and Concrete Research 41(9), 923-931.

García, R., Vigil de la Villa, R., Vegas, I., Frías, M., Sánchez de Rojas, M.I., 2008. The pozzolanic properties of paper sludge waste. Construction and Building Materials 22(7), 1484-1490.

Gashti, M.P., Bourquin, M., Stir, M., Hulliger, J., 2013. Glutamic acid inducing kidney stone biomimicry by a brushite/gelatin composite. Journal of Materials Chemistry B 1(10), 1501-1508.

Gursel, A.P., Maryman, H., Ostertag, C., 2016. A life-cycle approach to environmental, mechanical, and durability properties of "green" concrete mixes with rice husk ash. Journal of Cleaner Production 112, 823-836.

Gu, Y.M., Fang, Y.H., You, D., Gong, Y.F., Zhu, C.H., 2015. Properties and microstructure of alkali-activated slag cement cured at below-and about-normal

temperature. Construction and Building Materials 79, 1-8.

Güneyisi, E., Gesoğlu, M., Mermerdaş, K., 2008. Improving strength, drying shrinkage, and pore structure of concrete using metakaolin. Materials and Structures 41(5), 937-949.

Habert, G., De Lacaillerie, J.D.E., Roussel, N., 2011. An environmental evaluation of geopolymer based concrete production: reviewing current research trends. Journal of Cleaner Production 19(11), 1229-1238.

Haleem, A., Luthra, S., Mannan, B., Khurana, S., Kumar, S., Ahmad, S., 2016. Critical factors for the successful usage of fly ash in roads and bridges and embankments: Analyzing indian perspective. Resources Policy 49, 334-348.

Halliday, J.E., Jones, M.R., Dyer, T.D., Dhir, R.K., 2012. Potential use of UK sewage sludge ash in cement-based concrete. Waste and Resource Management 165, 57-66.

Han, H.M., Mikhalovsky, S.V., Phillips, G.J., Lloyd, A.W., 2007. Calcium phosphate sonoelectrodeposition on carbon fabrics and its effect on osteoblast cell viability in vitro. New Carbon Materials 22(2), 121-125.

Highways Department, 2014. Guidance Notes on Design and Construction of Pavements with Paving Units. RD/GN/044.

Hu, J., Ge, Z., Wang, K., 2014. Influence of cement fineness and water-to-cement ratio on mortar early-age heat of hydration and set times. Construction and Building Materials 50, 657-663.

Idir, R., Cyr, M., Tagnit-Hamou, A., 2010. Use of fine glass as ASR inhibitor in glass aggregate mortars. Construction and Building Materials 24, 1309-1312.

Ing, D.S., Chin, S.C., Guan, T.K., Suil, A., 2016. The use of sewage sludge ash (SSA) as partial replacement of cement in concrete. ARPN Journal of Engineering and Applied Sciences 11 (6), 3771-3775.

Istuque, D., Reig, L., Moraes, J., Akasaki, J., Borrachero, M., Soriano, L., Payá, J., Malmonge, J., Tashima, M., 2016. Behaviour of metakaolin-based geopolymers incorporating sewage sludge ash (SSA). Materials Letters 180, 192-195.

Itim, A., Ezziane, K., Kadri, E.H., 2011. Compressive strength and shrinkage of mortar containing various amounts of mineral additions. Construction and Building Materials 25(8), 3603-3609.

Jiang, Z., Sun, Z., Wang, P., 2005. Autogenous relative humidity change and autogenous shrinkage of high-performance cement pastes. Cement and Concrete Research 35(8), 1539-1545.

Jiao, Z.Z., Wang, Y., Zheng, W.Z., Huang, W.X., 2018. Pottery sand as fine aggregate for preparing alkali-activated slag mortar. Advances in Materials Science and Engineering (Accepted paper)

Kaufmann, J., Loser, R., Leemann, A., 2009. Analysis of cement-bonded materials by multi-cycle mercury intrusion and nitrogen sorption. Journal of Colloid and Interface Science 336(2), 730-737.

Kawano, M., Tomita, K., 1991. Mineralogy and genesis of clays in postmagmatic

alteration zones, Makurazaki volcanic area, Kagoshima Prefecture, Japan. Clays and Clay Minerals 39(6), 597-608.

Kiattikomol, K., Jaturapitakkul, C., Songpiriyakij, S., Chutubtim, S., 2001. A study of ground coarse fly ashes with different finenesses from various sources as pozzolanic materials. Cement and Concrete Composites 23, 335-343.

Koenig, A., Herrmann, A., Overmann, S., Dehn, F., 2017. Resistance of alkali-activated binders to organic acid attack: Assessment of evaluation criteria and damage mechanisms. Construction and Building Materials 151, 405-413.

Komonweeraket, K., Cetin, B., Aydilek, A.H., Benson, C.H., Edil, T.B., 2015. Effects of pH on the leaching mechanisms of elements from fly ash mixed soils. Fuel 140, 788-802.

Kong, D.L., Sanjayan, J.G., 2008. Damage behavior of geopolymer composites exposed to elevated temperatures. Cement and Concrete Composites 30(10), 986-991.

Kosior-Kazberuk, M., 2011. Application of SSA as partial replacement of aggregate in concrete. Polish Journal of Environmental Studies 20, 365-370.

Kou, S.C., Zhan, B.J., Poon, C.S., 2012. Properties of partition wall blocks prepared with fresh concrete wastes. Construction and Building Materials 36, 566-571.

Krizan, D., Zivanovic, B., 2002. Effects of dosage and modulus of water glass on early hydration of alkali-slag cements. Cement and Concrete Research 32(8), 1181-1188.

Kumarappa, D.B., Peethamparan, S., Ngami, M., 2018. Autogenous shrinkage of alkali activated slag mortars: Basic mechanisms and mitigation methods. Cement and Concrete Research 109, 1-9.

Lahoti, M., Wong, K.K., Tan, K.H., Yang, E.H., 2017. Use of alkali-silica reactive sedimentary rock powder as a resource to produce high strength geopolymer binder. Construction and Building Materials 155, 381-388.

Lam, C.S., Poon, C.S., Chan, D., 2007. Enhancing the performance of pre-cast concrete blocks by incorporating waste glass-ASR consideration. Cement and Concrete Composites 29, 616-625.

Langan, B., Weng, K., Ward, M., 2002. Effect of silica fume and fly ash on heat of hydration of Portland cement. Cement and Concrete Research 32(7), 1045-1051.

Lawrence, P., Cyr, M., Ringot, E., 2003. Mineral admixtures in mortars: effect of inert materials on short-term hydration. Cement and Concrete Research 33(12), 1939-1947.

Lecomte, I., Henrist, C., Liegeois, M., Maseri, F., Rulmont, A., Cloots, R., 2006. (Micro)-structural comparison between geopolymers, alkali-activated slag cement and Portland cement. Journal of the European Ceramic Society 26(16), 3789-3797.

Lee, G., Poon, C.S., Wong, Y.L., Ling, T.C., 2013. Effects of recycled fine glass aggregates on the properties of dry–mixed concrete blocks. Construction and Building Materials 38, 638-643.

Lee, W., Van Deventer, J., 2002. The effects of inorganic salt contamination on the strength and durability of geopolymers. Colloids and Surfaces A: Physicochemical and Engineering Aspects 211(2-3), 115-126.

Lemougna, P.N., MacKenzie, K.J., Jameson, G.N., Rahier, H., Melo, U.C., 2013. The role of iron in the formation of inorganic polymers (geopolymers) from volcanic ash: A ^{57}Fe Mössbauer spectroscopy study. Journal of Materials Science 48(15), 5280-5286.

Lemougna, P.N., Wang, K.T., Tang, Q., Kamseu, E., Billong, N., Melo, U.C., Cui, X.M., 2017. Effect of slag and calcium carbonate addition on the development of geopolymer from indurated laterite. Applied Clay Science 148, 109-117.

Li, J.S., Chen, Z., Wang, Q.M., Fang, L., Xue, Q., Cheeseman, C.R., Donatello, S., Liu, L., Poon, C.S., 2018. Change in re-use value of incinerated sewage sludge ash due to chemical extraction of phosphorus. Waste Management 74, 404-412.

Li, J.S., Poon, C.S., 2017. Innovative solidification/stabilization of lead contaminated soil using incineration sewage sludge ash. Chemosphere 173, 143-152.

Li, J.S., Xue, Q., Fang, L., Poon, C.S., 2017. Characteristics and metal leachability of incinerated sewage sludge ash and air pollution control residues from Hong Kong evaluated by different methods. Waste Management 64, 161-170.

Lin, D.F., Lin, K.L., Hung, M.J., Luo, H.L., 2007. Sludge ash/hydrated lime on the geotechnical properties of soft soil. Journal of Hazardous Materials 145 (1-2),

58-64.

Lin, D.F., Weng, C.H., 2001. Use of sewage sludge ash as brick material. Journal of Environmental Engineering 127 (10), 922-927.

Ling, T.C., Poon, C.S., 2014. Use of recycled CRT funnel glass as fine aggregate in dry mixed concrete paving blocks. Journal of Cleaner Production 68, 209-215.

Ling, T.C., Poon, C.S., Wong, H.W., 2013. Management and recycling of waste glass in concrete products: current situations in Hong Kong. Resources, Conservation and Recycling 70, 25-31.

Lin, K.L., Chang, W.C., Lin, D.F., Luo, H.L., Tsai, M.C., 2008. Effects of nano-SiO_2 and different ash particle sizes on sludge ash-cement mortar. Journal of Environmental Management 88, 708-714.

Lin, Y., Liao, Y., Yu, Z., Fang, S., Ma, X., 2017. A study on co-pyrolysis of bagasse and sewage sludge using TG-FTIR and Py-GC/MS. Energy Conversion and Management 151, 190-198.

Litke, A., Su, Y., Tranca, I., Weber, T., Hensen, E.J., Hofmann, J.P., 2017. Role of adsorbed water on charge carrier dynamics in photoexcited TiO_2. The Journal of Physical Chemistry C 121(13), 7514-7524.

Liu, Y., Zhu, W., Yang, E.H., 2016. Alkali-activated ground granulated blast-furnace slag incorporating incinerator fly ash as a potential binder. Construction and Building Materials 112, 1005-1012.

Li, X.G., Lv, Y., Ma, B.G., Chen, Q.B., Yin, X.B., Jian, S.W., 2012. Utilization of

municipal solid waste incineration bottom ash in blended cement. Journal of Cleaner Production 32, 96-100.

Luxan, M.P., Madruga, M., Saavedra, J., 1989. Rapid evaluation of pozzolanic activity of natural products by conductivity measurement. Cement and Concrete Research 19 (1): 63-68.

Lynn, C.J., Dhir, R.K., Ghataora, G.S., West, R.P., 2015. Sewage sludge ash characteristics and potential for use in concrete. Construction and Building Materials 98, 767-779.

Ma, J., Zou, J., Li, L., Yao, C., Zhang, T., Li, D., 2013. Synthesis and characterization of Ag_3PO_4 immobilized in bentonite for the sunlight-driven degradation of Orange II. Applied Catalysis B: Environmental 134, 1-6.

Maltais, Y., Marchand, J., 1997. Influence of curing temperature on cement hydration and mechanical strength development of fly ash mortars. Cement and Concrete Research 27(7), 1009-1020.

Mehta, A., Siddique, R., 2016. An overview of geopolymers derived from industrial by-products. Construction and Building Materials 127, 183-198.

Mijarsh, M., Johari, M.M., Ahmad, Z., 2014. Synthesis of geopolymer from large amounts of treated palm oil fuel ash: application of the Taguchi method in investigating the main parameters affecting compressive strength. Construction and Building Materials 52, 473-481.

Miller, M.A., Kendall, M.R., Jain, M.K., Larson P.R., Madden A.S., Tas A.C., 2012.

Testing of Brushite ($CaHPO_4 \cdot 2H_2O$) in Synthetic Biomineralization Solutions and In Situ Crystallization of Brushite Micro-Granules. Journal of the American Ceramic Society 95(7), 2178-2188.

Monzó, J., Paya, J., Borrachero, M.V., Peris-Mora, E., 1999. Mechanical behavior of mortars containing sewage sludge ash (SSA) and Portland cements with different tricalcium aluminate content. Cement and Concrete Research 29, 87-94.

Monzó, J., Paya, J., Borrachero, M.V., Girbes, I., 2003. Reuse of sewage sludge ashes (SSA) in cement mixtures: the effect of SSA on the workability of cement mortars. Waste Management 23, 373-381.

Nagarjuna, K., 2015. Sewage sludge ash (SSA) in precaste concrete blocks. International Journal of Engineering Science 1, 768-771.

Neuman, W., Toribara, T., Mulryan, B., 1962. Synthetic hydroxyapatite crystals I. Sodium and potassium fixation. Archives of Biochemistry and Biophysics 98(3), 384-390.

News.gov.hk, 2013. Legislative Council Questions 18: Extension of landfill. http://www.info.gov.hk/gia/general/201306/26/P201306260311.htm (accessed 16.03.18).

Niu, X., Shen, L.H., 2018. Release and transformation of phosphorus in chemical looping combustion of sewage sludge. Chemical Engineering Journal 335, 621-630.

Nunes, C., Slížková, Z., Stefanidou, M., Němeček, J., 2016. Microstructure of lime and lime-pozzolana pastes with nanosilica. Cement and Concrete Research 83, 152-163.

Pak, C.Y., Eanes, E.D., Ruskin, B., 1971. Spontaneous precipitation of brushite in urine: evidence that brushite is the nidus of renal stones originating as calcium phosphate. Proceedings of the National Academy of Sciences 68(7), 1456-1460.

Pan, S.C., Tseng, D.H., Lee, C.C., Lee, C., 2003. Influence of the fineness of sewage sludge ash on the mortar properties. Cement and Concrete Research 33, 1749-1754.

Park, J.P., Moon, S.O., Heo, J., 2003. Crystalline phase control of glass ceramics obtained from sewage sludge fly ash. Ceramics International 29, 223-227.

Park, S.B., Lee, B.C., Kim, J.H., 2004. Studies on mechanical properties of concrete containing waste glass aggregates. Cement and Concrete Research 34 (12), 2181-2189.

Parvinzadeh Gashti, M., Stir, M., Bourquin, M., Hulliger, J.R., 2013. Mineralization of calcium phosphate crystals in starch template inducing a brushite kidney stone biomimetic composite. Crystal Growth and Design 13(5), 2166-2173.

Paulnath, R.C.M., Aski, A.M.M., Hamsath, F., Jasekan, S., Pathirana, C.K., 2016. Suitability of Incinerated Sewage Sludge Ash to Produce Geopolymer Concrete. http://webcache.googleusercontent.com/search?q=cache:G8lMZOnvjs4J:www.dcee.ruh.ac.lk/images/donaimage/ACEPProceeding2016/Suitability%2520of

%2520Incinerated%2520Sewage%2520Sludge%2520Ash%2520to%2520Produce.pdf+andcd=1andhl=zh-CNandct=clnkandgl=hkandclient=opera (accessed 16.03.18).

Payá, J., Borrachero, M.V., Monzó, J., Peris-Mora, E., Amahjour, F., 2001. Enhanced conductivity measurement techniques for evaluation of fly ash pozzolanic activity. Cement and Concrete Research 31(1), 41-49.

Petrone, L., Easingwood, R., Barker, M., McQuillan, A., 2011. In situ ATR-IR spectroscopic and electron microscopic analyses of settlement secretions of Undaria pinnatifida kelp spores. Journal of The Royal Society Interface 8(56), 410-422.

Pérez-Carrión, M., Baeza-Brotons, F., Payá, J., Saval, J., Zornoza, E., Borrachero, M., Garcés, P., 2014. Potential use of sewage sludge ash (SSA) as a cement replacement in precast concrete blocks. Materiales de Construcción 64 (313).

Pimraksa, K., Chindaprasirt, P., Rungchet, A., Sagoe-Crentsil, K., Sato, T., 2011. Lightweight geopolymer made of highly porous siliceous materials with various Na_2O/Al_2O_3 and SiO_2/Al_2O_3 ratios. Materials Science and Engineering: A 528(21), 6616-6623.

Pinarli, V., 2000. Sustainable waste management-studies on the use of sewage sludge ash in the construction industry as concrete material. International Symposium in United Kingdom.

Pittman, D.W., Ragan, S.A., 1998. Drying shrinkage of roller-compacted concrete

for pavement applications. ACI Materials Journal 95(1), 19-26.

Poon, C.S., Chan, D., 2006. Paving blocks made with recycled concrete aggregate and crushed clay brick. Construction and Building Materials 20, 569-577.

Poon, C.S., Kou, S.C., Lam, L., 2002. Use of recycled aggregates in molded concrete bricks and blocks. Construction and Building Materials 16, 281-289.

Prahara, E., 2014. Compressive Strength and Water Absorption of Pervious Concrete that Using the Fragments of Ceramics and Roof Tiles. EPJ Web of Conferences 68, No. 00015.

Puertas, F., Palacios, M., Manzano, H., Dolado, J.S., Rico, A., Rodríguez, J., 2011. A model for the C-A-S-H gel formed in alkali-activated slag cement. Journal of the European Ceramic Society 31, 2043-2056.

Rajaokarivony-Andriambololona, Z., Thomassin, J., Baillif, P., Touray, J., 1990. Experimental hydration of two synthetic glassy blast furnace slags in water and alkaline solutions (NaOH and KOH 0.1 N) at 40 C: structure, composition and origin of the hydrated layer. Journal of Materials Science 25(5), 2399-2410.

RD/GN/044A, 2017. Guidance Notes on Design and Construction of Pavements with Paving Units. Research & Development Division, Highways department, Hong Kong.

Reddy, M.S., Dinakar, P., Rao, B.H., 2016. A review of the influence of source material's oxide composition on the compressive strength of geopolymer concrete. Microporous and Mesoporous Materials 234, 12-23.

Ruffell, A., Wiltshire, P., 2004. Conjunctive use of quantitative and qualitative X-ray diffraction analysis of soils and rocks for forensic analysis. Forensic Science International 145, 13-23.

Salih, M.A., Ali, A.A.A., Farzadnia, N., 2014. Characterization of mechanical and microstructural properties of palm oil fuel ash geopolymer cement paste. Construction and Building Materials 65, 592-603.

Sasaoka, N., Yokoi, K., Yamanaka, T., 2006. Basic study of concrete made using ash derived from the incinerating sewage sludge. International Journal of Modern Physics B 20, 3716-3721.

Schmitt, J., Flemming, H.C., 1998. FTIR-spectroscopy in microbial and material analysis. International Biodeterioration and Biodegradation 41(1), 1-11.

Schuur, H., 2000. Calcium silicate products with crushed building and demolition waste. Journal of Materials in Civil Engineering 12, 282-287.

Shannag, M.J., Yeginobali, A., 1995. Properties of pastes, mortars and concretes containing natural pozzolan. Cement and Concrete Research 25, 647-657.

Shi, C.J., 1996. Strength, pore structure and permeability of alkali-activated slag mortars. Cement and Concrete Research 26 (12), 1789-1799.

Shi, C.J, Zheng, K., 2007. A review on the use of waste glasses in the production of cement and concrete. Resources, Conservation and Recycling 52, 234-247.

Smidt, E., Böhm, K., Schwanninger, M., 2011. The application of FT-IR spectroscopy in waste management, Fourier transforms-new analytical

approaches and FTIR strategies. Prof. Goran Nikolic (Ed.), InTech.

Smolczyk, H.G., 1980. Structure et charactérisation des laitiers. 7th International Congress on the Chemistry of Cement, Paris.

Smol, M., Kulczycka, J., Henclik, A., Gorazda, K., Wzorek, Z., 2015. The possible use of sewage sludge ash (SSA) in the construction industry as a way towards a circular economy. Journal of Cleaner Production 95, 45-54.

Sopcak, T., Medvecky, L., Giretova, M., Stulajterova, R., Durisin, J., Girman, V., Faberova, M., 2016. Effect of phase composition of calcium silicate phosphate component on properties of brushite based composite cements. Materials Characterization 117, 17-29.

Stumm, W., 1992. Chemistry of the Solid-Water Interface. Wiley, New York.

Taha, B., Nounu, G., 2008. Using lithium nitrate and pozzolanic glass powder in concrete as ASR suppressors. Cement and Concrete Composites 30, 497-505.

Taylor, H.F.W., 1997. Cement Chemistry. Thomas Telford Publishing, London.

Taylor, H.F.W., Mohan, K., Moir, G.K., 1985. Analytical study of pure and extended portland cement pastes: I, pure portland cement pastes. Journal of the American Ceramic Society 68(12), 680-685.

Taylor, H.F.W., Mohan, K., Moir, G.K., 1985a. Analytical study of pure and extended portland cement pastes: II, fly ash- and slag-cement pastes. Journal of the American Ceramic Society 68(12), 685-690.

Theiss, F., Apelt, D., Brand, B., Kutter, A., Zlinszky, K., Bohner, M., Matter, S., Frei,

C., Auer, J.A., Von Rechenberg, B., 2005. Biocompatibility and resorption of a brushite calcium phosphate cement. Biomaterials 26(21), 4383-4394.

Tironi, A., Trezza, M.A., Scian, A.N., Irassar, E.F., 2013. Assessment of pozzolanic activity of different calcined clays. Cement and Concrete Composites 37, 319-327.

Toderaş, M., Filip, S., Ardelean, I., 2006. Structural study of the Fe_2O_3-B_2O_3-BaO glass system by FTIR spectroscopy. Advanced Materials 8(3), 1121.

Topçu, İ.B., Canbaz, M., 2004. Properties of concrete containing waste glass. Cement and Concrete Research 34, 267-274.

Turgut, P., Yahlizade, E., 2009. Research into concrete blocks with waste glass. International Journal of Civil and Environmental Engineering 1, 203-209.

Turner, L.K., Collins, F.G., 2013. Carbon dioxide equivalent (CO_2-e) emissions: a comparison between geopolymer and OPC cement concrete. Construction and Building Materials 43, 125-130.

Vaitkevičius, V., Šerelis, E., Hilbig, H., 2014. The effect of glass powder on the microstructure of ultra high performance concrete. Construction and Building Materials 68, 102-109.

Venkatanarayanan, H.K., Rangaraju, P.R., 2013. Decoupling the effects of chemical composition and fineness of fly ash in mitigating alkali-silica reaction. Cement and Concrete Composites 43, 54-68.

Wallah, S.E., Hardjito, D., 2014. Handbook of alkali-activated cements, mortars and

concretes, Chapter 10: Assessing the shrinkage and creep of alkali-activated concrete binders. Woodhead Publishing Ltd.

Wang, H., Li, H., Yan, F., 2005. Synthesis and mechanical properties of metakaolinite-based geopolymer. Colloids and Surfaces A: Physicochemical and Engineering Aspects 268(1-3), 1-6.

Wang, K.S., Chiou, I.J., Chen, C.H., Wang, D., 2005. Lightweight properties and pore structure of foamed material made from sewage sludge ash. Construction and Building Materials 19, 627-633.

Wang, L., Skjevrak, G., Hustad, J.E., Gronli, M.G., 2012. Sintering characteristics of sewage sludge ashes at elevated temperatures. Fuel Processing Technology 96, 88-97.

Wiskel, J.B., Li, X., Ivey, D.G., Henein, H., 2018. Characterization of X80 and X100 microalloyed pipeline steel using quantitative X-ray diffraction. Metallurgical and Materials Transactions B (Accepted paper).

Xuan, D.X., Zhan, B.J., Poon, C.S., 2016. Development of a new generation of eco-friendly concrete blocks by accelerated mineral carbonation. Journal of Cleaner Production 133, 1235-1241.

Xu, H.C., He, P.J., Gu, W.M., Wang, G.Z., Shao, L.M., 2012. Recovery of phosphorus as struvite from sewage sludge ash. Journal of Environmental Sciences 24(8), 1533-1538.

Yamaguchi, N., Ikeda, K., 2010. Preparation of geopolymeric materials from sewage

sludge slag with special emphasis to the matrix compositions. Journal of the Ceramic Society of Japan 118(1374), 107-112.

Yang, J., Li, D., Fang, Y., 2017. Synthesis of Nanoscale $CaO-Al_2O_3-SiO_2-H_2O$ and $Na_2O-Al_2O_3-SiO_2-H_2O$ Using the Hydrothermal Method and Their Characterization. Materials 10(7), 695.

Yang, T., Wu, Q., Zhu, H., Zhang, Z., 2017. Geopolymer with improved thermal stability by incorporating high-magnesium nickel slag. Construction and Building Materials 155, 475-484.

Yaseri, S., Hajiaghaei, G., Mohammadi, F., Mahdikhani, M., Farokhzad, R., 2017. The role of synthesis parameters on the workability, setting and strength properties of binary binder based geopolymer paste. Construction and Building Materials 157, 534-545.

Yip, C.K., Lukey, G., Van Deventer, J., 2005. The coexistence of geopolymeric gel and calcium silicate hydrate at the early stage of alkaline activation. Cement and Concrete Research 35(9), 1688-1697.

Yu, L., Zhang, Z., Huang, X., Jiao, B., Li, D., 2017. Enhancement Experiment on Cementitious Activity of Copper-Mine Tailings in a Geopolymer System. Fibers 5(4), 47.

Yu, Q., Sawayama, K., Sugita, S., Shoya, M., Isojima, Y., 1999. The reaction between rice husk ash and $Ca(OH)_2$ solution and the nature of its product. Cement and Concrete Research 29(1), 37-43.

Zhan, B.J., Poon, C.S., 2015. Study on feasibility of reutilizing textile effluent sludge for producing concrete blocks. Journal of Cleaner Production 101, 174-179.

Zhang, W., Hama, Y., Na, S.H., 2015. Drying shrinkage and microstructure characteristics of mortar incorporating ground granulated blast furnace slag and shrinkage reducing admixture. Construction and Building Materials 93, 267-277.

Zhang, W.Y., Hama, Y., Na, S.H., 2015. Drying shrinkage and microstructure characteristics of mortar incorporating ground granulated blast furnace slag and shrinkage reducing admixture. Construction and Building Materials 93, 267-277.

Zhang, W., Zakaria, M., Hama, Y., 2013. Influence of aggregate materials characteristics on the drying shrinkage properties of mortar and concrete. Construction and Building Materials 49, 500-510.

Zheng, D.D., Ji, T., Wang, C.Q., Sun, C.J., Lin, X.J., Hossain, K.M.A., 2016. Effect of the combination of fly ash and silica fume on water resistance of Magnesium-Potassium Phosphate Cement. Construction and Building Materials 106, 415-421.

Zhou, J., Ye, G., Van Breugel, K., 2010. Characterization of pore structure in cement-based materials using pressurization–depressurization cycling mercury intrusion porosimetry (PDC-MIP). Cement and Concrete Research 40(7), 1120-1128.

Zhu, X.H., Tang, D., Yang, K., Zhang, Z.L., Li, Q., Pan, Q., Yang, C.H., 2018. Effect of $Ca(OH)_2$ on shrinkage characteristics and microstructures of alkali-activated slag concrete. Construction and Building Materials 175, 467-482.

Ziolkowski, M., Kovtun, M., 2018. Confined-Direct Electric Curing of NaOH-activated fly ash based brick mixtures under free drainage conditions: Part 2. Confined-DEC versus oven curing. Construction and Building Materials 176, 452-461.